

NÃO CONFIDENCIAL



Laboratório Nacional de Engenharia Civil

APPLICATIONS OF COMPUTATIONAL MECHANICS TO UNDERGROUND STRUCTURES IN HYDRAULIC PROJECTS

REPORT

RELATÓRIO 52/92 – NOS

José J. J. - 92

MINISTÉRIO DAS OBRAS PÚBLICAS, TRANSPORTES E COMUNICAÇÕES

Laboratório Nacional de Engenharia Civil

NÃO CONFIDENCIAL

DEPARTAMENTO DE BARRAGENS

Núcleo de Obras Subterrâneas

Proc. 047/13/9246

Proc. 047/13/9249

APPLICATIONS OF COMPUTATIONAL MECHANICS TO UNDERGROUND STRUCTURES IN HYDRAULIC PROJECTS

REPORT

RELATÓRIO 52/92 – NOS

Lisbon, March 1992

I&D
BARRAGENS

Copyright © LABORATÓRIO NACIONAL DE ENGENHARIA CIVIL, I. P.
AV DO BRASIL 101 • 1700-066 LISBOA
e-mail: lnec@lnec.pt
www.lnec.pt

Digitalizado no Setor de Divulgação Científica e Técnica do LNEC

2023

**APPLICATIONS OF COMPUTATIONAL MECHANICS TO UNDERGROUND
STRUCTURES IN HYDRAULIC PROJECTS**

**APLICAÇÕES DE MECÂNICA COMPUTACIONAL A ESTRUTURAS
SUBTERRÂNEAS DE OBRAS HIDRÁULICAS**

**APPLICATIONS DE MÉCANIQUE COMPUTATIONNELLE À DES
STRUCTURES SOUTERRAINES D'OUVRAGES HYDRAULIQUES**

ABSTRACT:

A brief description of the phenomena and problems associated with underground structures in hydraulic projects is presented, namely in what concerns the powerhouses, surge chambers and pressure tunnels and shafts. An analysis of the calculation methodologies followed in the structural design of this works is presented, as well as of the numerical models usually adopted, namely finite and boundary element models. Finally, some applications of computational mechanics are presented. First, a parameter study for underground powerhouses, with special emphasis in the definition of shapes, existence of several caverns, and in the tridimensional equilibria is described. Afterwards, examples of application to some hydraulic projects are illustrated: a large underground powerhouse in Mozambique, the Alto Lindoso hydroelectric power scheme in construction in the north of Portugal, and the Castelo do Bode tunnel, in operation, integrated in the water supply system to Lisbon.

RESUMO:

Apresenta-se uma breve descrição dos fenómenos e problemas associados a estruturas subterrâneas em obras hidráulicas, nomeadamente em relação a centrais hidroeléctricas, chaminés de equilíbrio e túneis e poços em carga. Procede-se a uma análise das metodologias

de cálculo seguidas no projecto estrutural destas obras e dos modelos numéricos adoptados, de que se salientam os modelos por elementos finitos e por elementos de fronteira. Finalmente, ilustram-se aplicações da Mecânica Computacional a um estudo de índole paramétrica de cavernas de centrais hidroeléctricas, com especial incidência na definição de formas, na existência de cavidades múltiplas e no efeito dos equilíbrios tridimensionais, e a vários empreendimentos hidráulicos, uma central hidroeléctrica de grandes dimensões em Moçambique, o aproveitamento hidroeléctrico do Alto Lindoso em construção no Norte de Portugal, e o tunel do Castelo do Bode, em exploração, integrado no sistema de adução de água à região de Lisboa.

RESUMÉ

On décrit brièvement les phénomènes et les problèmes associés aux structures souterraines d'ouvrages hydrauliques, particulièrement les centrales hydroélectriques, les cheminées d'équilibre, les galeries et les puits en charge. On fait l'analyse des méthodes de calcul suivies pour le projet structural de ces ouvrages, ainsi que des modèles numériques adoptés, notamment les modèles par éléments finis et les modèles par éléments de frontière. Pour finir, on décrit des applications de Mécanique Computationnelle à une étude paramétrique de cavernes de centrales hydroélectriques, concernant surtout la définition des formes, l'existence de cavités multiples et l'effet des équilibres tridimensionnels. Des exemples d'application à plusieurs projets hydrauliques sont rapportés: une centrale hydroélectrique de grandes dimensions au Mozambique, l'aménagement hydroélectrique d'Alto Lindoso, en construction au Nord du Portugal, et la galerie de Castelo do Bode, déjà en service, qui fait partie du système d'adduction d'eau à la région de Lisbonne.

TABLE OF CONTENTS

	Page
1 - INTRODUCTION	1
1.1 - General	1
1.2 - Hydroelectric powerhouses	2
1.3 - Surge chambers	5
1.4 - Pressure tunnels and shafts	6
2 - CONCEPTION AND CALCULATION OF UNDERGROUND STRUCTURES	9
2.1 - Preliminary considerations	9
2.2 - Conception of works	10
2.3 - Structural calculation	13
3 - COMPUTATIONAL METHODS	17
3.1 - Numerical methods	17
3.2 - Mechanical behaviour models	20
3.3 - Models for the hydromechanical behaviour	21
4 - PARAMETRIC STUDY OF THE STRUCTURAL BEHAVIOR OF HYDROELECTRIC POWERHOUSES	25
4.1 - Nature of the study	25
4.2 - Analysis of the shapes	26
4.3 - Multiple caverns	28
4.4 - Tridimensional equilibria	29
LNEC - Proc.047/13/9246	
Proc.047/13/9249	III

	Page
5 - ANALYSIS OF AN UNDERGROUND POWERHOUSE IN MOZAMBIQUE	33
5.1 - General description	33
5.2 - Finite element models	33
5.3 - Laboratory model	34
5.4 - Comparison between experimental, numerical and observed values	35
6 - ANALYSIS OF THE BEHAVIOUR OF THE ALTO LINDOSO UNDERGROUND POWER SCHEME	 37
6.1 - Description of works	37
6.2 - Rock mass characterization	38
6.3 - Quantification of the in-situ state of stress	41
6.4 - Structural behaviour of the powerhouse complex	43
6.5 - Structural behaviour of the surge chamber	46
7 - APPLICATION TO THE CASTELO DO BODE TUNNEL	49
7.1 - General description of the tunnel	49
7.2 - Observation of the tunnel	50
7.3 - Numerical and analytical solutions for the simulation of the loading test	51
7.4 - Comparison between the calculated and the observed values	55
ACKNOWLEDGEMENTS	57
REFERENCES	59

LIST OF FIGURES

FIGURE

- 1.1 - Alto Lindoso hydroelectric power scheme (after EDP, 1991)
- 1.2 - Cahora Bassa underground powerhouse complex
- 1.3 - Shapes of underground powerhouses
- 1.4 - Types of surge chambers
- 1.5 - Drakensberg pumped storage scheme (after Pyzikowski, 1982)
- 1.6 - Castelo do Bode tunnel (after EPAL, 1988)
- 2.1 - Optimization of cavern orientation with respect to main discontinuities
- 2.2 - Pressures on the supports of caverns (after Cording et al., 1971)
- 2.3 - Deterministic assessment of potentially unstable blocks (after Croney et al., 1978)
- 3.1 - Flow around Paulo Afonso IV powerhouse cavern
- 3.2 - 3D boundary element model for the Castelo do Bode tunnel
- 3.3 - Displacements computed at the final excavation stage for the Inagawa No.2 powerhouse (after Kawamoto et al., 1988)
- 3.4 - Failure zones due to bedding and two joint sets for the Siah Bishe powerhouse (after Honisch, 1988)
- 3.5 - Free surface under (1) no coupling; (2) coupling elastic; (3) coupling plastic (after Wei and Hudson, 1990)
- 4.1 - Parametric studies of powerhouse caverns
- 4.2 - 2D and 3D boundary element models
- 4.3 - Boundary displacements for isolated caverns
- 4.4 - Convergence curves for isolated caverns
- 4.5 - Boundary tangential stresses for isolated caverns
- 4.6 - Failure zones for isolated caverns
- 4.7 - Boundary displacements for multiple caverns
- 4.8 - Failure zones for multiple caverns
- 4.9 - Results of 3D boundary model for hydrostatic initial state of stress
- 4.10 - Displacements of 3D model for several longitudinal initial stresses

FIGURE

- 4.11 - Tangential stresses of 3D model for several longitudinal initial stresses
- 4.12 - Influence of cavern orientation on displacements and stresses
- 5.1 - Cahora Bassa scheme. General plan of the powerhouse and hydraulic circuit (after Silveira et al., 1974)
- 5.2 - Block for the 3D calculation model
- 5.3 - Construction sequence simulated by 3D model at section S_1
- 5.4 - 2D finite element mesh
- 5.5 - Schematic drawing of the laboratory model
- 5.6 - Principal stresses in the powerhouse cavern for a state of triaxial stress in the rock mass corresponding to $\sigma_v = 15$ MPa and $\sigma_H = 10$ MPa (after Silveira et al., 1974)
- 5.7 - Principal stresses in the powerhouse cavern
- 5.8 - Principal stresses in the walls of the south surge chamber
- 5.9 - Displacements at section S_1
- 5.10 - Plasticity zones
- 5.11 - Observation plan of the powerhouse underground complex
- 5.12 - Comparison of observed and predicted behaviour
- 6.1 - Hydraulic circuit of Alto Lindoso power scheme. Longitudinal profile (after EDP, 1991)
- 6.2 - Sites of rock tests
- 6.3 - Discontinuity sets
- 6.4 - View of the boundary element mesh
- 6.5 - Displacements at the boundaries along the cross-sections
- 6.6 - Construction sequence at section S_2
- 6.7 - Detail of the finite element mesh
- 6.8 - Displacements at phase 8
- 6.9 - Principal stresses at phase 8
- 6.10 - Displacements around powerhouse cavern for the different phases
- 6.11 - Failure zones around cavities with application of Coulomb criteria
- 6.12 - Observation plan of the powerhouse complex

FIGURE

- 6.13 - Comparison of observed and numerical convergences
- 6.14 - Boundary element model considering concrete arches (after Castro, 1989)
- 6.15 - Displacements obtained with boundary element model (after Castro, 1989)
- 6.16 - Principal stresses obtained with boundary element model (after Castro, 1989)
- 6.17 - Tangential stresses along the boundaries of the powerhouse cavern (after Castro, 1989)
- 6.18 - 3D boundary element mesh for the surge chamber
- 6.19 - Displacements and principal stresses for phase 3, hypothesis C_1
- 6.20 - Displacements and principal stresses for phase 3, hypothesis C_2
- 6.21 - Observation plan of the surge chamber
- 6.22 - Convergence measurements at section A of the surge chamber
- 7.1 - Castelo do Bode tunnel: vertical section
- 7.2 - Loading test: internal water pressure and strains in the Carlson extensometers in the instrumented section
- 7.3 - Conceptual model and construction sequence for the finite element model
- 7.4 - Conceptual models for the analytical solutions of the thick walled pervious rings (after Schleiss, 1986)
- 7.5 - Tangential stresses in the centre of the concrete lining
- 7.6 - Normal stresses in the lining/rock contact
- 7.7 - Flow rates through the concrete lining
- 7.8 - Extensometers A1 and A2. Tangential stresses
- 7.9 - Extensometer A3. Tangential stresses
- 7.10 - Extensometer A4. Tangential stresses

LIST OF TABLES

TABLE

- 4.1 - Parameters used for the analyses of shapes
- 5.1 - Summary of in-situ parameters
- 6.1 - Stability of blocks of an exploration gallery
- 6.2 - Summary of joint shear tests result
- 6.3 - Results of SFJ and STT tests
- 6.4 - In-situ state of stress calculated

APPLICATIONS OF COMPUTATIONAL MECHANICS TO UNDERGROUND STRUCTURES IN HYDRAULIC PROJECTS

1 - INTRODUCTION

1.1 - General

Amongst the hydraulic projects that make use of the underground space, the hydroelectric power schemes are the most important ones. They are composed, mainly, by the dam, the hydraulic circuit and the powerhouse.

The use of the underground space for the powerhouse and the hydraulic circuit surge chamber, has been widely implemented where adequate conditions exist, mainly since the second World War, because of the advantages that it brings when compared with surface solutions. Such advantages include weather independent construction, safety from landslides, avalanches, military actions and sabotages and solutions with less environmental impact. The costs with the excavations and supports are usually balanced with the costs of the foundation and superstructure of surface powerhouses. In good rock masses, the supports of the tunnels, caverns and shafts can be considerably reduced or even eliminated, which can result in more economical solutions. Furthermore, the expropriation costs are reduced, and smaller economical and environmental impacts are originated.

On the other hand, significant advances in underground technology, in Rock Engineering and in computational methods have allowed an increasingly rational approach to the design of these underground structures.

The first underground powerhouse, Edward Dean Adam, was built in 1885 in USA, followed by Snoqualmie Falls in 1899. Since then about 500 have been constructed worldwide (Lang, 1971), (Benson, 1989a). In Portugal, the first project totally built underground was

Salamonde, in the Cávado river, in operation since 1953. In Brazil, the first underground project was Cubatão, inaugurated in 1927, but Paulo Afonso I, inaugurated in 1952, was the first one totally built underground (Martins, 1985).

In these projects several types of underground openings exist: the powerhouse complex, high and low pressure tunnels and shafts, surge chambers, water intakes and adits. Several possible types of arrangements exist for the hydraulic circuit. Initially they were almost totally at the surface, but with time the use of the underground space became more and more frequent.

A very good example of the complexity of these projects is given by the Alto Lindoso power scheme, now under construction in the north of Portugal (Fig. 1.1). The underground powerhouse is located 70m south of the left abutment of a double curvature concrete arch dam, and its main floor is at the depth of 340m (EDP, 1991).

The tunnels for water supply for irrigation or urban centres are another kind of hydraulic projects, that can have a considerable extension and internal pressure, and sometimes are also built at considerable depths. They are composed mainly by a water intake, the pressure tunnel and the tunnel portal. They have similar problems as those put by the pressure tunnels of hydroelectric schemes, and what will be said for these also applies to them.

1.2 - Hydroelectric powerhouses

The set of underground works associated with the powerhouses form an essential part of a hydroelectric scheme, whose satisfactory performance is dependent on their suitable location as well as on the correct design of the supports in order to ensure the stability and safety.

In addition to the powerhouse cavern, some other underground works exist, some of which are caverns, such as the transformers room, spherical and butterfly valve chambers and sometimes, the downstream surge chamber; other works are of the linear type, such as the access shafts and tunnels, ventilation shafts, and connection tunnels. Thus the general arrangement of the complex of works must be suitably planned. In fact rational use of space

is still more necessary for underground works than it does for surface solutions owing to the high cost involved in excavation.

An example of the complexity of an underground power house is given by Cahora Bassa power plant located in Mozambique. Fig.1.2 gives a schematic perspective of the powerhouse and the associated surge chambers. The underground openings are situated at a depth that, in the case of the powerhouse, varies from about 130 m at one of the ends to about 230 m at the other end (Silveira et al., 1974).

A whole project implies the need for good geologic, geotechnical and hydrogeological survey of the rock mass where the caverns will be located, reason why it is necessary to provide access shafts and/or tunnels direct to the rock mass concerned, chiefly for deep underground works. In general, once the characteristics of the rock mass have been ascertained and a site has been selected, the design of these works involves the definition of the main axes of orientation of the openings, definition of the shapes of caverns and associated shafts and tunnels, taking into account mainly factors related to mechanical characteristics, discontinuity surfaces and the in-situ state of stress in the rock mass. Moreover the design of the different parts of the underground powerhouse complex should be such as to provide an optimum solution from the points of view of safety, functionality and economy.

Design of these works calls for the definition of supports to be applied at the different construction phases of the caverns, namely using concrete arches and/or rock bolting with reinforced shotcrete, which is established on basis of the experience acquired in numerous works and on the stability analyses using numerical models, like finite element, boundary element and block methods. These numerical methods give an important contribution to the design of these works and to the interpretation of their monitored behaviour.

As regards the analysis of these works, emphasis should be laid upon the importance of observation and of the construction procedure itself. Observation of the works permits to calibrate the numerical models, to improve construction sequence and provide safety control and acquisition of knowledge in the domain of phenomena involved. As to construction procedures, many variables intervene in the execution methods, some being directly related

to the works, namely the characteristics of the rock mass, whereas other variables are related to external circumstances, such as deadlines and conditioning factors of the project.

As regards the cavern execution systems, several construction sequences are considered which comprise the different sequences of excavation and provision of support. They largely influence the behaviour of these underground structures during the construction phase and consequently the final states of strain and stress.

The general arrangement of the different underground works for the power station is strongly influenced by topographic and geological conditions. The inside arrangement of the powerhouse is dependent on the number and size of the turbo-generator units and by the space required for erection and loading. Once the type of turbo-generator and the arrangement of the corresponding shaft have been defined, the different equipments are located in the powerhouse cavern, bearing in mind that the arrangement must be as compact as possible. The overall dimensions of the powerhouse cavern are then defined taking into account the different equipments to be installed.

As to the shape of the powerhouse cavern, the most common cross-section used to be a mushroom type with vertical walls and concrete arch ceiling; at present egg-shaped or horseshoe shaped sections are more recommended, in an attempt to avoid high vertical walls. Use has also been made of other shapes, with nearly circular ceilings whose span can exceed the distance between the walls of the caverns. In some underground powerhouses at small depth, when there are no conditions for the arch effect owing to the small thickness of the overburden or to poor rock quality, the power house is installed in a shaft. Fig. 1.3 shows different shapes adopted for underground powerhouses.

Other caverns can be adopted for accommodation of other equipments as occurs at Alto Lindoso (Fig. 1.1), in such a way as to form a multiple-cavity system separated by rock pillars, comprising a complex of connecting tunnels and shafts. In this case one should try to study the effects that the excavation of an underground structure may have over other neighbour openings. Occurrence of zones with high stress concentration may modify the general arrangement initially foreseen or the excavation procedure and the supports adopted,

and the distance between parallel cavities is an important parameter to be considered (Duffaut, 1982).

1.3 - Surge chambers

Surge chambers in hydraulic works are intended both to limit the effects of the water hammer, and to supply the turbines with the necessary volume of water, in case of sudden loading variations.

Surge chambers may be located in the hydraulic circuit upstream/or downstream of the powerhouse, depending on the general arrangement of the hydraulic circuit and, particularly, on the length of the pressure circuit. The upstream surge chambers are located in the transition from the headrace tunnel to the high pressure shaft. The downstream surge chambers, located between the draft tube and the tailrace tunnels, may sometimes be part of the powerhouse underground complex. Depending on the number of power units and the number of draft tube tunnels, one or more surge chambers can be adopted, which may be caverns to receive flows from all draft tubes and to discharge into the tailrace tunnel.

There are several types of surge chambers (Fig. 1.4), all with devices for producing energy losses and damping the water mass oscillation inside the chamber.

Recently smaller surge chambers have been constructed, partially filled with high pressure air. Formation of an air cushion reduces the inertia effect of the water mass in the plant and hydraulic circuit thus providing stability to the hydraulic system. The surge chamber is preferably located near to the powerhouse to avoid large distances between the surge chamber and the compressed air system (Goodall et al., 1989). The larger the head the more economical this type of surge chamber proves with reference to other types.

Referring to the Alto Lindoso scheme, Fig. 1.1 shows the downstream surge chamber which is a composite structure (throttled and gallery types). This is a large structure with a cylindrical shaft, about 65m in height and 23m in diameter, a concrete cylindrical arch, a

380m long circular feeding chamber, and an expansion chamber about 300m long, which ends by a ventilation shaft.

Lastly mention should be made of the importance of the design of supports and linings required for ensuring the stability of these works. Surge chambers are concentrated structures, in which tridimensional equilibria develop. Therefore the problems and phenomena involved in their construction and structural design are similar to those found in the caverns of the powerhouse complex.

1.4 - Pressure tunnels and shafts

The pressure tunnels and shafts that form the hydraulic circuit of hydroelectric schemes, as well as the pressure tunnels of water supply systems, can be of considerable importance due to the high water pressures (internal and external) that may be present, to the great length that they sometimes have, and therefore to the variety of geotechnical conditions that may occur.

The hydraulic circuit is formed by a variety of works. Normally, after the water intake, at the upper reservoir, starts a low pressure tunnel, that ends at a vertical or inclined shaft, which is followed by a high pressure tunnel, that brings the water to the powerhouse. After passing the turbines, the water is conducted to the lower reservoir by a low pressure tunnel. The hydraulic circuit of the Drakensberg Pumped Storage Scheme in South Africa, is a good illustration of all these types of conduits, and is shown in Fig. 1.5 (Pyzikowski, 1982). As an illustration of a water supply pressure tunnel, a horizontal and a vertical sections of the Castelo do Bode tunnel are shown in Fig. 1.6.

The choice of the alignment of the power tunnels and shafts depends on several economical and technical factors. According to Benson (1989b), the primary factors that are likely to have a dominant role in overall economics are the schedule for completion of the works, the available contractors and equipment as well as the geological conditions. Many other important technical factors affect the selection of the alignment, namely the water heads and the internal pressures they generate, the surface topography, the in situ stresses and the

prevention of hydraulic jacking, the position of the water table and the external pressures they may provoke, the need of temporary supports and final linings, as well as the requirements for access, ventilation and drainage.

During the last decades there has been a tendency to bring the hydraulic circuits underground, due to the efficiency of the excavation methods available, and to the smaller environmental implications. Also, the better rock quality that is found underground, increases its contribution of the rock mass to resist, together with the supports, to the internal pressures, leading to smaller linings, and therefore to more economical solutions.

The static water heads in pressure tunnels and shafts have been increasing steadily worldwide in the last decades. The special topographical and geological conditions in Norway made of this country the leader in terms of projects with high water heads, with the unlined pressure shaft of the Nyset-Steggje project reaching a water head of nearly 1000m. The maximum static water head on a steel lined section is also to be found in Norway, at the Lang-Sima project, with a value of 1150m (Brekke and Ripley, 1987).

The choice of the adequate location and the design of the supports of the pressure tunnels and shafts can only be done on the basis of a detailed geotechnical study. Once all the necessary information is available, numerical models are of great usefulness in order to correctly define an alignment and supports that obey all the safety and economical requirements.

2 - CONCEPTION AND CALCULATION OF UNDERGROUND STRUCTURES

2.1 - Preliminary considerations

Structural design of underground works is an all-embracing process that takes into account the various aspects dependent on the specific nature of such works. It covers two stages, the conception stage and the calculation stage. Conception of an underground work is basically related with choice of the site, location and orientation, and shape and geometry of the cavities, while the calculation is concerned with determining structural solutions for achieving a certain performance.

A great effort is made in order to ensure greater structural safety of works, and every step is therefore taken to integrate progress in the various fields connected with the theory of structural safety and other theories of which that theory is a subsidiary.

The theory of structural safety includes the study of the factors and the establishing criteria that condition decision as regards quality and which must be met, and the research of calculation models and methodologies, with the aim of reaching solutions which can satisfy the quality standards concerned. Problems related with characterization of actions and the determination of the structural behaviour are of great importance in these works and belong to the domain of the theory of actions, mechanical behaviour of materials (rock mass) and structural behaviour.

The theory of structural reliability concerns the study of models and methodologies, taking into consideration existing uncertainties in order that the structures will not reach certain unfavouring states from the point of view of their functioning.

Activities relating to monitoring of the behaviour of underground works fall within the scope of the theory of control processes during the various stages in their life, with a view to obtaining adequate levels of structural quality.

2.2 - Conception of works

One of the processes used in designing these underground structures consists of defining the following stages (Martins, 1985), (Benson, 1989a):

- Choice of the site that from the point of view of stability offers optimum conditions, taking into account the geotechnical characteristics of the rock mass.
- Definition of the main axes of orientation of the cavities, so as to minimize stability problems.
- Definition of the shapes of the caverns and tunnels, taking into consideration, namely, the mechanical properties and discontinuities of the rock mass and the in-situ state of stress.
- Dimensioning of the different parts of the underground complex, so as to achieve an optimum solution from an economic viewpoint; this must involve a calculation stage for verifying the stability and safety conditions of the structures.
- Choice of the construction process for excavation and supports, taking account of the type of works, equipment, dimensions of the works and topographical and geological conditions.
- Monitoring of the works during the construction stage, in order to obtain information relating to the structural response, the actions and the geotechnical conditions, which will make it possible to gauge the adequacy of the structural and constructional solutions used and modifications in the light of the information obtained.

Any decisions that may be taken at any of the stages of the design influence the decisions in the other stages, so that progressive optimization of the design requires an interactive sequence until a suitable solution is reached as regards economy and safety.

Conception of the underground structures is basically linked to the first three stages. Accordingly, choice of the site and location of the works may be considered as the most important stage in the preliminary design of a project of this type, because that decision will affect the following stages, and a wrong choice may lead to great risks from a technical and economic point a view, if decisions are taken prematurely, owing to the great uncertainties

at the time about the geotechnical characteristics of the rock mass and then in-situ state of stress. In any decisions taken, there are important restrictions that must be respected; in case of hydro-electric power plants these are mainly concerned with location of the upper and lower reservoirs, topography of the terrain and economic factors related with the profitability of the project. In the preliminary design stage, there must be analysis of various possible locations of the powerhouse and hydraulic circuit, deciding on the location that offers the best solution.

After these prerequisites have been met, there is a certain flexibility in choosing the site, so that location of the works will depend mainly on the quality of the rock mass, avoiding certain rock formations that are unsuitable for the functions to be carried out by the works and unfavourable to the stability of the structures, and also major geological accidents. Once the site has been chosen, location of works, above all as regards the cavities of the powerhouse complex, must be defined as to ensure a field of stresses that is favourable to its stability. Thus the cavities must be at a depth which, if possible, enables an important zone of the rock mass to be left unaltered above the roof of the cavities.

Optimization of the orientation of the cavities depends basically on the field of stresses and the geotechnical structure of the rock mass. At this stage, two limit situations may be considered: i) a sound rock mass without any relevant discontinuities; ii) a fractured rock mass with several sets of discontinuities.

In the first situation, which is usually related with works at great depths where fracturing of the rock mass is small or even non-existing, the stability of the cavities depends mainly on the in-situ state of stress, the geometry of the excavation and the strength of the rock mass. Orientation of the main axis of the cavities must be defined so as to minimize the zones subject to tension (Richards et al., 1977). The most favourable orientation will be obtained when the axis of the cavern coincides with the direction of the major principal stress and the ratio between the height and the span is equal to the ratio between the vertical and horizontal stresses. In the case of caverns of hydro-electric projects, there is not much flexibility in defining this ratio, since the dimensions of those cavities are imposed by other factors, such as the electromechanical equipment.

In the second situation mentioned, orientation of the cavity is determined by the most important discontinuity, so as to minimize any problems connected with disarticulation of the rock mass (Fig. 2.1). The basis rule consists of orientating the main axis of the cavern according to the line bisecting the maximum angle of two directions corresponding to the most important discontinuities (Olsen and Broch, 1977).

In intermediate situations, however, which are the most common, optimization of the orientation of the main axis must at the same time consider the in-situ state of stress and fracturing of the rock mass. On the basis of the Norwegian experience, it is recommended, for cavities that are not very deep, that the main axis should be orientated according to the bisector of the greater angle between two families of important discontinuities, while for cavities at greater depths this axis should be orientated as to be offset by 15° to 30° from the direction of the greatest horizontal principal stress, avoiding parallelism with the main discontinuity set. In specific cases it is possible to prepare a numerical model of the problem concerned, bringing the in-situ state of stress and the discontinuity set and, by an iterative process, to determine the best orientation, having in mind the stability of the works.

As regards definition of the shape of the cavities, it is necessary to bear in mind the considerations already mentioned in analyzing the problems and phenomena associated with underground hydro-electric schemes, concerning the establishment of the minimum dimensions required for the cavern of the powerhouse, its internal arrangement and the overall arrangement of the powerhouse complex. Generally speaking, the shapes of the openings take into account the function for which they are intended, the excavation method used and the in-situ state of stress. As a fundamental principle, the aim is to obtain a distribution of essentially compressive stresses round the periphery of the cavities. The simplest shape of cavity is therefore that of a cavity with an arch ceiling. There are empirical criteria, namely in keeping with Norwegian experience, adopted for defining shapes of openings according to the initial state of stress (moderate and high level) and the orientation of the maximum principal stress (Broch, 1982).

As regards the shape of the powerhouse cavern, however, essentially symmetrical cross-sections have been adopted, mushroom-shaped, egg-shaped and with a circular ceiling

(Fig.1.3). It is found that in terms of structural behaviour the egg shape generally provides best solution, and the girders of the gantry crane can be fixed to the walls of the cavern by means of prestressed stays. This enables them to be fixed earlier and thus allows them to be used in the excavation work.

As regards the other caverns of the powerhouse complex, definition of their shapes is generally less conditioned by instability factors because their dimensions are smaller. The shape of the surge chambers may be as varied as possible, as has been mentioned previously, but it is to be noted that problems arise in analyzing the stability of these cavities, since in many projects there are large dimensions involved. As for the works of the hydraulic circuit, the definition of shapes is conditioned by their function and by the excavation process used, a circular and horseshoe shape generally being adopted.

2.3 - Structural calculation

Structural calculation corresponds to the stage when there is full definition of the characteristics of the structures resulting from the conception stage. The need or not of a support will be established, and in the first case its characteristics will be defined. Dimensioning of the supports is based mainly on an analysis of the most important actions and consideration of the characteristics of the rock mass, in which it is necessary to distinguish the approximations of continuous medium and discontinuous medium. The calculations for verifying the stability of the structures are based on analyses of deformation-stresses, generally making use of numerical models and limit equilibrium techniques applied to given failure mechanisms; on the interpretation of data obtained from monitoring the works, and on empirical rules obtained on the basis of the experience of many works in different types of rock masses and under stress conditions (Hoek and Brown, 1982).

As regards the use of supports, a distinction must be made between primary and definitive supports, for which are defined safety criteria that are necessarily different, since the former are dimensioned so as to prevent rupture and disarticulation of the rock mass during the

construction stage, whereas the latter are intended to ensure the safety and functionality of the work throughout its life.

It is therefore necessary, in dimensioning the supports or in considering that the rock mass is self-supporting, to adopt safety criteria that establish given limits for displacements, deformations or stresses, both for the rock mass and for the support. Safety criteria constitute a fundamental problem, both in relation to the population and the economy of the works.

Structural safety has been thoroughly discussed in recent years, drawing attention to its probabilistic nature. In underground works, there is a great difficulty as regards the lack of information on the characteristics of the rock masses and the actions, so that the probabilistic concept of safety applied in other types of works is hard to apply, and use is therefore made of the traditional concept of coefficients of safety, which in recent years has been considered on a semi-probabilistic basis.

The safety criteria most commonly used normally consist of limiting the displacement values at the boundaries of underground works, which is an indirect way of limiting deformations in the rock mass. Criteria may also be established for limiting the magnitude of stresses in the rock mass in order to prevent failure, but is inadvisable for economic reasons. It is therefore considered more convenient to establish safety criteria for the supports, bringing in ways of considering safety stresses and carrying out dimensioning in relation to failure. As regards the last mentioned method, it is impossible to fix values of probability of failure, and so values have been adopted for the properties of the rock mass by assessing each case.

In dimensioning the supports, it is necessary to consider the mechanical characteristics of the rock mass and the actions acting during the various stages of the project, i.e. construction and operation. As regards the characteristics of the mass, the main difficulties are concerned with consideration of fracturing and heterogeneity. It must also be pointed out that the different types of works that occur in these projects call for different dimensioning criteria, these being more empirical for linear works, a greater refinement being allowed for the caverns, where it is usual to undertake a more ample characterization of the rock masses and actions.

For considering fracturing, the rock mass may be idealized as a continuous medium or as a discontinuous medium. If a continuous medium is used, the mechanical characterization is determined on the basis of stress-strain relationships, in which case there is great difficulty in obtaining that information exclusively from tests, owing to the large dimensions required in view of the spacing between fractures. Therefore, empirical models of behaviour of the rock mass are often used, or certain stress-strain relationships are adopted, according to the project designer's experience and intuition.

The discontinuous medium approach in principle calls for a mechanical characterization of the rock material and geometrical and mechanical characterization of the system of fractures, with use often being made of empirical or deterministic methods which, on the basis of the surfaces of principal discontinuities and on the use of limit equilibrium methods, make it possible to quantify the forces that will act on the supports owing to the fall of blocks (Croney et al., 1978), (Priest, 1985), (Goodman and Shi, 1985), (Lamas, 1986). It is supposed that a certain volume of rock mass, determined on the basis of the geometrical and strength characteristics of the discontinuities, is subject to becoming detached, and sometimes the weights of the volumes so considered are assimilated to distributed forces.

Fig. 2.2 shows pressures acting on the supports of caverns of underground power plants, on the basis of a study by Cording et al. (1971). It is found that as regards the ceiling the pressures on the support correspond to the weight of a volume of rock mass equal in width to the span of the opening and in height between 0.1 and 0.3 of the span; and as regards the walls of the caverns, the pressures are equivalent to a volume equal in height to that of the cavity and in width between 0.05 and 0.15 of the height.

Deterministic models have also been developed; once the characteristics of the most important discontinuity surfaces have been obtained, these models make it possible to examine the blocks resulting from compartmentation of the rock mass and excavation surfaces, and to identify those in which mechanisms of failure are kinematically possible. After this analysis, and on the basis of calculations of stability of potentially unstable blocks, adequate supports are determined for the safety of the work. Fig. 2.3 gives a geometrical representation of the intersections of the surfaces of discontinuity with the boundaries of excavation for the

Dinorwic powerhouse. The same figure shows, on the basis of a deterministic model, the potentially unstable blocks of rock, considering relative simple rupture mechanisms involving the fall and sliding of blocks.

As a concluding remark, the calculation methods used in the design may be systematized in the following groups:

- i) Empirical methods - Based on the use of geomechanical classifications, from which recommendations may be established for the characteristics of the supports or the applied forces, for the estimated conditions of the rock mass.
- ii) Numerical methods - Based on the analysis of the field of stresses/strains, using physical and numerical models, especially in the latter case finite element models, boundary element models.
- iii) Observation methods - Related with the observation of displacements round the cavities in order to detect possible instability, using empirical rules and results of numerical models, as well as analysis of the interaction between the rock mass and support.

3 - COMPUTATIONAL METHODS

3.1 - Numerical methods

The calculation methods implicate the setting up and application of models, that result from an idealization of the reality, with the simplifications inherent in the different situations met in structural design. In order to choose the computational methodologies for representation of the phenomena and processes, technical and scientific criteria and pragmatic criteria must be taken into account. If the former prevail, the models sometimes present great complexity and the optimum model is the one that best fits the available results and/or information. If a pragmatic approach prevails, simplified models are adopted that result from selection criteria based mainly on empirical considerations. For calculation of underground structures, there are also highly complex numerical and/or experimental models, used for investigation purposes, which are intended to throw light on several phenomena associated with these works.

Description of the uncertainties that affect the parameters of the models can be made by using a probabilistic description, in which parameters are considered as random variables characterized by a probability distribution total or partially defined through some of their moments. For underground works, the parameters are as a rule quantitatively established, setting limits of variation. Thus parametric studies of the sensitivity to certain parameters are conducted.

In the different conceptual models used in the methodologies for predicting the structural behaviour and quantifying the actions, use is made of analytical solutions, experimental and numerical methods. One has to acknowledge the importance of analytical solutions of the Theory of Elasticity and Plasticity, though for simpler cavity shapes, since they are solutions that allow to acquire knowledge on the influence of some basic parameters on which the behaviour of these underground works depend.

Numerical models have provided an important contribution, in spite of the numerous uncertainties regarding the characterization of the rock masses and even of the design. They are based either on continuous mechanics (essentially differential and integral methods such as the finite element method and the boundary element method) or on the mechanics of discontinuous media, namely the discrete element method. There are, also, limit equilibrium methods through which the behaviour of the support is investigated for loads determined under the assumption that limit equilibria have been established in the rock mass. The shape and dimensions of the limit equilibrium surfaces depend on the depth (surface or deep underground) and they vary following the different procedures proposed by several authors. Once load has been defined, the support is studied without considering its compatibility with the rock mass; later appropriate numerical methods are adopted for calculations.

Particular reference should be made to deterministic methods which make it possible to analyze the stability of underground works in rock masses, once the orientation, the geometry and strength characteristics of the discontinuity surfaces have been obtained. Assessment of stability and definition of the geometry of the excavation as a rule comprise the following steps: i) characterization of the most important discontinuity surfaces; ii) identification of the potentially unstable blocks; iii) analysis of the stability of the potentially unstable blocks and appropriate supports. These methods have known an important development with the method of blocks by Goodman and Shi (1985), whose importance has to be acknowledged in underground cavities.

Some general considerations should also be made as regards the potentialities of the different numerical methods already mentioned and on their scope of application to underground structures of hydraulic schemes.

Finite element models are widely used owing to their versatility and to the ease of application, namely to consider different types of constitutive laws of the rock masses and supports, different construction sequences and in situ-states of stress. These methods are also important for the quantification of actions in underground works. For the case of water percolation in discontinuous media such as rock masses, models have been developed for the calculation of its mechanical and hydraulic actions. As an example of application, Fig. 3.1

gives the equipotential lines determined by finite elements for the flow around the Paulo Afonso IV powerhouse cavern (Martins, 1985).

As concerns the integral methods, mentioned should be made of the increasingly used boundary element models. With these models discretization is introduced only along the boundaries, thus reducing by one the dimensionality of the problem. In these models, the main advantages essentially lie on the simplicity of the discretization process, with easy data preparation, and on the generation of the system of equations with a reduced number of unknowns. Nevertheless, application of these models to non-linear behaviour has not yet been developed as far as necessary. As an example of application, Fig. 3.2 shows a tridimensional boundary element model developed for the evaluation of the in-situ state of stress in the rock mass for the Castelo do Bode water supply tunnel (Sousa et al., 1986).

For a discontinuous medium approach finite element and boundary element models can also be used, as an extension of the methods established for the continuum approach, as well as the distinct element method.

Finite element models to be used in a discontinuous medium include special elements, known as joint elements, which make it possible to simulate the behaviour of rock joints and of interfaces between the rock mass and the supports. These elements have been developed to analyze several types of problems, involving non-linear behaviour of the discontinuity surfaces (Goodman and St. John, 1977). Boundary element models could also be extended to the analysis of rock media crossed by discontinuities, by using a formulation of non-linear problems comprising slip and separation along discontinuities (Crouch and Starfield, 1983).

The discrete element method considers the discontinuous medium as a set of independent blocks, rigid or deformable, and allows the representation of the non-linear behaviour of the rock discontinuities (Cundall, 1971), (Vargas, 1982), (Lemos, 1987). This is an entirely discontinuous formulation where slip, separation, rotation and large movements of the blocks can be simulated.

3.2 - Mechanical behaviour models

In order to simulate the continuum, one of the most widely used solutions is still the adoption of elastic behaviour models. The reason lies in their simplicity and they are found to provide an acceptable practical approximation for the analysis of some problems in view of the scarce geotechnical information available. These models make it possible easily to identify zones where non-linear behaviours may be expected, namely in domains in which concentration of compression and tensions do occur. The use of linear elastic models doesn't always prove adequate, reason why continuous models that simulate non-linear behaviour of materials have been increasingly developed. Usually idealizations such as no-tensile strength, elastoplasticity, and shear failure along low-strength surfaces are assumed.

The models adopted for continuous media for underground structures of hydraulic schemes have followed multiple approaches, that have been published by many authors. Among the empirical models, special relevance should be given to the Hoek and Brown criterion (Hoek and Brown, 1982), that permits the evaluation of its parameters as a result of geomechanical classifications, namely the RMR and the Q systems. In what follows, two particular approaches are focused: the damage mechanics and the multilaminated models.

In the damage mechanics theory the damage introduced in the rock mass by the distributed discontinuities is characterized by a second-order symmetric tensor. With this concept, the deformation and fracturing behaviour of the rock mass can be treated in a framework of continuum mechanics. Numerical procedures using the finite elements method have already been developed (Resende and Martin, 1988), (Ohashi et al., 1986). Fig. 3.3 shows some results of an application of these models to the Inagawa No.2 powerhouse, located in Japan (Kawamoto et al., 1988). Deformation modes on the surfaces are computed for a damage analysis and a conventional finite element analysis. Some comparisons are made for the displacements of an extensometer at the final excavation stage.

Multilaminate models have also been applied to hydraulic underground openings, and simulate in a homogeneous way, using the finite element method, the presence of several joint sets. They assume that all joints in a set are parallel and continuous, and that the volume occupied

by the joint sets is small compared to the total volume of the rock mass. For each of the joint sets a rheological model is established, and the rheological model of the jointed rock mass consists of several units, representing each joint set, arranged in series. An additional unit represents the intact rock (Zienkiewicz and Pande, 1977), (Pande, 1985), (Erban, 1986). These models make use of a viscoplastic algorithm which allows time dependent calculations. Recently, constitutive laws for rock masses reinforced by passive or active rock bolts have been derived and incorporated in multilaminate models (Gerrard and Pande, 1985), considering the reinforcements, like the discontinuities, in a homogeneous way. As an example of application of multilaminate models, Fig. 3.4 shows some results obtained by Hönisch (1988) for the powerhouse cavern of the Siah Bishe pumped storage project, in Iran. Bedding planes and joint set J1 strike with 60° deviation from the cavern axis, and dip angles are 60° opposite to each other, and joint set J2 is vertical, striking parallel to the cavern axis. In the figure are shown the shear failure zones in the discontinuity planes, been clearly visible their asymmetry due to the different orientation and characteristics of the joint sets.

When a discontinuous medium approach is to be used, the discontinuity surface or surface groups are individualized and thus their mechanical characterization is required as well as that of the rock material. For the representation of the mechanical behaviour of discontinuity surfaces, many models have been established and many implementations in numerical procedures have been accomplished. Therefore, an analysis of these models is considered out of the scope of this work.

3.3 - Models for the hydromechanical behaviour

In underground hydraulic projects computational models are necessary not only for the analysis of the mechanical behaviour of the rock openings, but also for the analysis of the water flow. The presence of the water has to be taken into account because of the influence that it has on the definition of the actions, because of the changes that the creation of underground openings originates on the ground water conditions, and also because of the effect of the circulation of water under high pressure in the tunnels and shafts has on the stability of the rock mass. Since the state of stress variations influence the permeability of the

rock mass, namely of the joints, and the forces induced by the water flow provoke changes in the state of stress, a correct analysis of these two phenomena can only be done by models that simulate this hydromechanical interaction.

The first models that have been developed to simulate the hydromechanical behaviour of rock masses were two-dimensional finite element models (Brekke et al., 1972), (Witherspoon et al., 1974), and made use of two different models, one for the stress analysis and the other for the water flow, and of a hydromechanical coupling law. The interaction was simulated using an iterative procedure between the two models. This procedure is still used by many authors, but the models can now be much more sophisticated, like the one presented by Erban and Gell (1988) where a tridimensional multilaminate mechanical model is coupled with a homogeneous fluid flow model, like the one of Mendonça (1989), which couples two tridimensional models for continuous media, or like the one of Wei and Hudson (1990), which couples a non-linear tridimensional model for continuous and discontinuous media with a model for non-confined fluid flow in the permeable rock matrix and the joints.

The distinct element method has also been used for the study of coupled hydromechanical problems namely by Vargas (1982), and by Lemos (1987), that introduced in distinct element models the fluid flow along the fractures. Making use of the specificity of the dynamic relaxation technique used in their models, they were able to show the importance of transient flow in dynamic problems. Barton et al. (1987) also adapted a distinct element model to the study of excavation induced joint aperture variations. More recently, a distinct element model based on a static relaxation technique (Stewart, 1981), has also been adapted to include the water flow (Wei and Hudson, 1991).

Many other techniques for coupled hydromechanical analysis have been developed, mainly devoted to other kind of problems, like oil extraction, waste disposal and pollutant migration, and geothermal energy. They are having a quick development in these fields, due to the importance that nowadays is given to them.

Example of application of hydromechanical models to hydraulic tunnels are presented by Faihrurst and Lemos (1988) and by Wei and Hudson (1990). The latter is shown in Fig. 3.5,

which shows the flow around a tunnel calculated using the iterative finite element model above mentioned, for three cases: (1) no hydromechanical coupling; (2) coupling, but rock and joints are elastic; (3) coupling, and both rock and joints are considered perfect elasto-plastic materials. It can be seen that the permeability clearly changes with tunnel excavation, and that if elastic conditions are assumed permeability decreases significantly.

4 - PARAMETRIC STUDY OF THE STRUCTURAL BEHAVIOUR OF HYDROELECTRIC POWERHOUSES

4.1 - Nature of the study

Advances in knowledge in rock engineering have led to the construction of underground power plants involving cavities with spans of great size, and mention may be made of some of such plants with spans over 25m, namely Churchill Falls (Canada), Cahora Bassa (Mozambique), Leytaux (Switzerland), Alto Lindoso (Portugal), Waldeck II (Germany) and Imaichi (Japan). In nearly all the cavities, the shape is as a rule elongated, with ratios between the height and the span of more than unity.

The shape traditionally used for the powerhouse cavern has been that of a mushroom shaped cross section, with vertical walls and concrete arch ceiling supported on the rock mass or on pillars. It induces important stresses in the support zone of the arch, and for greater spans other hypotheses are considered, such as the egg shape (or horseshoe) with straight or curved walls, the ceiling as a rule being supported by rock bolts. In the case of the horseshoe, an appreciable reduction of the plasticized zones is achieved, these being restricted to small zones adjacent to the walls, as was the case in Waldeck II (Pahl and Glogglar, 1982) and Imaichi (Mizukoshi, 1982), which are the powerhouses with the largest spans. The powerhouse complex may consist of a single cavern, of larger dimensions, or several caverns, in which case it is necessary to analyze aspects relating to interference between cavities, dimensions of the rock pillars, forces concerned, mechanical characteristics of the rock mass and excavation sequences. The surge chamber, when it forms part of the powerhouse complex, as a rule considerably affects the field of deformation and stresses round the cavities.

A study was then carried out for analyzing the structural behaviour of the main cavities associated with the powerhouse complex, in order to try to quantify the influence of the principal parameters (Martins, 1985). This study made it possible, on one hand, to quantify in adimensional terms the sensitivity to a variation of the most significant parameters on the

stability of the works and, on the other hand, to assess the observed behaviour of the works, apart from providing better understanding of the phenomena involved in these underground structures. It was thus accepted as a prior hypothesis that the rock mass was a continuous and homogeneous medium, and the influence of the following parameters was considered (Fig.4.1):

i) Different shapes for the powerhouses - An analysis was made, in the case of a single cavern of mushroom and horseshoe shape, of its stability, making a variation of the actions due to release of the in-situ state of stress and corresponding main directions. In the case of multiple caverns (two caverns), the influence between cavities was studied, the thickness of the rock pillar and the in-situ state of stress being variable. Concomitantly, an attempt was made to quantify the effect of the tridimensionality of these structures, taking as variable the in-situ state of stress, for a single cavern.

ii) Mechanical characteristics of the rock mass - An anisotropic behaviour was considered for the rock mass for a transversely isotropic material, assuming various ratios of moduli of elasticity and various angles of anisotropy, and for non-linear behaviours the Coulomb criterion was assumed for different values of cohesion and internal angle of friction. In all situations a single mushroom-shaped cavern was considered.

iii) Sequences of construction - For the simulation, which involved stages of excavation and introduction of the support, for a single mushroom-shaped cavern, four stages were considered, with a continuous concrete support being introduced in the first stage.

Various plane models were established by boundary elements and finite elements, and a tridimensional model by boundary elements. Fig. 4.2 shows the models by boundary elements used.

4.2 - Analysis of the shapes

Table 4.1 shows the parameters used for studying the several shapes of the powerhouse. Fig. 4.3 shows displacements calculated in the walls for both shapes. Fig. 4.4 gives curves of

convergences between points, as a function of β , angle defining the orientation of the major principal initial stress. The convergences for the mushroom-shaped cavern as a rule are greater than for the horseshoe cavern, with the exception of the curves C_{25} and C_{34} .

As regards the single cavern, it is found that there are displacements preferentially directed to the interior, and in the case of hydrostaticity, the greatest values occur in the side walls, about half way up, while in the ceiling the values are about half of those. Consideration of a non-hydrostatic state of stress considerably affects the deformation field. When the initial state of stress is predominantly vertical, it is found that the points on the surface and in the interior show displacements to the interior of the cavity, the greatest values being in the ceiling and about 1.5 times greater than the hydrostatic state, while on the side walls the displacements are about 1/4 of the displacements in the ceiling. When, on the other hand, the in-situ state of stress is predominantly horizontal, there occur divergent displacements at points located in the zones of the ceiling and sill. For intermediate values of β , the field of displacements is strongly conditioned by the direction of the greatest main stress, with zones in which the displacements are nearly null or divergent, in the ceiling and the sill, in a direction approximately orthogonal to that of the greatest main stress.

As regards the stress field, the following is noted: i) concentration of stresses in the vicinity of the caverns and in particular at angular points; ii) non-hydrostatic states of stress imply a field of stress that is preferentially orientated according to the direction of the greatest principal stress; iii) for the case of $\beta=0^\circ$, it is noted that the stresses are greater by the walls and preferentially vertical when compared with those of the sill and the ceiling; iv) for $\beta=90^\circ$, the stresses are preferentially horizontal, being of small magnitude by the walls, unlike what occurs in the ceiling and sill. Fig. 4.5 represents tangential stresses along the boundaries of the cavities. In comparing the two shapes of cavities, there is seen to be a greater homogeneity of the stress field and displacements round the surfaces of excavation for the horseshoe shape.

Considering various hypotheses of strength of the rock mass (tensile strength of 0.1MPa; shear strength for four pairs of value of cohesion and angle of friction), the following is observed (Fig 4.6): i) in relation to tensile failures, the largest areas of failure occur for a

preferentially horizontal state of stress, on the side walls; failures in the support zone of the future mushroom-shaped arc; less thickness and extent in the areas of failure for the horseshoe shape; ii) as regards areas of shear failure, it is found that they are considerably less in the case of the hydrostatic state when compared with the other hypotheses; the areas of failure demonstrate the influence of the direction of the greatest initial principal stress; and it is seen that for $\beta=0^\circ$ the failures occur in the side walls and for $\beta=90^\circ$ basically in the ceiling and sill; the images of failure naturally reflect the direct influence of the strength characteristics.

4.3 - Multiple caverns

In the situation of multiple caverns, the existence of two openings was considered, both of them mushroom-shaped, with the larger cavity for the powerhouse having a width of 20m and a height of 35m, and the other cavity a width of 12m and a height of 14m, which refers to a secondary cavity. The dimensions adopted for the rock mass pillar between cavities were considered in accordance with the height of the greater cavity ($D/H=0.5; 1$ and ∞) and different states of stress were taken (Table 4.1).

As regards the field of displacements, and for the hypotheses assumed for the state of stress, it is observed that the introduction of a secondary cavity has little influence on the respective field of displacements in the vicinity of the principal cavity, whereas for the secondary cavity there is a deformational movement in the direction of the greater cavity that is accentuated as the distance decreases between them and for the predominantly horizontal state of stress. Fig. 4.7 gives a synthesis of the displacements at the boundaries of both cavities for the situations analyzed. These results clearly demonstrate the influence of parallel cavities, and it is to be noted that there is a significant disturbance in the field of displacements of the smaller cavity, even for $D/L=1$, this effect being accentuated as the distance decreases. If the initial state of stress is predominantly vertical, the effect is not so striking, unlike what happens with hydrostatic or predominantly horizontal states of stress, the last case being that which most strongly conditions this occurrence.

Assuming identical strength characteristics for the rock mass in the case of an isolated cavity. Fig. 4.8 shows the failure zones for a hydrostatic initial state of stress. There is seen to be a generalized increase in the areas of tensile failure next to the larger cavity, mainly for a distance of $0.5H$ between cavities and a predominantly horizontal state of stress, though this is less accentuated for $1.0H$. For the secondary cavity it is found, generally speaking, that there is a reduction in the tensile zones round it, with the exception of the case of a predominantly vertical state of stress in which there occurs an increase in the ceiling and sill. As regards zones of shear failure, there is a considerable increase in such areas, principally for materials with more precarious characteristics. The conclusions previously mentioned as regards the influence of the pillar on the tensile failure areas remain valid.

4.4 - Tridimensional equilibria

In the caverns tridimensional equilibria develop, and the aim was therefore to analyze their influence, bearing in mind the plane analyses made. An analysis was made of the influence of the distance of the cross section to the top of the cavern, as regards the evolution of the displacements and stresses, taking as variable the initial state of stress and for the hypotheses shown in Table 4.1. It was considered that the longitudinal direction was a principal direction, taking longitudinal stresses of 1, 3 and 9MPa.

In Fig. 4.9, for the hydrostatic case, are shown graphs of displacements and stresses along the surface marked in the figure for three transverse cross sections.

On comparing the graphs corresponding to the different states of stress, it is found that a horizontal initial state of stress causes higher horizontal displacements in the zone half way up the height of the caverns, with the displacements in the ceiling occurring towards the interior of the rock mass, unlike what takes place in the other situations. In the situation in which the main initial stresses do not coincide with the ordinate axes, it is noted that the direction of the displacements reflects the anisotropy of the in-situ state of stress. As the cross sections approach the top, the effect of the tridimensionality, which is represented by a

diminution of the displacements, acquires greater importance, until in the cross-section coinciding with the top its expression is clearly different.

The stresses are always compressive, with the exception of the vertical stress in the intermediate zone of the wall of the cavity for the horizontal initial state of stress higher than the vertical. The depth of the zone subject to tension is, however, relatively reduced. For this case, the greatest compressions occur in the ceiling of the cavern. They also have important values for a hydrostatic initial state of stress, diminishing markedly for a predominantly vertical initial state of stress. The variation in the stresses with the distance to the top of the cavern is less than noted for displacements.

With the aim of quantifying the influence of the longitudinal initial stress, Fig. 4.10 presents normal and longitudinal displacements for two points, according to the distance of the cross section to the top of the cavity. An analysis of the figure shows that: i) with the increase in the σ_{III} there is a decrease in the normal displacements and increases in longitudinal displacements; ii) for a hydrostatic state of stress in the transverse plane, the greatest displacements occur in the side walls and towards the interior, longitudinal displacements being noted towards the interior of the rock mass in the cross section of the top of the cavity for $\sigma_{III}=1\text{MPa}$; iii) for $\beta=0^\circ$, the greatest normal displacements occur in the ceiling and towards the interior, in the walls being divergent for $\sigma_{III}=9\text{MPa}$ and greater longitudinal displacements in the walls directed to the interior in the cross section of the top; iv) for a hydrostatic state of stress, the greatest normal displacements occur in the walls and to the interior of the cavity, in the ceiling being divergent, and the greatest longitudinal displacements occur in the walls, directed to the cavern, in the cross section of the top, except in the case $\sigma_{III}=1\text{MPa}$.

As regards stresses, Fig. 4.11 gives graphs of tangential stresses according to the distance to the top of the cavity. Among other conclusions, it is found that: i) as regards tangential stress, there is a decrease with σ_{III} , and the stress is compressive, except for points in the walls, for a case of $\beta=90^\circ$, where tensions occur; ii) as regards longitudinal tangential stresses, it is noted that there is an increase of σ_{II} with σ_{III} , an occurrence of high stresses in

the cross-sections near the top and also the appearance of tensile stresses in the walls for $\sigma_{III}=1\text{MPa}$, the greatest occurring in the ceiling.

An effort was also made to analyze the question associated with definition of the best orientation for the cavern, taking into account the influence of the state of stress. A vertical stress of 3MPa was adopted, with horizontal principal stresses of 1 and 3MPa, the axis of the cavern being orientated, in one case, according to $\sigma_{III}=1\text{MPa}$ and, in the other case, according to $\sigma_{III}=3\text{MPa}$. Fig. 4.12 shows displacements and tangential stresses calculated for the selected cases. It may be observed that the greatest normal displacements occur in the side wall for $\sigma_{III}=1\text{MPa}$, and are about 5 to 6 times greater than those corresponding to the other case, while in the ceiling the greatest displacements occur for $\sigma_{III}=3\text{MPa}$ and are about 1.5 times greater. As regards σ_{II} stresses, the greatest stresses in the cross section occur in the ceiling for $\sigma_{III}=1\text{MPa}$ and are about 10 times greater than those corresponding to the other case, while in the walls they occur for $\sigma_{III}=3\text{MPa}$ and are about 1.5 times greater. For σ_{II} , the greatest stresses occur for $\sigma_{III}=3\text{MPa}$ and in the wall are about 11 times greater and two times in the ceiling. It can thus be concluded that the best orientation to be chosen for the cavern is that in which the axis coincides with the greatest horizontal stress.

5 - ANALYSIS OF AN UNDERGROUND POWERHOUSE IN MOZAMBIQUE

5.1 - General description

To analyze the results obtained from an experimental model and from the monitoring displacements, numerical models were developed for a large underground powerhouse located in Mozambique (Silveira et al., 1974), (Sousa, 1983). Fig. 5.1 gives the general plan of the powerhouse and hydraulic circuit. In Fig. 1.2 a schematic perspective of the powerhouse, surge chamber and annexes is shown. The underground openings are situated at a depth that, in the case of the powerhouse, varies from about 130m at one of the ends to about 230m at the other end. The dimensional characteristics of this cavern are 216.7m in length, 28.9m in width and 24 and 57m in minimum and maximum height. The two surge chambers are located in parallel to the powerhouse and the dimensional characteristics of the cavern are as follows: 82.5 and 87.7m in length for the north and the south chambers; 19.0m in width; 72.0 and 70.3m in height for the north and the south chambers, respectively.

The rock mass consists of granitic gneisses with several dyke intrusions. The existence of lamprophyric dykes becomes important in the behaviour of such underground structures. Three principal discontinuity sets were detected and geological accidents like faults are scarce.

The geotechnical structure of the site was analyzed with particular attention by LNEC. The in situ tests performed essentially consisted in the determination of the deformability of the rock mass and of the shear strength of the discontinuities and of the rock. The initial stresses were also determined in tests carried out using the small flat jack and the stress tensor gauge methods developed at LNEC. Some significant results are summarized in Table 5.1.

5.2 - Finite element models

For the purpose of the stability analysis of the underground openings of the power house, a 3-D finite element idealization was selected, considering a block that contains part of the

cavern corresponding to the powerhouse, and half of the south surge chamber and respective diffuser. In Fig. 5.2 is represented the block adopted for the calculation model. Because the power house is situated at a great depth, it can be assumed that the presence of the ground surface has a negligible effect on the boundaries of the excavation. For this reason and by introducing some simplifications, the boundaries of the model were assumed fixed with reference to normal displacements.

Following the continuous approach, the rock mass was supposed to be linearly elastic and isotropic, described by a Young's modulus equal to 70GPa and a Poisson's ratio equal to 0.2. The initial state of stress was supposed equal to a vertical stress $\sigma_v=15\text{MPa}$, a horizontal stress $\sigma_h=10\text{MPa}$ and a shear stress $\tau_{vh}=0\text{MPa}$. The concrete supports used in the principal caverns were assumed to present a Young's modulus equal to 40GPa and a Poisson's ratio equal to 0.2, taking into account results of tests.

To study the behaviour of the openings, two hypotheses were made: i) a one-stage excavation sequence deactivating finite elements, corresponding to the openings and to the concrete supports; ii) a four-stage construction excavation sequence for a section considered in the Observation Plan (S_1), (Fig 5.3).

Finally a plane finite element model containing a cross section through section S_1 was built for the purpose of comparing results with the 3-D idealization, and for analyzing more correctly the influence of other openings, like the transformer room, penstocks and tailrace tunnels (Fig. 5.4).

5.3 - Laboratory model

LNEC conducted a series of tests in a 3-D experimental model trying to know what stresses would set up in the boundaries of the powerhouse and of the surge chambers (Silveira et al., 1974). The model used had the form of a cube with 1.75m edge, inside which were reproduced the underground openings (Fig. 5.5).

The experimental model was obtained by assembling various blocks made of a material consisting of a mixture of plaster of Paris, diatomite and water. The tests carried out for measuring the strains in the caverns of the powerhouse and surge chambers consisted of applying an isolated compression according to each of three main directions (vertical pressure; lateral pressure according to the direction of the longitudinal axis of the powerhouse; and lateral pressure applied according to the direction perpendicular to the longitudinal axis). The distribution of stresses in the prototype for any ratio between the vertical pressure and the lateral pressure considered as the initial state of stress in the rock mass were determined by using the method of superposition of the effects and the laws of elastic similarity.

Considering a vertical pressure of 15MPa and a lateral pressure, equal in all directions, of 10MPa, Fig. 5.6 shows principal stresses in the powerhouse cavern. The stress field is practically compressive, the highest compressions recorded in the ceiling arch was 55MPa and the highest compression in the walls was 31MPa, in the lower part of the downstream wall by Group 5. As regards tensions, approximately vertical stresses of about 3 and 2MPa are observed in the lower part of the zone of the groups, next to Group 5 and 1, respectively, and horizontal stresses of about 2 and 1MPa in the zone of Group 5 (Silveira et al., 1974).

5.4 - Comparison between experimental, numerical and observed values

The laboratory results show that in the main cavern the stress field is practically compressive since the few tensile stresses recorded are of little importance. These results were compared with those obtained in the first hypothesis used in the 3-D finite element model.

In Fig. 5.7 are shown the principal stresses in the powerhouse cavern, whereas Fig. 5.8 shows the principal stresses in the walls of the south surge chamber. There is a reasonable agreement between these two kinds of values, taking into account that the finite element mesh was not refined enough for computation difficulties (Sousa, 1983). Nevertheless there is a better agreement in the walls.

The results in terms of displacements of the 2-D finite element model are shown in Fig. 5.9 calculated for the section mentioned before. For simplicity a one-stage excavation was adopted. One can clearly see the displacements towards the surge chamber, which shows the large influence of this cavern on the overall displacement field.

In this plane model a non-linear behaviour was considered, characterized by the Coulomb criterion, using a cohesion of 0.3MPa and an angle of friction of 41° according to the values referred to in Table 5.1. As Fig. 5.10 shows, the failure zones around the cavities are very important, but it is worth mentioning that the presence of reinforcements produces a considerable reduction in the extent of the plasticity zones.

The behaviour of the underground structures was analyzed by measurements performed during and after the opening of the caverns (LNEC, 1975). Three sections were selected and the monitored displacements were determined by convergence measurements and multi-stage extensometers MPBX (Fig 5.11).

Fig. 5.12 shows displacements observed and predicted by the numerical models. As concluding remarks it can be said that there is a reasonable agreement between the numerical and the observed results. At section AA in the powerhouse cavern a divergence of 1.4mm was measured at the end of the excavation, while the 3-D calculation gave a value of 3.6mm. On the other hand the 2-D calculation gave a contradictory result, with a convergence in the same section due to the fact that the excavation was considered in one stage.

6 - ANALYSIS OF THE BEHAVIOUR OF THE ALTO LINDOSO UNDERGROUND POWER SCHEME

6.1 - Description of works

The Alto Lindoso hydroelectric power scheme essentially consists of an arch dam, an underground powerhouse complex and an underground hydraulic circuit (Fig. 1.1).

The underground powerhouse is located, in plan, about 70m of the dam left abutment with the main floor at the depth of 340m. The overall size of the cavern is as follows: 20.85m wide between walls, 20.3m high between the roof and the main floor, and 91.0m long. It is equipped with two generating units, each one composed of a 317MW Francis turbine and of a 350MVA generator. The maximum and minimum effective heads are 280.8 and 218.6m. The powerhouse is connected to the control building by a busbar shaft, 6.8m in diameter and 341m in high, and its main access tunnel is 1780m long.

The spherical valve chamber is part of the underground powerhouse complex. The main dimensions of the chamber is as follows: 9.0m in width, 60.0m in length and 20.0m in height. Downstream of the powerhouse is located the butterfly valve chamber which has the following dimensions: 9.8m in width, 65m in length and about 28m in maximum height.

The hydraulic circuit comprises two independent high pressure circuits located in the left bank at small distance from the dam, and a low pressure circuit (tailrace tunnel), a surge chamber, water intakes and outlet (Fig. 6.1). A reservoir is created by the Touvedo hollow gravity dam located some kilometers downstream of the hydraulic circuit outlet, which is intended to modulate the high flows turbined by the Alto Lindoso scheme.

The surge chamber is an underground structure with the shape of a large cylindrical shaft, with a diameter of 23m, and a height of 65m. A concrete cylindrical arch closes the chamber at the top. It is throttled by its base and has associates a 380m long feeding chamber, 9.5m in diameter, and a 300m long expansion chamber, about 12m in diameter.

Other works worth mentioning are the provisional diversion tunnel for the river flows, which made it possible to keep the old power station in operation, and two flood discharge spillways located underground in the right bank.

6.2 - Rock mass characterization

In the design stage a detailed geologic and geomechanical study was conducted, based on surface observation, mechanical exploration, geophysical surveys, stress measurements in boreholes, deformability measurements with conventional systems and with LNEC's dilatometer, shear tests and other laboratory tests (Neiva et al., 1983). The rock consists of a medium to coarse grained granite, sound in general.

Though boreholes had not reached depths exceeding about 100m, they made it possible to take decisions as to the options initially put forward in the preliminary design stage. However, it was foreseen that a more detailed geotechnical characterization should be performed in the vicinity of the main underground structures during the construction.

The geotechnical study of the rock mass comprised in situ tests aiming at the quantification of the in-situ state of stress and the deformability of the rock mass, the characterization of the discontinuity sets and laboratory tests that comprised unconfined compression and joint shear tests (Sousa et al., 1988). In-situ state of stress measurements will be analyzed in section 6.3.

The in situ tests that were made to determine the deformability were performed using the LFJ (Large Flat Jack) method developed at LNEC. Tests were performed near the powerhouse gallery (Fig. 6.2). In one of the tests the slots were made horizontal in the wall of the test chamber and in the other they were vertical, with one or two flat jacks placed one next to the other. The stress-strain diagrams obtained showed a nearly linear elastic behaviour of the rock mass almost in all cases. The mean values resulting from the LFJ tests, in terms of deformability modulus, for vertical and horizontal directions, are respectively 90 and 58GPa.

As regards the evaluation of the dynamic characteristics of the rock mass of the powerhouse cavern, mention should be made also of geophysical exploration tests by micro-seismic refraction, by using small length seismic bases. The profiles obtained made it possible to determine velocities of propagation of the longitudinal wave (between 5150 and 6250 m/sec), from which were derived dynamic elasticity moduli (74 to 78GPa). Similarly to the LFJ results, these results gave evidence of rock mass with excellent mechanical properties.

The discontinuity data collection process was carried out on the walls of an exploratory gallery open along the axis of the powerhouse cavern, using a scanline sampling technique. This technique involves the setting up of a measuring tape on the rock surface and recording the characteristics of all the discontinuities that intersect the tape.

A statistical analysis of the discontinuity orientation data was performed, in order to study the degree of clustering of the several concentration areas found with polar projection and to define a mean orientation for each set. In Fig. 6.3 are shown the mean orientations and the limits of variation of each of the five discontinuities sets that were identified.

Simultaneously with the characterization of the joint sets, an analysis was made of the blocks that may form in the walls and top of the exploration gallery that crossed the powerhouse (Lamas, 1989). A graphical method with inclined stereographic projections was used, which was proposed by Priest (1985), for the analysis of the stability of tetrahedral blocks. The 5 joint sets may combine in 10 different ways, forming equal number of types of blocks. The stability conditions of each block under gravitational forces depend on the joints forming it, on the orientation of the exposed rock face, and were classified in the following types:

- N - stable block that cannot move;
- D_i - if unstable, block can slide along a joint of set i;
- D_{ij} - if unstable, block can slide along the intersection line of two joints of sets i and j;
- V - unstable block, falling in vertical if supports are not provided.

Table 6.1 indicates what blocks can be formed, the type of the stability conditions, and for the blocks that can slide, the angle of the direction of the potential movement with the horizontal.

The laboratory tests comprised unconfined compression and joint shear tests. A stiff testing machine, electronically controlled, was used for the unconfined compression tests, making it possible to study the deformational behaviour of the rock up to failure. The evolution of the transverse and axial deformations up to yield generally followed a pattern that reveals considerable variation of the Poisson's ratio contrasting with the stability of the modulus of elasticity. The values of the moduli of elasticity and ultimate strengths were not markedly scattered, and had mean values of 60GPa and 140MPa respectively.

For the joint shear tests, use was made of a conventional shear box with samples of the main joint sets. Roughness profiles were also recorded in order to characterize the tested joints as well as possible. Table 6.2 presents mean, maximum and minimum values of the apparent cohesion with and without dilatancy (c and c'), the tangent of the friction angle with and without dilatancy ($tg\phi$ and $tg\phi'$), normal and shear stiffness (KN and KT) and the dilatancy angle (i), obtained in the first group of joints tested.

During construction, it was decided to carry out complementary tests in the zone of the powerhouse ceiling, on rock specimens and joints. Thus some boreholes were driven in a pilot gallery near the powerhouse. Measurement of the joint orientations were done, and more laboratory shear tests were performed.

From the tests results and the site investigations, the parameters for the Bieniawski geomechanical classification were determined. Unconfined compressive strengths presented a fairly small dispersion; a mean stress of 134MPa was obtained, close to that obtained in earlier tests (141MPa). The RQD index presented a mean value of 93; joint spacing ranged from 0.2 to 0.6m; the characteristics of the discontinuities nearly always corresponded to slightly rough surfaces, the opening width being less than 1mm, and small degree of surface weathering; as regards water pressure, discontinuities are dry in general. The final RMR index obtained was equal to 77, and thus the rock mass fits in class II, i.e. good quality rock

mass, almost in transition to class I (Bieniawski, 1984). For the sampled zone of the powerhouse, the modulus of deformability of the rock mass was estimated at 54GPa, using the Bieniawski correlation, valid for RMR > 50. The cohesion and the angle of friction of the rock mass vary respectively between 0.2 and 0.3MPa and 40 and 45°.

Using Hoek and Brown strength criteria, the rock mass was given the following strength envelope (Hoek and Brown, 1982):

$$\sigma_1 = \sigma_3 + \sqrt{8.5\sigma_c\sigma_3 + 0.062\sigma_c} \quad (6.1)$$

For the rock mass surrounding the surge chamber, the Bieniawski geomechanical classification was also applied. The final RMR index obtained was 72, the rock mass fitting again into class II, good quality rock mass. The modulus of deformability estimated was 44GPa, using the Bieniawski correlation.

6.3 - Quantification of the in-situ state of stress

The geotechnical study of the rock mass included a test programme aiming at quantifying the in-situ state of stress. Tests were made using the SFJ (Small Flat Jack) and the STT (Stress Tensor Tube) methods, both based on stress relief, the former by opening of slots and the latter by overcoring in the zone of measurements. Before construction, SFJ and STT tests were carried out in a test chamber and in the walls of a gallery, whose location is shown in Fig. 6.2. During construction several SFJ tests were performed in slots located in the walls of the powerhouse cavern and in the bottom of the surge chamber (LNEC, 1991). In Table 6.3 are summed up the results obtained with the former tests (Sousa et al., 1988).

The stresses were measured at small depths and do not correspond in general to those existing at the excavation surfaces. There is a dispersion of the test results, mainly of those of the STT method, which derives from the difficulties of test technique and from the interpretation model.

In order to ascertain the state of stress inside the rock mass and on the excavation surfaces, a numerical methodology was defined for the resolution of the inverse problem, making use of the results obtained and of a 3-D boundary element model. The model was prepared for the zone of the gallery around the test chamber. The boundary element model makes use of a direct formulation and uses curved sided boundary elements with eight nodal point and second order interpolation functions, identical for displacements and stresses (Lamas, 1984). For the region of the test chamber, the model was prepared considering a zone of influence of about 3 times the width of the gallery (equal to 7m) upstream and downstream of the chamber. The mesh used is shown in Fig. 6.4. The rock mass was assumed to be linear, elastic, homogeneous and isotropic.

The methodology proposed consists of determining a matrix A_{ij} for the structural model, which represents the components of the state of stress at the different test points for the unitary states of stress acting in the rock mass. Representing by S_j , the components of the initial state of stress, supposed uniform in the whole domain, the following expression is obtained:

$$A_{ij}S_j = M_i \quad (6.2)$$

$$(i = 1, 2, \dots, N)$$

$$(j = 1, 2, \dots, 6)$$

where the vector M_i represents the components of the state of stress obtained by tests at various points and N total number of components of the state of stress measured by tests.

The system of equations (6.2) presents a highly redundant number of equations being the most probable in situ state of stress calculated using the least-square method

$$X_{ij}S_j = U_i \quad (6.3)$$

$$(i, j = 1, 2, \dots, 6)$$

with

$$U_i = A_{ik}M_k \quad (k = 1, 2, \dots, N)$$

The coefficients A_{ij} ($j = 1, 2, \dots, 58$) were obtained for the test locations, for the different unitary actions, by means of the tridimensional boundary element model. Fig. 6.5 shows results in terms of displacements at the boundaries, for the actions due to relief of the unitary states of stress in the direction of two coordinate axes and of a hydrostatic unitary state of stress for two cross-sections. Then by means of equations (6.2) and (6.3), the most probable initial state of stress was calculated and the error between the measured and the calculated stresses:

$$\epsilon_i = M_i - A_{ij} S_j \quad (6.4)$$

$$(i = 1, 2, \dots, N)$$

$$(j = 1, 2, \dots, 6)$$

The error or residual sum of squares is given by

$$Q = \sum \epsilon_i^2 - U_j S_j \quad (6.5)$$

and the value $Q/(\epsilon_i^2)$ is a measure of the scattering of the stress measurements.

Using this error analysis, the values measured by SFJ₃ and ST₁₁ tests were excluded, and then the initial state of stress was obtained (Table 6.4). The relation between average horizontal and vertical stresses is about 1.5.

6.4 - Structural behaviour of the powerhouse complex

The continuous safety evaluation intended for the detection of any incidents in the behaviour of the underground structures during construction, was based on comparison of the results obtained by observation with the values predicted from numerical solutions, taking into account experience with similar works (LNEC, 1991).

Some numerical models were developed for the underground powerhouse complex. A finite element plane model was established for the analysis of the different construction sequences; more simplified boundary element models were adopted for a secondary section; a finite

element self-adaptive model was also used to check the results already obtained with other models, particularly the boundary element models (Sousa et al., 1991).

The plane finite element model covered the powerhouse complex and included the surge chamber in an approximate way. It was built to simulate the different excavation sequences. Eight zones with different material properties are used to simulate the rock mass and concrete, as well as the equivalent materials adopted for simulating the opening of some tunnels and shafts. Fig. 6.6 shows the excavation sequence adopted in the numerical model for a section through power unit 2, considering 10 phases, which follows the construction process as close as possible. Fig. 6.7 shows a detail of the finite element mesh in the zone of the powerhouse.

In the structural idealization, a continuous medium was assumed for the different materials. First, a linear elastic behaviour was assumed, with modulus of elasticity of 50 and 21GPa, respectively for the rock mass and the concrete, and a Poisson's ratio of 0.2 was considered. The elastic characteristics of the rock mass were obtained from the RMR system and all the tests performed. For the concrete, the values were obtained from tests performed in samples of the arch, following the empirical approach of Bazant and Panula (1978, 1979). Afterwards, non-linear behaviour was considered for the rock mass, following the Hoek and Brown strength criterion defined by equation 6.1 ($m=8,5$ and $s=0,062$) and the Coulomb criterion, using a cohesion of 0.2MPa and an angle of friction of 40° . The in-situ state of stress was assumed to be homogeneous and hydrostatic, with a value of 10MPa, in this phase of the study. This value corresponds approximately to the vertical stress estimated from the in-situ stress measurements.

Besides the actions associated with stress release in the different construction sequences, the following were considered: i) in phase 4, weight of concrete of the powerhouse ceiling arch; ii) in phase 5, 0.5MN anchoring forces inclined at 10% and 1.5m apart; iii) in phase 10, 0.165MN/m forces applied on the two crest beams.

For the last phase of excavation of the powerhouse complex (phase 8), Fig.s 6.8 and 6.9 present vectors of displacements and principal stresses around the main cavities, for the linear

elastic calculation. In Fig. 6.10 displacements in the boundaries of the powerhouse for the different phases are shown. It can be clearly see the large influence of the opening of the surge chamber on the displacement field. This is due to the approximation considered in this plane model, that intends to represent a limit situation. The application of the non-linear Hoek and Brown criterion doesn't produce any failures in the rock mass. On the other hand the application of the Coulomb criterion, that considers adverse parameters, gives important failure zones around all the cavities as shown in Fig. 6.11.

An observation plan was established for the underground powerhouse complex, including the monitoring of the structural effects during the excavation process. Several types of measurements were made (LNEC, 1991): convergences in several sections using a special convergence-meter developed at LNEC; displacements inside the rock mass using rod-extensometers; strains in the concrete arch ceiling with Carlson extensometers; and movements of some relevant discontinuities. Three important sections (S1, S2 and S3) of the powerhouse were instrumented, as shown in Fig. 6.12. Each section has 12 rod-extensometers and a large number of convergence measurements were taken, two of which in the powerhouse cavern are indicated in the figure (for section S2).

Fig. 6.13 shows the convergences observed and calculated for two pairs of points (S2 and S2.1), for all the excavation steps considered. The maximum calculated value is 17mm for section S2.1, after the complete excavation of the powerhouse, and before deactivating the elements corresponding to the surge chamber. Considering that the convergence measurements began when the calculated displacement had already started, as illustrated in the figure, the agreement between the calculated and the observed values is good, which indicates a good behaviour of the cavern. For step 9 the model gives a decrease in the convergences, that is due to the excavation of the surge chamber, which was simulated in a very severe way. The observed values indicate the almost negligible influence of the surge chamber on the structural behaviour of the powerhouse complex.

Boundary element models applied to the monitored section S_3 of the powerhouse cavern were also developed (Castro, 1989). They are plane equilibrium models and use a direct formulation applicable to isotropic materials with linear elastic behaviour, where

heterogeneities can be simulated and body forces referring to dead weight can be considered. Use is made of curved boundary elements with three nodal points and second order interpolation functions (Frazillio and Martins, 1984).

For the structural idealizations adopted, plane strain conditions were considered, with the following elastic characteristics (modulus of elasticity and Poisson's ratio) and unit weight of the rock mass: $E_m = 40$ and 20GPa ; $\nu_m = 0.2$; and $\gamma_m = 27\text{KN/m}^3$. For the concrete, the following parameters were adopted: $E_c = 30\text{GPa}$; $\nu_c = 0.2$; and $\gamma_c = 25\text{KN/m}^3$. The hypotheses for the modulus of elasticity of the rock mass correspond to the values adopted in a preliminary design phase (EDP, 1983), being the former value more approximate to those obtained by the in situ tests. As in the previous finite element model, a hydrostatic state of stress of 10MPa was assumed.

Two boundary element models were set up, one for multiple unsupported cavities, the other considering concrete arches for the powerhouse cavity and the butterfly valve chamber (Fig. 6.14). Figs 6.15 and 6.16 present displacements and principal stresses for the calculations that include concrete supports. Fields of displacements are found to be only slightly influenced by the existence of the two other cavities. Introduction of concrete supports does not markedly affect the deformational movement towards the inside of the cavities. The order of magnitude of the displacements obtained in the boundary of the powerhouse cavern is about 5mm at mid-arch and 5.5mm at mid-floor. Fig. 6.17 indicates the tangential stresses along the walls of the powerhouse cavern, with and without concrete support.

6.5 - Structural behaviour of the surge chamber

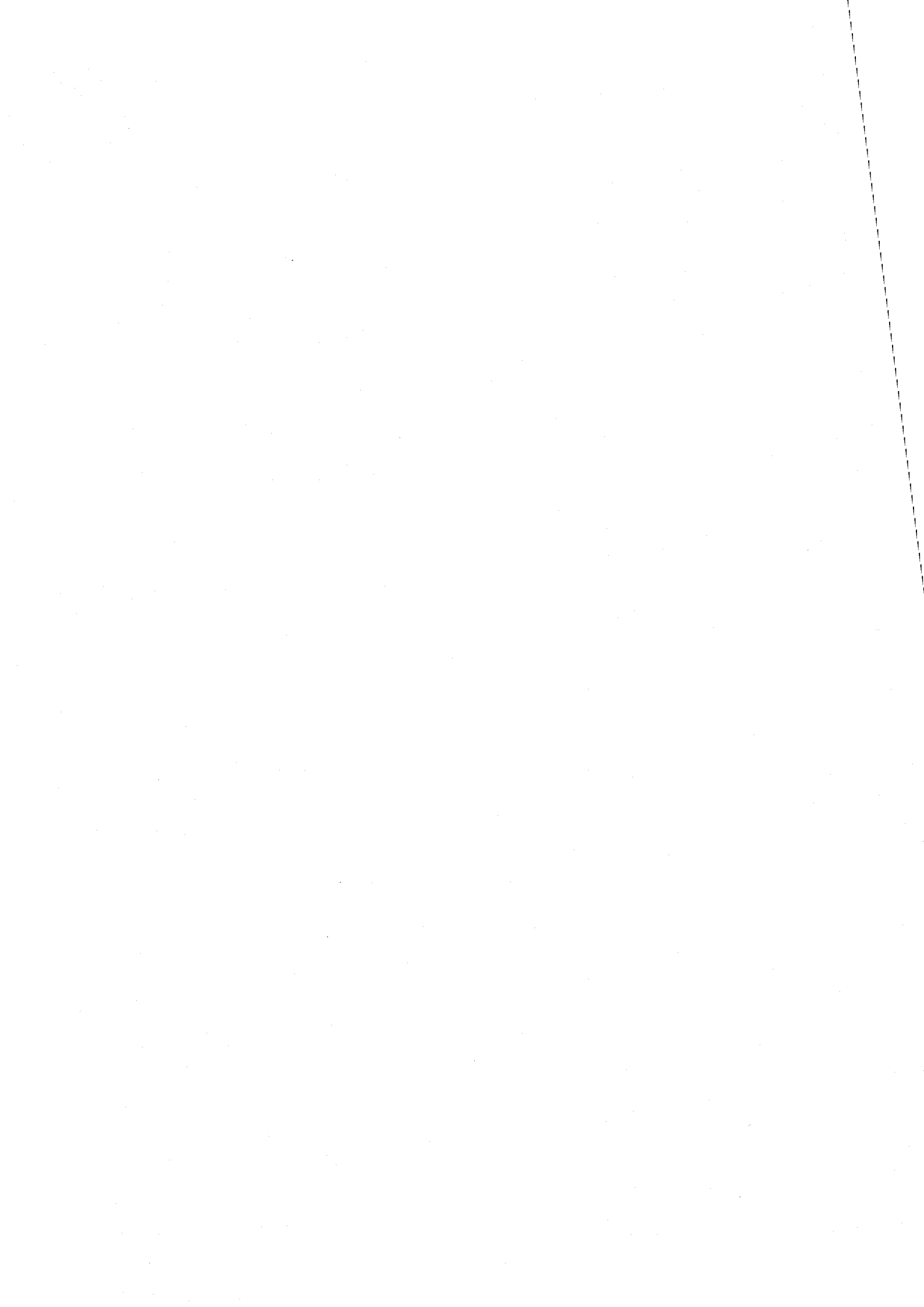
For the surge chamber, only 3-D boundary element models were applied at the moment, which simulated several excavation depths and considered several calculation hypotheses regarding the in-situ state of stress. The computational system use is the same mentioned in section 6.3.

The numerical models used covered a part of the expansion surge chamber and the surge shaft for three depths; for simplicity, the feeding surge chamber was not considered. The boundary element meshes comprise the same number of nodal points and of boundary elements. Fig. 6.18. shows in perspective the last mesh (phase 3), use for the whole shaft.

For calculation purposes, a homogeneous, linear elastic rock mass was assumed, characterized by a modulus of elasticity of 50GPa and a Poisson's ratio of 0.2. Nine distinct actions involving stress release were considered. The hypothesis C_1 corresponds to a hydrostatic initial state of stress equal to 10MPa, such as adopted for the powerhouse. C_2 corresponds to the state of stress estimated from STT and SFJ tests (section 6.3). Calculations C_3 and C_4 correspond to a horizontal axisymmetric state of stress of 10MPa and a lower (2/3) and a higher (3/2) vertical stress. C_5 , C_6 and C_7 are uniaxial states of stress of 10MPa, following the three coordinate axes. Calculations C_8 and C_9 are similar to C_3 and C_4 , respectively; C_8 presents double vertical stress whereas the vertical stress in C_9 is half the horizontal stress.

In Fig.s 6.19 and 6.20 are presented the displacements and the principal stresses in a vertical plane containing the expansion chamber for phase 3, for hypotheses C_1 and C_2 .

According to the observation plan, several measurements were performed in the surge chamber during the excavation process: convergences in several horizontal sections; displacements inside the rock mass using rod-extensometers; and strains in the concrete arch ceiling with Carlson extensometers. Fig. 6.21 shows the monitoring scheme used for the rod-extensometers. Fig. 6.22 shows the convergence measurements at section A located at the top of the shaft. The maximum value obtained is of the same order of the calculated one.



7 - APPLICATION TO THE CASTELO DO BODE TUNNEL

7.1 - General description of the tunnel

The new water supply system to the Lisbon area starts at the Castelo do Bode reservoir, and includes a 125 km long conduit. The Castelo do Bode tunnel is part of this system and is located immediately after the reservoir. It has a 3 meter diameter circular section, a length of 1088m, and allows a maximum flow of $10^6\text{m}^3/\text{day}$ (EPAL, 1988). The support is a reinforced concrete lining with the exception of the last 150m, where a steel lining exists. Fig. 1.6 shows the location of the tunnel in a horizontal and a vertical section.

The tunnel was excavated in a pre-cambrian metamorphic rock mass, formed by gneisses and migmatites very similar to those found in the dam foundation. The orientation of the gneiss foliation is nearly constant along the tunnel, and the main discontinuity set occurs with the same orientation as the foliation (Oliveira et al., 1983).

The geotechnical study of the rock mass had two different phases (LNEC, 1982 and 1986): i) before the tunnel construction, a geotechnical survey and a testing programme were carried out, which consisted in the execution of dilatometer tests for the assessment of the rock mass deformability and of special loading tests for the determination of the in situ state of stress, as well as on the drilling of integral samples for the study of the discontinuity pattern; ii) during the excavation, the characterization of the rock mass along the tunnel was initiated, in situ stress measurements as well as strength and deformability laboratory tests were performed, and microseismic refraction tests were carried out in some sections in order to determine the thickness of the rock mass damaged by the blasting. During the drilling of the boreholes for the rod-extensometers, permeability tests were also conducted at different depths by the drilling company (Tecnasol, 1989).

The results of the in situ stress measurements by special dilatometer tests, performed during the preliminary studies, led to relations between horizontal and vertical stresses ranging from 0.2 to 0.8. However, one should notice that these tests were made at small depths, far from

reaching the depth of the tunnel. The in situ stress measurements performed during the excavation using the small flat jack (SFJ) and overcoring (STT) techniques were carried out in two test chambers inside the tunnel (Sousa et al., 1986). Using the same methodology as for the Alto Lindoso underground power scheme, a 3-D boundary element model was built for the zone of tunnel around the first test chamber, and the most probable initial state of stress in the rock mass was obtained. The value calculated for the vertical stress is close to the weight of the overlying material, while the horizontal stress is a fraction of the vertical stress.

7.2. Observation of the tunnel

The observation of the tunnel during the construction consisted on the measurement of convergences in tunnel sections, between the walls and the roof. Subsequently, a Plan of Observation concentrating on the period of time before the exploration of the tunnel was established, since afterwards the direct observation would only be possible for short periods. The observations proposed in this plan concern the control of the structural effects in the concrete support and the rock mass, of the actions and of the properties of the materials.

The quantification of the structural effects focused on the observation of the displacements, strains and stresses in the support and the rock mass, induced by the most relevant actions. In the concrete lining, it was only possible to monitor the strains and stresses in one section of the tunnel, located at 156m from the tunnel portal, as shown in the vertical section of Fig. 7.1. This section has four active Carlson extensometers, and two dummy ones for corrections (Fig. 7.2). The observation of the vertical displacements in the rock mass included the positioning of two vertical triple borehole rod-extensometers, with fixed points near the tunnel, in an intermediary zone and near the surface (Fig. 7.1). Surface displacements were measured by means of a precision trigonometric levelling.

Particular importance was given to the verification of the safety and serviceability of this underground structure, because it is part of an important water supply system and is located

near a large dam. Having this in mind, a loading test with a slow filling up of the tunnel took place in August 1986, followed by others with fast filling up.

During the tests, a trigonometric levelling of the adjacent slopes between the boreholes SCB₁ and SCB₁₆ was performed (Fig. 7.1). The results obtained have small variations, but show an evolution of the vertical displacements in accordance with the internal pressure in the tunnel. The structural effects in the tunnel were evaluated only by means of the Carlson extensometers in the concrete support, because the borehole rod-extensometers were placed only afterwards. In Fig. 7.2 are presented the effects produced by the loading-unloading test, namely the strains in the support and the pressure at the tunnel portal. In Fig. 7.1 are presented the water levels at the end of the loading and of the unloading stages, as well as, in an amplified scale, the intermediate levels. It is possible to conclude that the water table near the tunnel changes considerably with the internal pressure, but is always far from reaching the medium level before the tunnel excavation.

7.3. Numerical and analytical solutions for the simulation of the loading test

The most important actions are a consequence of the presence of the water, mainly the internal and the external water pressures. Another action is temperature variation caused by the circulation of the water coming from the surface, which may have important consequences on the stresses in the lining, mainly when the internal pressure is small. The temperature of the water at the surface of the reservoir has important variations between 10 and 25°C, which is confirmed by the observations done with the Carlson extensometers. The release of the state of stress is also an important action, but for the analyses presented here it was not relevant.

The mechanical characteristics adopted for the rock mass in the zone of the instrumented section took into account the available geotechnical information, that resulted from the Bieniawsky geomechanical classification and from the dilatometer and SFJ tests. An RMR index of 63 was determined, which corresponds to a class II rock mass; and a Young's modulus of 26GPa was calculated. From the dilatometer tests lower values had been obtained:

a mean value of 12GPa in borehole SCB₁₄, but not reaching the depth of the tunnel, and a mean value of 18GPa in borehole SCB₁₅, with 20GPa at the depth of the tunnel. For the rock in contact with the lining a lower Young's modulus of 13GPa was assumed, which corresponds to the indications given by the microseismic tests and to the average values given by the SFJ tests performed in the tunnel walls.

The calculation of the effective Young's modulus of the concrete lining took into account the effect of creep of the concrete, using the empirical formulation of Bazant and Panula (1978, 1979). The value obtained for a concrete with the age of 1 year was 22GPa.

The stresses due to the temperature variation inside the tunnel were calculated assuming the following values for the thermal and thermo-mechanical characteristics of the concrete and rock: i) thermal conductivity of the concrete, $K_b = 2.4 \text{ W/mK}$; ii) relation between the thermal conductivities of the rock and the concrete, $K_r/K_b = 1$; iii) linear dilation coefficient of the concrete, $\alpha_b = 10.8 \times 10^{-6} \text{ } ^\circ\text{C}^{-1}$; and iv) relation between the linear dilation coefficient of the rock and the concrete, $\alpha_r/\alpha_b = 1/2$.

The coefficient of permeability of the concrete was taken from the literature for good massive concrete, and is $k_b = 5 \times 10^{-10} \text{ m/s}$. The value $k_r = 2 \times 10^{-7} \text{ m/s}$ used for the gneisses is the average from the permeability tests performed in the closest borehole, and is in agreement with values of literature for this type of rock. For the grouted zone around the tunnel a coefficient of permeability ten times lower than for the rock was taken, $k_c = 2 \times 10^{-8} \text{ m/s}$.

The calculations of the stresses in the support were performed on the assumption of two different possibilities:

a) Impervious support

Analytical solutions for thick walled rings were adopted for the external pressure, considering one ring of rock effectively linked to the concrete due to the consolidation grouting, (Martins, 1985). In the present case a 0.75m thick inner ring was considered (0.35m of the concrete lining plus 0.40m of grouted rock).

For the analysis of the structural effects on the support and surrounding rock induced by the release of the state of stress and by the internal pressure, a finite element model was built. The concrete and the rock mass were considered as a continuous, homogeneous and isotropic medium with linear elastic behaviour. In Fig. 7.3 is shown the conceptual model which was adopted as well as the parameters that were used. Two different states of stress were considered, having in mind the values obtained in the tests. A two step construction sequence was adopted, where the first one corresponds to the release of the state of stress in the rock mass, and the second to placing the lining and applying the internal pressure.

For the consideration of the effect of temperature variations due to the circulation of water on the structural behaviour of the tunnel, the mathematical expressions developed by Lelli (1952) were adopted. For the calculation of the temperatures in the lining and the rock, a variation of temperature T_0 in the support for the case of steady flow was assumed, and the corresponding stress changes due to the temperature variations were calculated.

This model for impervious support was presented in detail in a report of LNEC (1990), and is here named model A.

b) Pervious support

Schleiss (1986) did an exhaustive work on the derivation of analytical solutions for the stresses, displacements and flows in the support and the rock mass around pressure tunnels, considering the fact that concrete supports are pervious and therefore flow can occur to or from them. He studied porous and fractured supports, with several zones of rock around it in order to consider the damage effect introduced by blasting or the improvement brought by consolidation grouting, considered different possibilities of the water table location and the effect of non-tension resistance of the concrete/rock contact, and used several conceptual models. In the application of his work to the Castelo do Bode tunnel it is assumed that the concrete support is not fractured (which is reasonable, having in mind the stresses that were calculated). Several conceptual models, represented in Fig. 7.4, were used, and different combinations of parameters were considered.

Model B - Single thick walled ring under internal and external pressures, subdivided in:

- B1) only the concrete support was considered, $r_a = 1.85\text{m}$, $E_b = 22\text{GPa}$, $k_b = 5 \times 10^{-10}\text{m/s}$;
- B2) a ring of rock of 0.40m was considered to participate, together with the support, to resist the internal and external pressures, $r_a = 2.25\text{m}$, $E_b = 22\text{GPa}$, $k_b = 10^{-8}\text{m/s}$.

Model C - Two concentric rings under internal and external pressures, one for the support and one for the rock, subdivided in:

- C1) concrete support and a 0.75m thick ring of rock contributing for the resistance, $r_a = 1.85\text{m}$, $r_c = 2.60\text{m}$, $E_b = 22\text{GPa}$, $E_F = 13\text{GPa}$, $k_b = 5 \times 10^{-10}\text{m/s}$, $k_F = 2 \times 10^{-8}\text{m/s}$;
- C2) inner ring of 0.75m (taking together the support and 0.40m of rock), and a large ring of rock contributing for the resistance, $r_a = 2.25\text{m}$, $r_c = 15.00\text{m}$, $E_b = 22\text{GPa}$, $E_F = 22\text{GPa}$, $k_b = 10^{-8}\text{m/s}$, $k_F = 2 \times 10^{-7}\text{m/s}$.

Model D - Three concentric rings, one for the support, one for the rock under the influence of the flow to/from the tunnel, and one outside this zone of influence. In this model only the internal pressure was considered explicitly and, as a simplification, a linear variation of the water pressure in the lining and the rock was considered. The external pressure was calculated from the internal pressure and from the position of the water table, which is considered stable outside the zone of influence, in the position measured in the beginning of the loading test ($p_R = 0.152\text{MPa}$). This model was subdivided in:

- D1) concrete support and a zone of influence of 10 times the inner radius: $r_a = 1.85\text{m}$, $R = 15.00\text{m}$, $E_b = 22\text{GPa}$, $E_F = 22\text{GPa}$, $k_b = 5 \times 10^{-10}\text{m/s}$, $k_F = 2 \times 10^{-7}\text{m/s}$;
- D2) inner ring of 0.75m (taking together the support and 0.40m of rock), and a zone of influence of 10 times the inner radius: $r_a = 2.25\text{m}$, $R = 15.00\text{m}$, $E_b = 22\text{GPa}$, $E_F = 22\text{GPa}$, $k_b = 10^{-8}\text{m/s}$, $k_F = 2 \times 10^{-7}\text{m/s}$.

Model E - Four concentric rings, one for the support, one for the rock affected by the blasting (and grouted), one for the rock inside the zone of influence of the flow to/from the tunnel, and one outside the zone of influence, $r_a = 1.85\text{m}$, $r_c = 2.60\text{m}$, $R = 15.00\text{m}$, $E_b = 22\text{GPa}$, $E_c = 13\text{GPa}$, $E_F = 26\text{GPa}$, $k_b = 5 \times 10^{-10}\text{m/s}$, $k_c = 2 \times 10^{-8}\text{m/s}$, $k_F = 2 \times 10^{-7}\text{m/s}$.

The values of the coefficient of permeability of the rings containing concrete and rock is an intermediate value between those of these two materials. The Poisson's ratio of the concrete is 0.2 and of the rock is 0.15.

The value of the stresses due to the temperature variations were assumed to be equal to the ones obtained for the impervious lining.

7.4. Comparison between the calculated and the observed values

In this section, a comparative study of the values calculated by means of the numerical and analytical solutions for impervious and pervious linings with the values of the observation in the instrumented section, for the loading test of the tunnel, will be presented.

The stress variations in the support during the loading stages were computed from the values of the strains obtained with the Carlson extensometers, using the Young's modulus calculated for the concrete. Subsequently the stress variations in the points where the extensometers are located were computed using the numerical and analytical solutions.

In Fig. 7.5 are represented the observed and the calculated stresses in the tangential direction for extensometers A1 and A2, for the maximum pressure during the loading test. Models B1 and B2, where the contribution of the rock is not taken into account, give much higher stresses than those observed, which indicates that the contribution of the rock mass in this tunnel is effective and must be considered for an economical design. With model C1 high unrealistic stresses were also obtained, due to the low E_r considered for the zone of rock affected by the blasting and consolidated with grouting. The other 5 models (A, C2, D1, D2 and E) provided good results, when compared with the observed values, and therefore were the only ones considered in what follows.

The normal stresses on the lining/rock contact are shown in Fig 7.6. With the exception of model E2 where a very small tension was obtained, all the models gave compressions, which means that the assumption established in the beginning of a support effectively linked to the

rock mass can be considered realistic. Fig. 7.7 indicates the flows of water from the tunnel into the rock mass for the previous models. Models C2 and D2, although giving good results in term of stresses, lead to extremely high values of flow through the lining, quite unrealistic, as they would represent for the whole length of the tunnel a considerable fraction of the total water transported by the tunnel from one end to the other. Therefore, for the final comparison of the results, only models D1, E and A were considered.

The observed values for the extensometers A1, A2, A3 and A4 are compared in Figs 7.8, 7.9 and 7.10 with those obtained by models D1, E and A. As can be seen, a good agreement exists for extensometers A1, A2 and A3, despite the simplifications and indetermination that exist. For extensometer A4 the agreement is not so good, mainly during the unloading. Since this extensometer is located in the outside of the lining, close to the rock mass, the values obtained may be affected by the irregularity of the concrete/rock contact surface. The good general agreement between the observed and calculated values indicate a normal behaviour of the tunnel and the reliability of the instrumentation used.

During the exploration of the tunnel, based on the continuous comparison between the calculated and the observed values, not only for this section but also for the sections that include the rod-extensometers, reasonable agreements have been achieved. It has been possible to state as a general conclusion, that the tunnel has the adequate safety and serviceability conditions.

ACKNOWLEDGEMENTS

The authors are indebted to Electricidade de Portugal - EDP, for permission to publish results from the Alto Lindoso hydroelectric power scheme.

The authors also wish to thank Empresa Pública das Águas Livres - EPAL, for permission to include results from the Castelo do Bode tunnel.

Thanks are also due to Mr. J. Almeida e Sousa for the collaboration in the calculations for the Alto Lindoso Scheme.

Lisboa, Laboratório Nacional de Engenharia Civil, November, 1991.

APPROVED BY

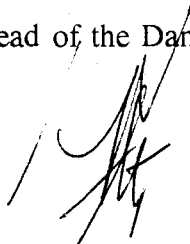
AUTHORS

Head of the Underground
Construction Division



F. Guedes de Melo

Head of the Dams Department



José Oliveira Pedro



Luís Ribeiro e Sousa

Civil Engineer, Principal Research Officer



Luís Nolasco Lamas

Civil Engineer, Research Assistant

Carlos Souza Martins

Civil Engineer, Research Officer

REFERENCES

- BARTON, N.; MAKURAT, M. & BANDIS, B. (1987) - Modelling rock mass conductivity changes in disturbed zones. Proc. 28th U. S. Rock Mechanics Symposium, Tucson, Arizona.
- BAZANT, Z. & PANULA, L. (1978, 1979) - Practical prediction of time-dependent deformations of concrete. Materials and Structures No. 65, 66 and 69.
- BENSON, R. (1989a) - The design of underground powerhouses. Int. Congress of ITA, Vancouver, Canada.
- BENSON, R. (1989b) - Design of lined and unlined pressure tunnels. Tunnelling and Underground Surface Technology, Vol. 4, No. 2.
- BIENIAWSKI, Z. (1984) - Rock Mechanics design in mining and tunnelling. Ed. A. Balkema, Rotterdam.
- BREKKE, T.; NOORISHAD, J.; WITHERSPOON, P. & MAINI, Y. (1972) - Coupled stress and flow analysis of fractured dam foundations and rock slopes. Proc. ISRM Int. Symp. on Percolation Through Fissured Rock, Stuttgart, Germany.
- BREKKE, T. & RIPLEY, B. (1987) - Design guidelines for pressure tunnels and shafts. Electric Power Research Institute, research report AP-5273, USA.
- BROCH, E. (1982) - Designing and excavating underground powerplants. Water Power and Dam Construction, Vol. 34, No. 4.
- CASTRO, L. (1989) - The boundary element method; developments for the analysis of underground structures (in Portuguese). LNEC internal report, Lisbon.
- CORDING, E.; HENDRON, A. & DEERE, D. (1971) - Rock engineering for underground caverns. Underground Rock Chambers, Arizona.
- CRONEY, P.; LEGGE, T. & DHALLA, A. (1978) - Location of block release mechanisms in tunnels from geological data and the design of associated support. Computer Methods in Tunnel Design, London.
- CROUCH, S. & STARFIELD, A. (1983) - Boundary element methods in solid mechanics. Ed. George Allen & Unwin, London.
- CUNDALL, P. (1971) - A computer model for simulating progressive large scale movements in blocky rock systems. Int. Symposium of ISRM, Nancy.

- DUFFAUT, P. (1982) - The factors that influence the shape of the cavities (in French). Int. Symposium on Caverns and Pressure Shafts, Aachen.
- EDP (1983) - Hydroelectric system of river Lima; preliminary design of the Alto Lindoso scheme (in Portuguese). Porto.
- EDP (1991) - Alto Lindoso hydroelectric scheme (in Portuguese). Porto.
- EPAL (1988) - Castelo do Bode sub-system. Technical Session of the Portuguese Society for Geotechnique, Lisbon.
- ERBAN, P. (1986) - Tridimensional finite element calculations of idealized discontinua under the consideration of the shear and dilation behaviour of the joints (in German). Report 14, RWTH, Aachen.
- ERBAN, P. & GELL, K. (1988) - Consideration of the interaction between dam and bedrock in a coupled mechanic-hydraulic FE-program. Rock Mechanics and Rock Engineering, 21.
- FAIHRURST, C. & LEMOS, J. (1988) - Influence of in-situ stresses on fluid penetration in jointed rock from unlined pressure tunnels. ISRM Int. Symp. on Power Plants, Madrid.
- FRAZÍLLIO, E. & MARTINS, S. (1984). Boundary element model developed for two-dimensional equilibria (in Portuguese). LNEC, Report, Lisbon.
- GERRARD, C. & PANDE, G. (1985) - Numerical modelling of reinforced jointed rock masses; I: Theory. Computers and Geotechnics I.
- GOODALL, D.; KJORHOLT, H.; DAHLO, T. & BROCH, E. (1989) - High pressure air cushion surge chambers. ITA Int. Cong. Progress and Innovation in Tunnelling, Toronto.
- GOODMAN, R. & ST. JOHN, C. (1977) - Finite element analysis for discontinuous rocks. Numerical methods in geotechnical engineering, Desai, C. and Christian, J. ed., McGraw Hill.
- GOODMAN, R. & SHI, G. (1985) - Block theory and its application to Rock Mechanics. Prentice-Hall, New Jersey.
- HÖNISCH, K. (1988) - Rock mass modelling for large underground powerhouses. Numerical Methods in Geomechanics (Insbruck), Swoboda ed., Balkema, Rotterdam.
- HOEK, E. & BROWN, E. (1982) - Underground excavations in rock. The Institution of Mining and Metallurgy, London.

- KAWAMOTO, T.; ICHIKAWA, Y. & KYOYA, T. (1988) - Deformation and fracturing behaviour of discontinuous rock mass and damage mechanics theory. Int. J. for Numerical and Analytical Methods in Geomechanics, Vol. 12.
- LAMAS, L. (1984) - Three-dimensional boundary element model for underground structures (in Portuguese). LNEC, Internal Report, Lisbon.
- LAMAS, L. (1986) - Statistical analysis of the stability of rock faces. MSc. dissertation, Imperial College, London.
- LAMAS, L. (1989) - Study of the compartmentation of rock masses by a scanline technique, and of the blocks formed by the joints; application to a gallery of Alto Lindoso (in Portuguese). 3rd Portuguese National Congress on Geotechnique, Porto.
- LANG, T. (1971) - Underground rock structures challenge the engineer. Int. Symposium on Rock Chambers, Arizona.
- LELLI, M. (1952) - The statical behaviour provoked by the hydrostatic pressure and the temperature variations of the tunnels and shafts excavated through fractured rock (in Italian). L'Energia Elettrica, No. 1, Vol. XXIX.
- LEMOS, J. (1987) - A distinct element model for dynamic analysis of jointed rock with application to dam foundation and fault motion. PhD Thesis, Univ. of Minnesota.
- LEMOS, J.; HART, D. & CUNDALL, P. (1985) - A generalized distinct element program for modelling jointed rock mass. Proc. Int. Symp. on Fundamentals of Rock Joints, Bjorkliden.
- LNEC (1975) - Observation of the underground works of Cahora-Bassa dam (in Portuguese). Internal Report, Lisbon.
- LNEC (1982) - Contribution for the geotechnical study of the new Castelo do Bode tunnel (in Portuguese). Internal Report, Lisbon.
- LNEC (1986) - Microseismic refraction tests in the Castelo do Bode Tunnel (in Portuguese). Internal Report, Lisbon.
- LNEC (1990) - Observation of the Castelo do Bode Tunnel; Analysis of the behaviour after entering into service (in Portuguese). Internal Report, Lisbon.
- LNEC (1991) - Observation of the underground works of Alto Lindoso hydro-electric scheme. Results obtained during construction in 1989 and 1990 (in Portuguese). Internal Report, Lisbon.

- MARTINS, S. (1985) - Contribution to the study of underground structures associated with hydroelectric developments (in Portuguese). LNEC Thesis, Lisbon.
- MENDONÇA, T. (1989) - Tridimensional finite element models for the study of the hydromechanical behaviour of concrete dams foundations (in Portuguese). LNEC report, Lisbon.
- MIZUKOSHI, T. (1982) - The design and construction of the Imaichi underground power plant. ISRM Int. Symp. on Caverns and Pressure Shafts, Aachen.
- NEIVA, C.; GUIMARAES, N. & AZEVEDO, M. (1983) - Geology of the hydraulic circuit of the hydro-electric development of Alto Lindoso (Portugal). Proc. Int. Symp. on Engineering Geology and Underground Construction, Lisbon.
- OHASHI, T.; KUSABUKA, M.; KYOYA, T. & KAWAMOTO, T. (1986) - The damage mechanics approach to the analysis of an underground opening excavated in a jointed rock mass. Proc. Int. Symp. on Large Rock Caverns, Helsinki.
- OLIVEIRA, R.; COSTA, P. & DAVID, J. (1983) - Engineering geological studies and design of Castelo do Bode tunnel. Proc. Int. Symp. on Engineering Geology and Underground Construction, Lisbon.
- OLSEN, R. & BROCH, E. (1977) - General design procedure for underground openings in Norway. Int. Symp. Rockstore'77, Stockholm.
- PAHL, A. & GLOGGLER, W. (1982) - Control of the stability of large caverns in rock (in German). ISRM Int. Symp. on Caverns and Pressure Shafts, Aachen.
- PANDE, G. (1985) - A constitutive model for rock joints. Proc. Int. Symp. on Fundamental of Rock Joints, Bjorkliden.
- PRIEST, S. (1985) - Hemispherical projection methods in Rock Mechanics. George Allen & Unwin, London.
- PYZIKOWSKI, W. (1982) - The Drackensberg pumped storage scheme. Description of scheme and principal data. The Civil Engineer in South Africa, Vol. 24, n°8.
- RESENDE, L. & MARTIN, J. (1988) - Parameter identification in a damage model for rock mechanics. Int. J. for Numerical and Analytical Methods in Geomechanics, Vol. 12.
- RICHARDS, L.; SHARP, J. & PINE, R. (1977) - Design considerations for large unlined caverns at shallow depths in jointed rock. Int. Symp. Rockstore '77, Stockholm.

- SCHLEISS, A. (1986) - Design of pervious pressure conduits, Part II: Influence of water flow on the concrete support an rock mass, stress-permeability interaction, design criteria (in German). ETH report No 86, Zurich.
- SILVEIRA, A.; AZEVEDO, C. & COSTA, P. (1974) - Contribution to the study of the underground structures of Cahora-Bassa. LNEC, Memory n° 430, Lisbon.
- SOUSA, J.; SOUSA, L. & VIOLANTE, V. (1991) - Error estimates and adaptive procedures in geotechnical problems. International Workshop on Applications of Computational Mechanics in Geotechnical Engineering, Rio de Janeiro.
- SOUSA, L. (1983). Three-dimensional analysis of large underground power stations. 5th Congress of ISRM, Melbourne.
- SOUSA, L.; MARTINS, S. & LAMAS, L. (1986) - Development of the techniques of measurement and the interpretation of the state of stress in rock masses. Application to Castelo do Bode tunnel. 5th International IAEG Congress, Buenos Aires.
- SOUSA, L.; BARROSO, M. & LAMAS, L. (1988) - Alto Lindoso underground power station; Geotechnical characterization. International Symposium on Rock Mechanics and Power Plants, Madrid.
- STEWART, I. (1981) - Numerical and physical modelling of underground excavations in discontinuous rock. PhD thesis, Univ. of London.
- TECNASOL (1989) - Execution of the boreholes for positioning the rod-extensometers; report on the works performed (in Portuguese). Lisbon.
- VARGAS, E. (1982) - Development and application of numerical models to simulate the behaviour of fractured rock masses. PhD thesis, Univ. of London.
- VARGAS, E. (1985) - Application of the dynamic relaxation technique to coupled stress-flow problems in fractured media. Int. Conference on Numerical Methods in Geomechanics, Nagoya University.
- WEI, L. & HUDSON, J. (1990) - Permeability variation around underground openings: a numerical study. Rock Joints (Loen), Barton and Stephanson (ed.), Balkema, Rotterdam.
- WEI, L. & HUDSON, J. (1991) - DEM modelling of water flow in jointed rock. (to be published).

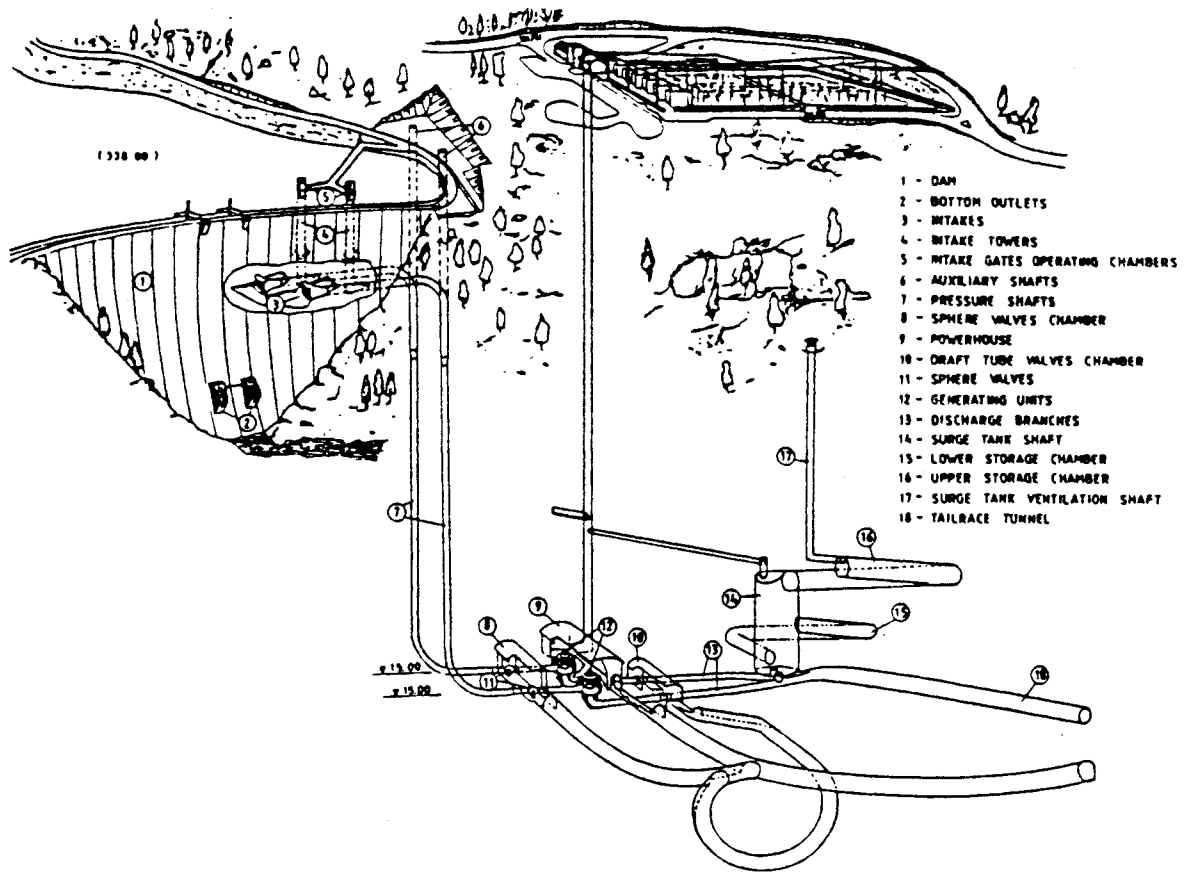


Fig. 1.1 - Alto Lindoso hydroelectric power scheme (after EDP, 1991).

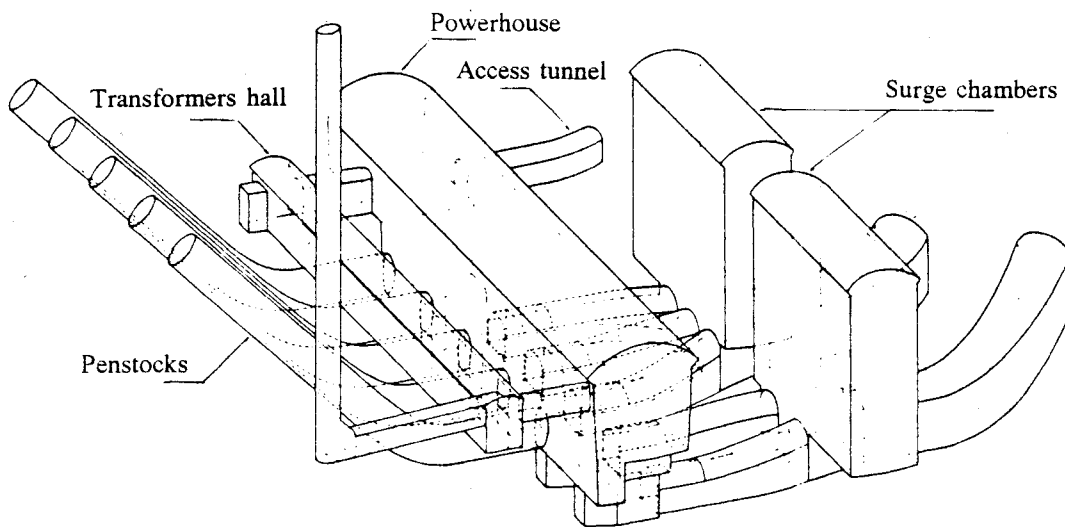
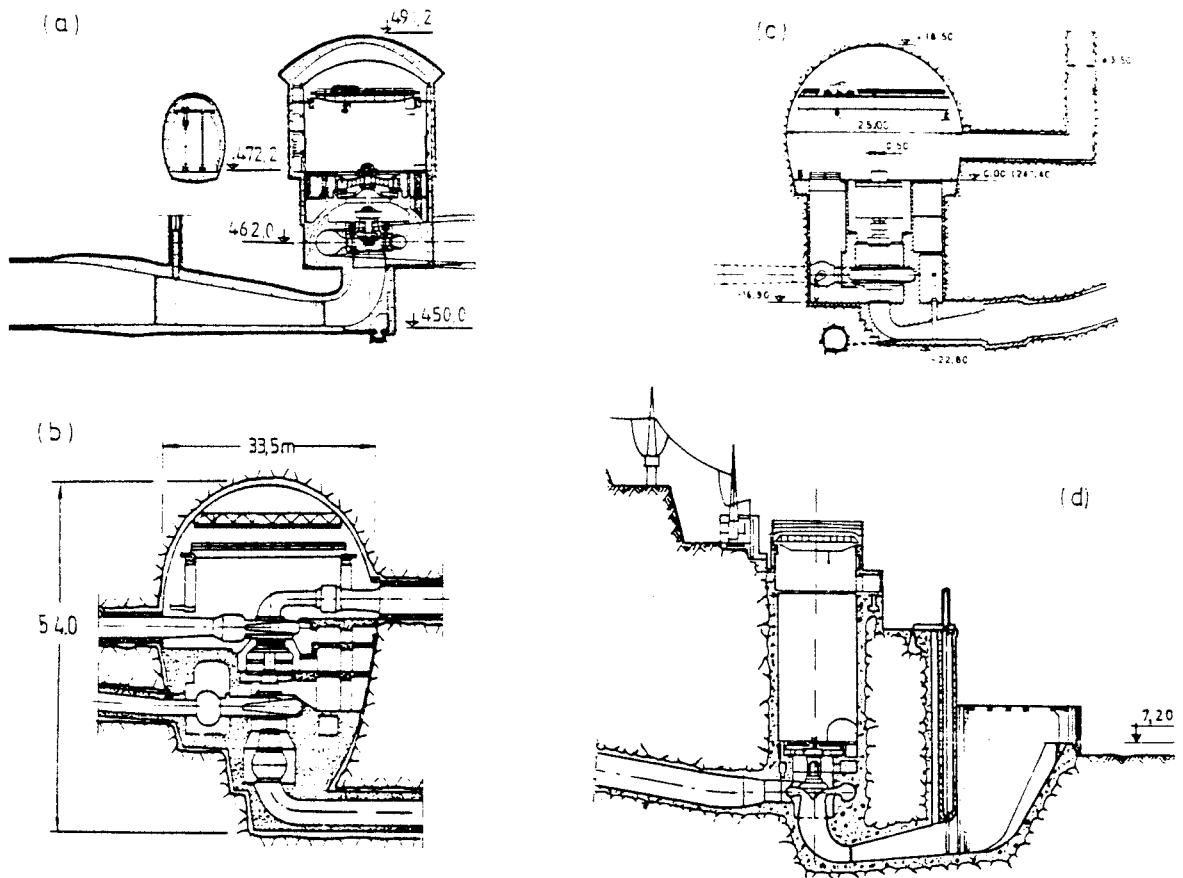


Fig. 1.2 - Cahora Bassa underground powerhouse complex.



(a) Miranda powerhouse (Portugal) - mushroom type
 (b) Waldeck II powerhouse (Germany) - horseshoe type
 (c) Montézic powerhouse (France) - circular ceiling
 (d) Torrão powerhouse (Portugal) - in shaft

Fig. 1.3 - Shapes of underground powerhouses.

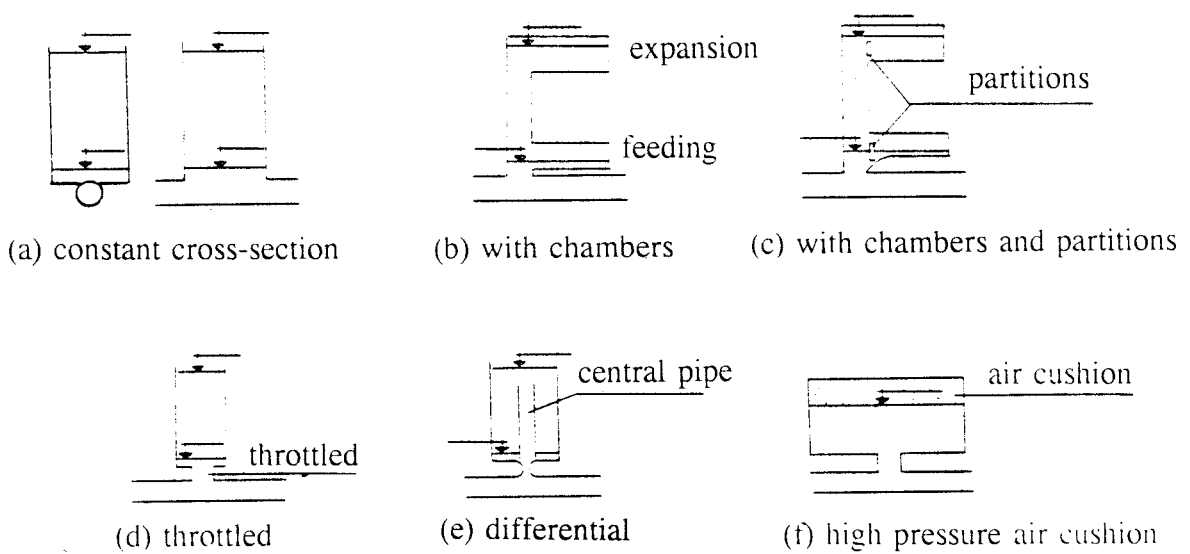


Fig. 1.4 - Types of surge chambers.

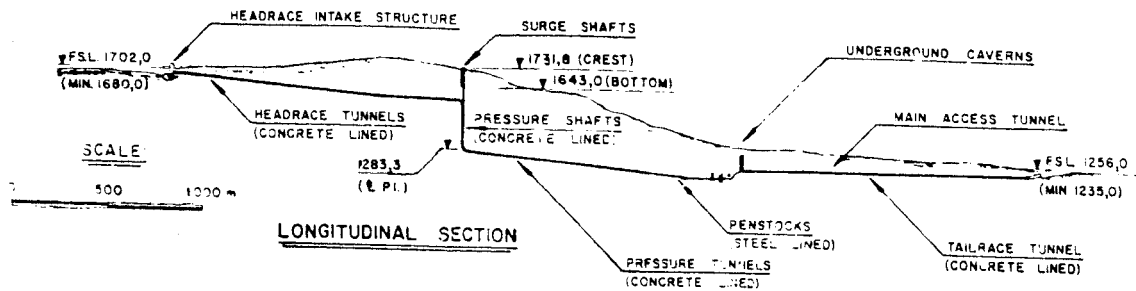


Fig. 1.5 - Drakensberg pumped storage scheme (after Pyzikowski, 1982)

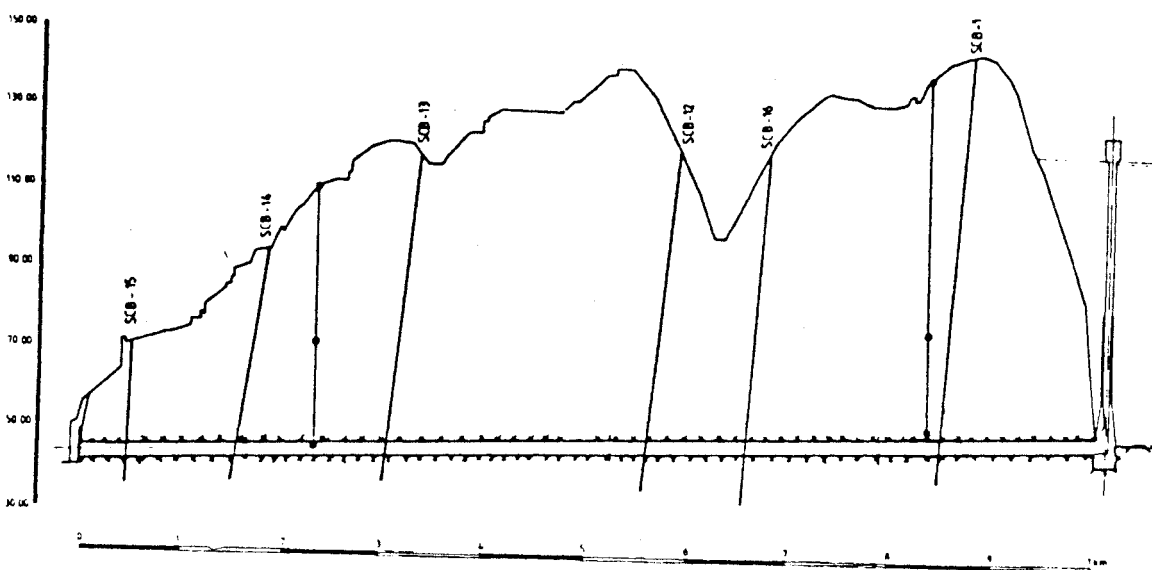
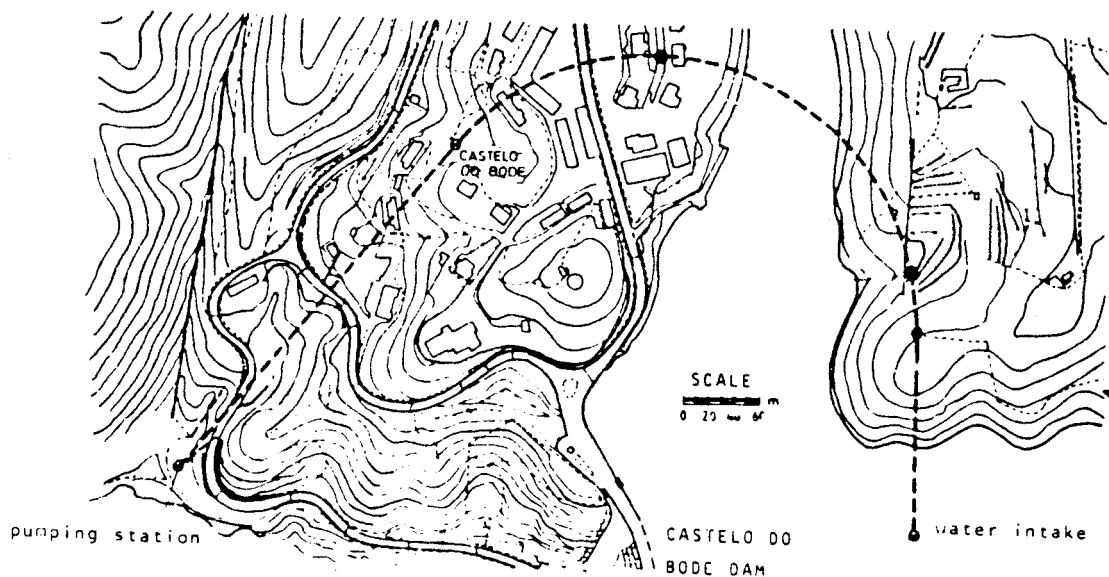


Fig. 1.6 - Castelo do Bode tunnel (after EPAL, 1988).

LNEC - Proc.047/13/9246
Proc.047/13/9249

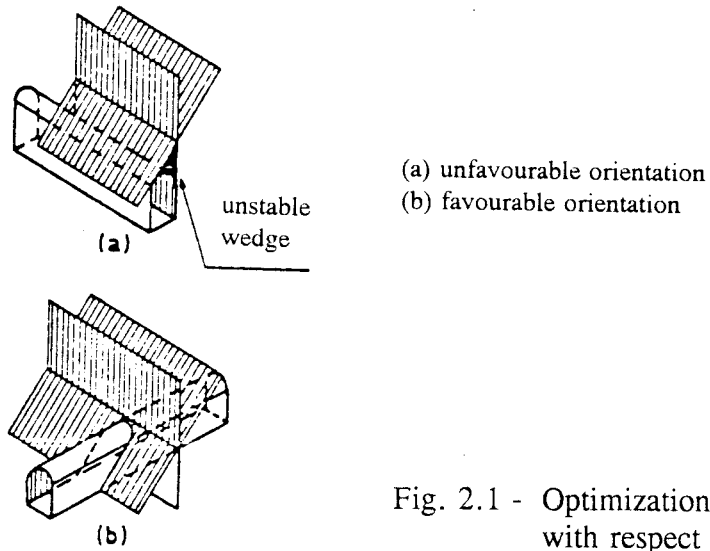


Fig. 2.1 - Optimization of cavern orientation with respect to main discontinuities

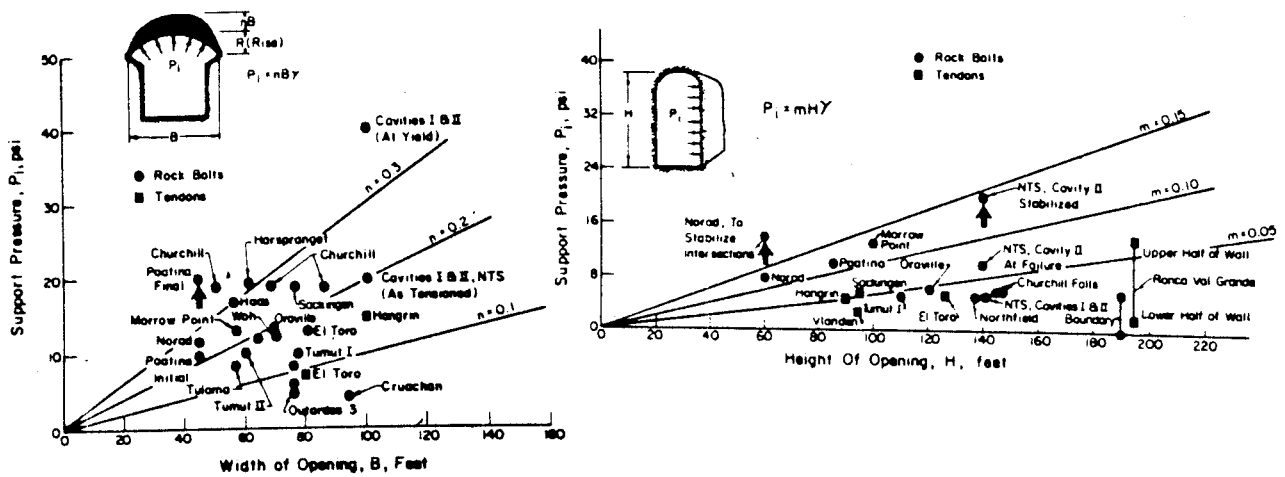


Fig. 2.2 - Pressures on the supports of caverns (after Cording et al., 1971)

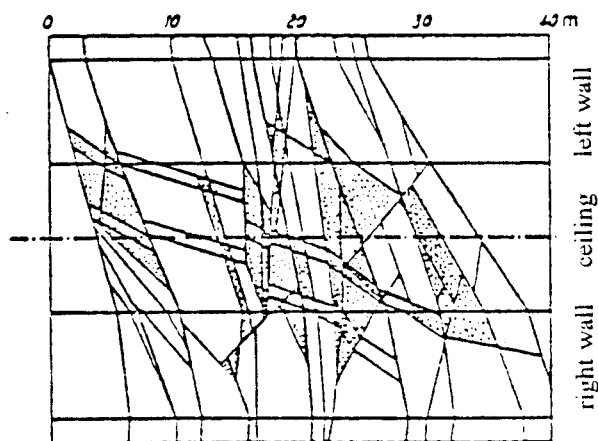


Fig. 2.3 - Deterministic assessment of potentially unstable blocks (after Croney et al., 1978)

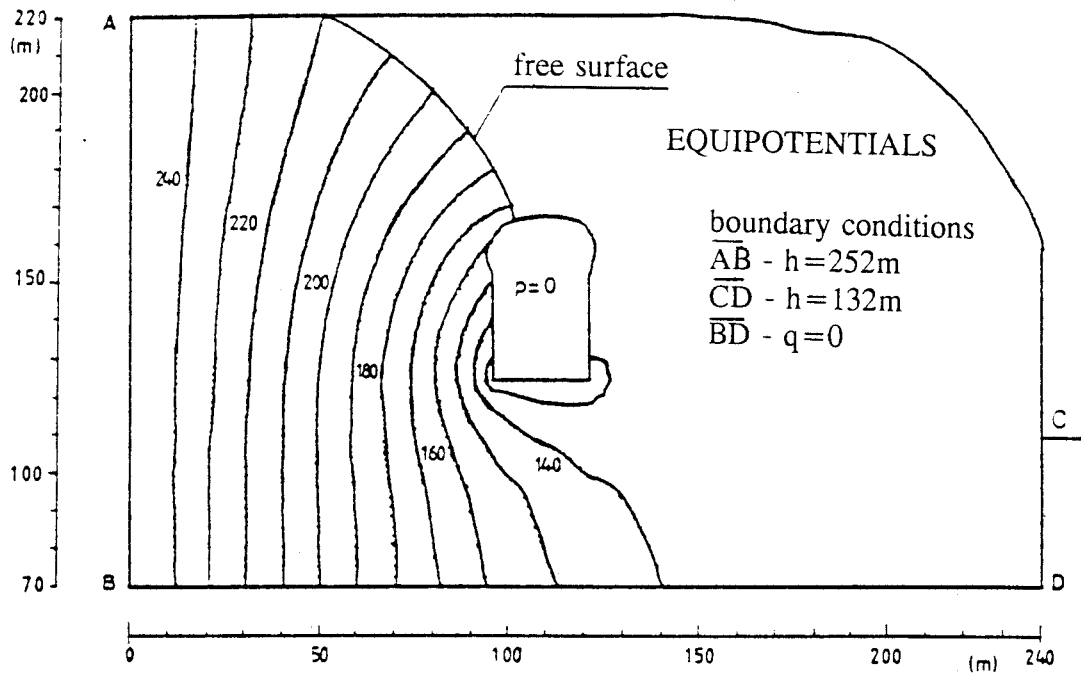


Fig. 3.1 - Flow around Paulo Afonso IV powerhouse cavern.

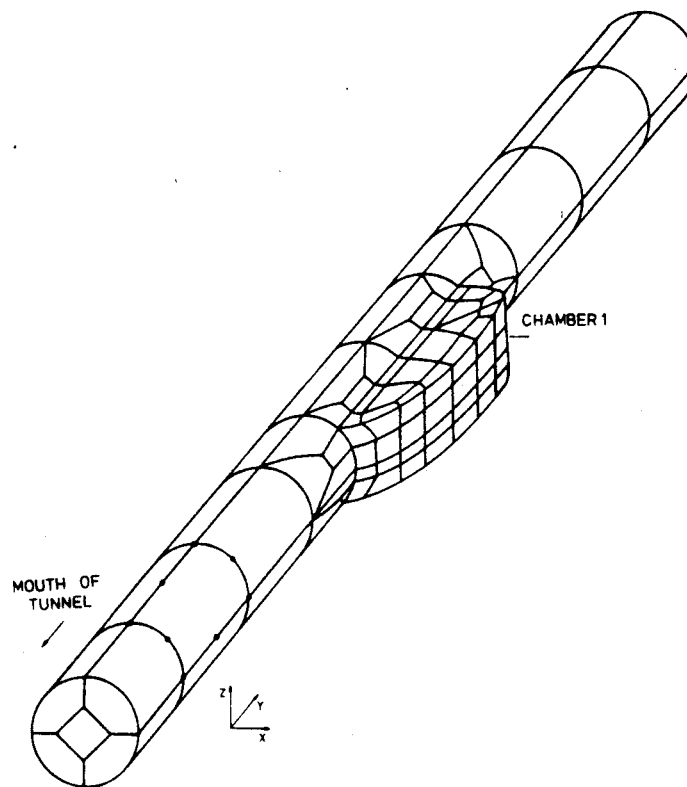


Fig. 3.2 - 3D boundary element model for the Castelo do Bode tunnel.

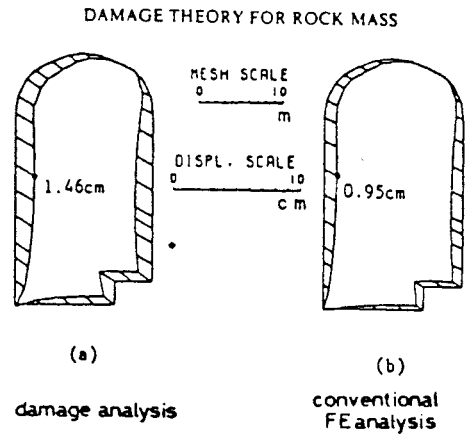
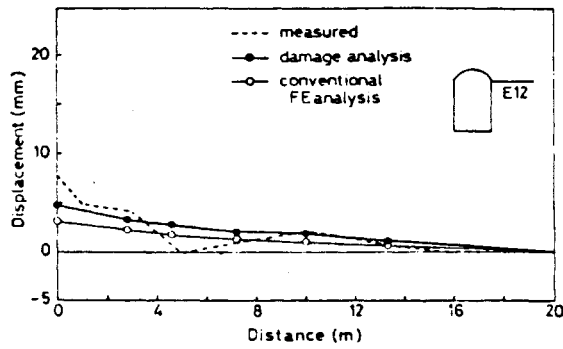
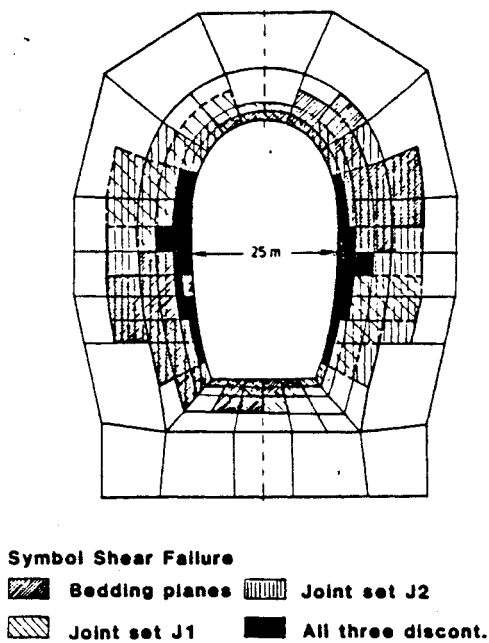


Fig. 3.3 - Displacements computed at the final excavation stage for the Inagawa No.2 powerhouse (after Kawamoto et al., 1988).



Symbol Shear Failure
 Bedding planes Joint set J2
 Joint set J1 All three discont.

Fig. 3.4 - Failure zones due to bedding and two joint sets for the Siah Bishe powerhouse (after Hönisch, 1988).

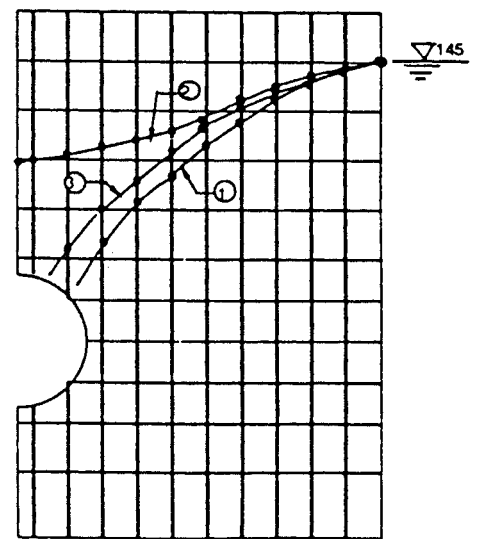
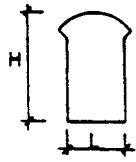


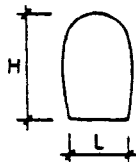
Fig. 3.5 - Free surface under (1) no coupling; (2) coupling elastic; (3) coupling plastic (after Wei and Hudson, 1990).

1 - DIFFERENT SHAPES

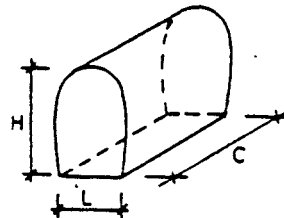
L - span
H - height
C - length
D - distance
between
cavities



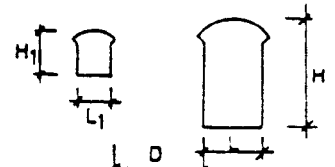
- MUSHROOM SHAPED



- HORSESHOE SHAPED



- 3D CAVERN

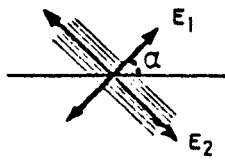


- MULTIPLE CAVITIES

2 - MECHANICAL PROPERTIES

LINEAR BEHAVIOUR

- isotropy
- anisotropy



NON-LINEAR BEHAVIOUR

- shear strength (Coulomb criteria)

$$\sigma_1 = A\sigma_3 + B$$

where

$$A = \frac{1 + \sin\phi}{1 - \sin\phi}$$

$$B = \frac{2C\sqrt{A}}{1 - \sin\phi}$$

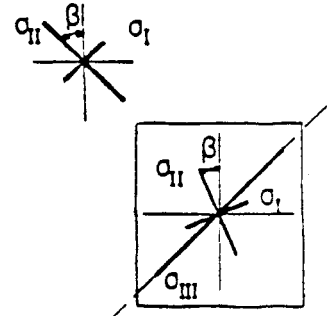
- tension strength

$$\sigma > R_T \rightarrow \sigma = 0$$

3 - IN-SITU STATE OF STRESS

- 2D analysis

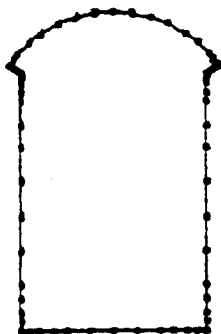
- 3D analysis



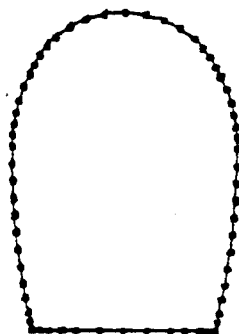
4 - CONSTRUCTION SEQUENCE

- one-stage excavation
- four-stage excavation

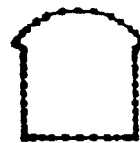
Fig. 4.1 - Parametric studies of powerhouse caverns.



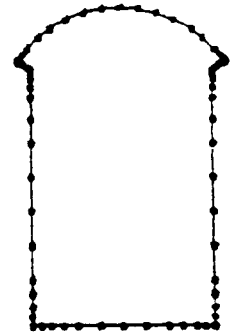
MODEL 1



MODEL 2



MODEL 3



MODEL 4

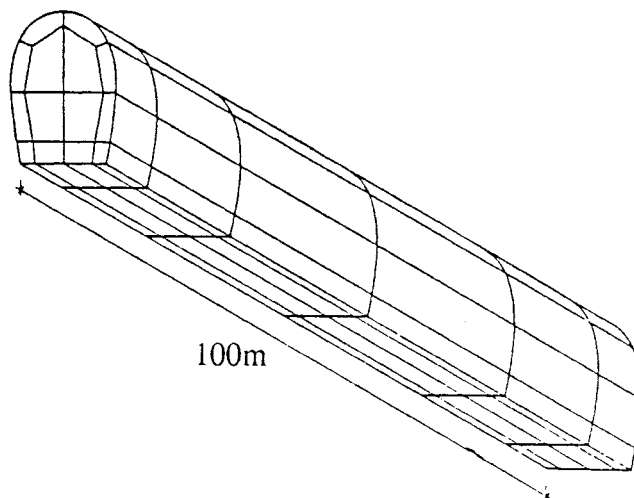


Fig. 4.2 - 2D and 3D boundary element models.

Table 4.1
Parameters used for the analyses of shapes

SINGLE CAVITY (H/L=1.75)			MULTIPLE CAVITIES H/L=1.75; H ₁ /L ₁ =1.17			3D EFFECT H/L=1.75 ; C/L=5.0			
Shape			Distance between cavities (D/H)						
mushroom		horseshoe	∞	1,0	0,5				
σ_1	σ_{11}	β	σ_1	σ_{11}	β	σ_1	σ_{11}	β	σ_{111}
3,0	3,0	hidr.	3,0	3,0	hidr.	3,0	3,0	hidr.	1,0
		1,0				3,0	0°	1,0	
1,0	3,0	0°				1,0	3,0	45°	1,0
1,0	3,0	22,5°	1,0	3,0	0°	1,0	3,0	90°	1,0
		3,0				3,0	hidr.	3,0	
1,0	3,0	45°				1,0	3,0	0°	3,0
		1,0	3,0	90°	3,0				
1,0	3,0	67,5°	1,0	3,0	90°	3,0	3,0	hidr.	9,0
		1,0				3,0	0°	9,0	
1,0	3,0	90°				1,0	3,0	90°	9,0

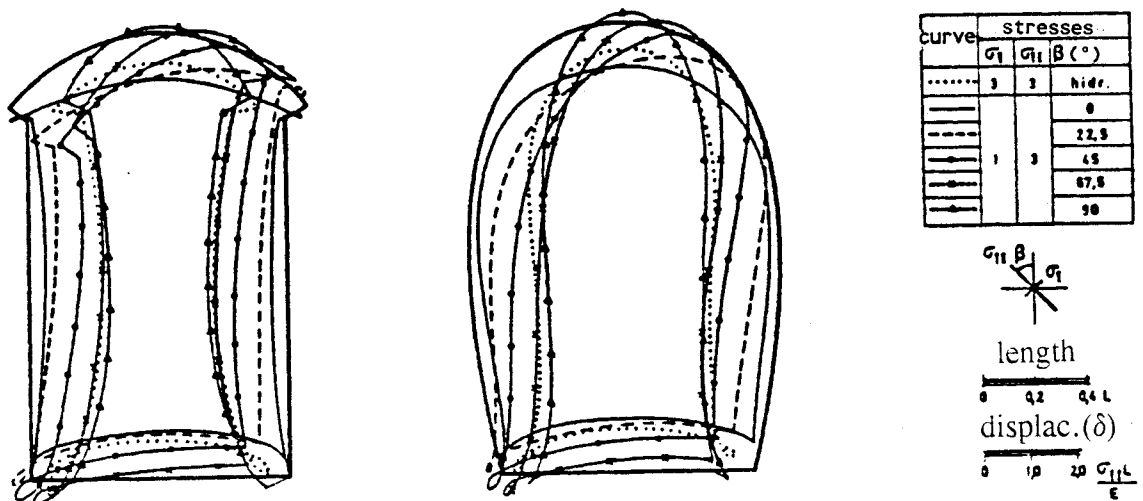


Fig. 4.3 - Boundary displacements for isolated caverns.

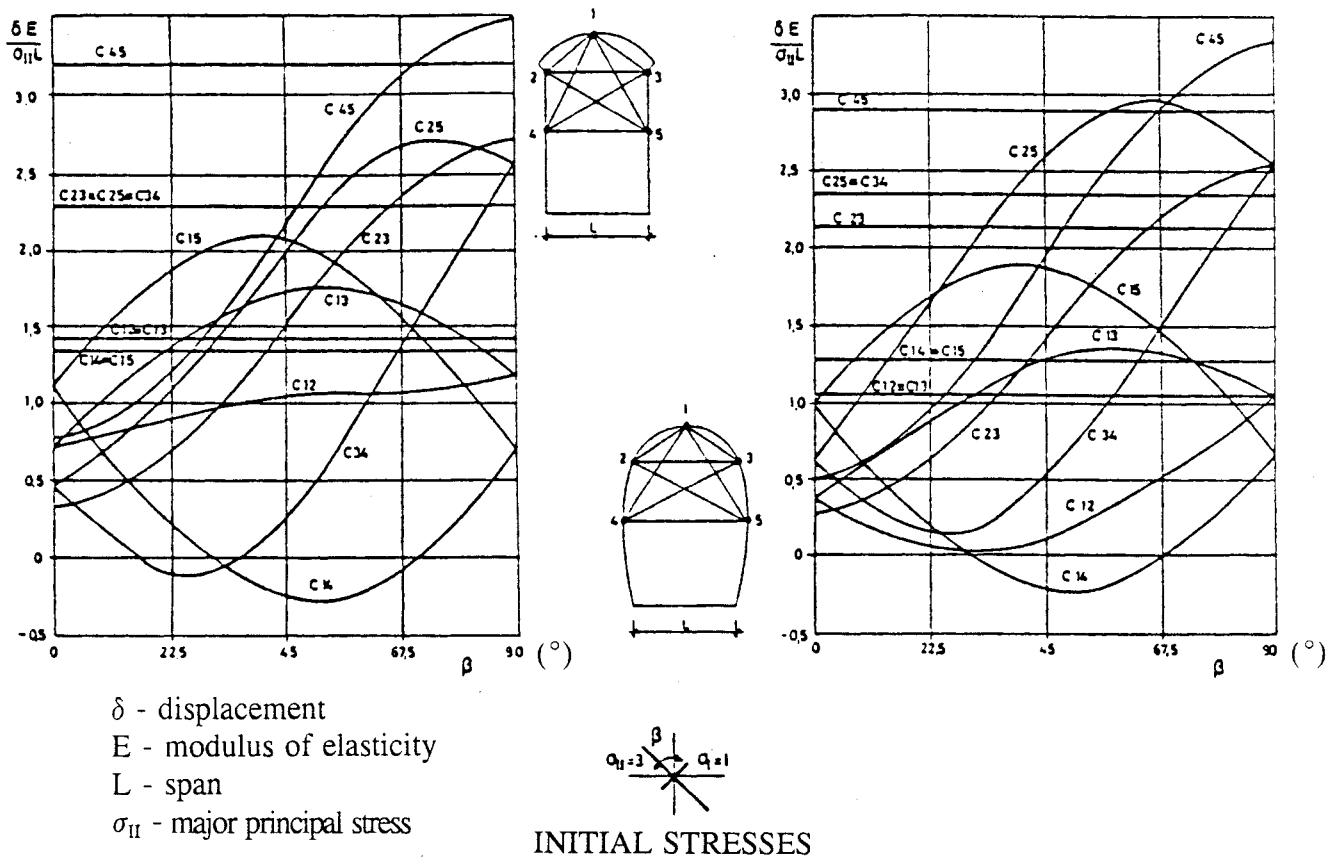


Fig. 4.4 - Convergence curves for isolated caverns.

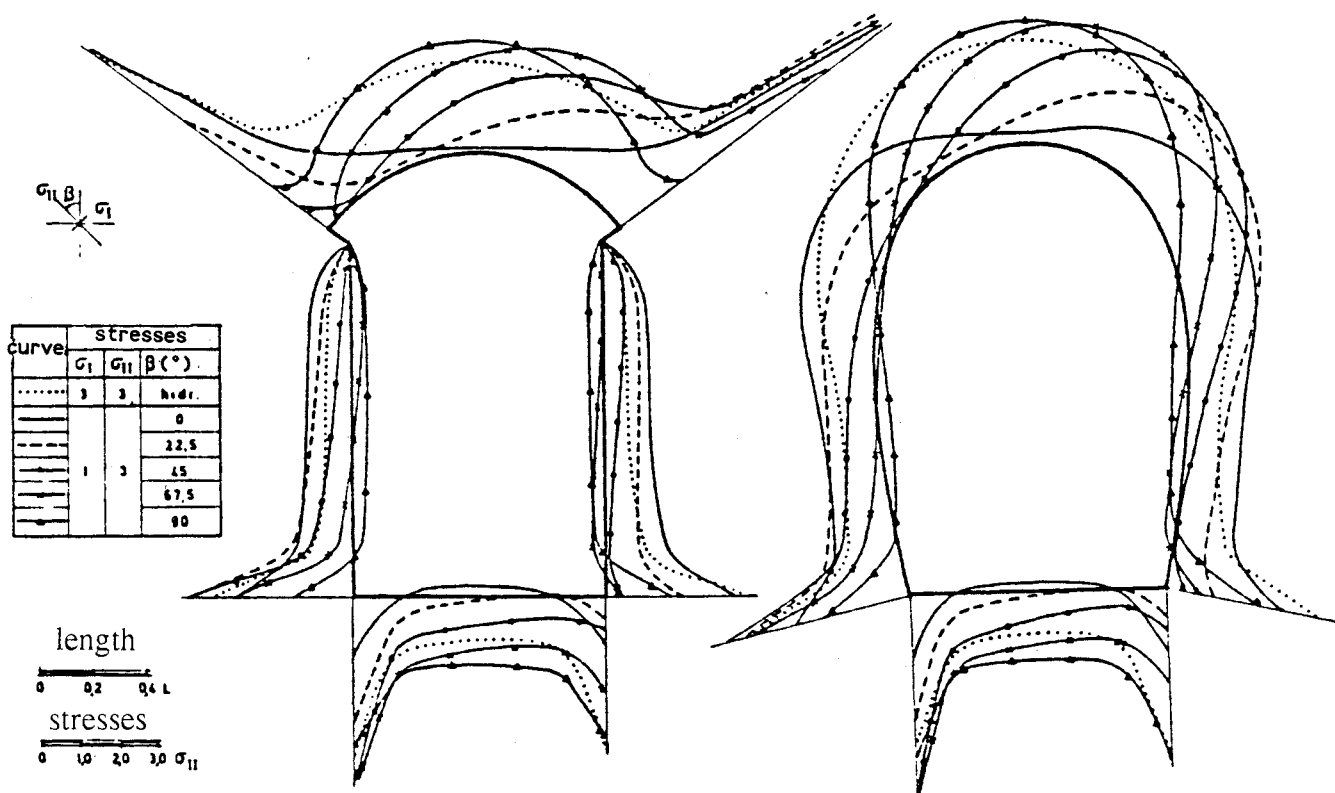


Fig. 4.5 - Boundary tangential stresses for isolated caverns.

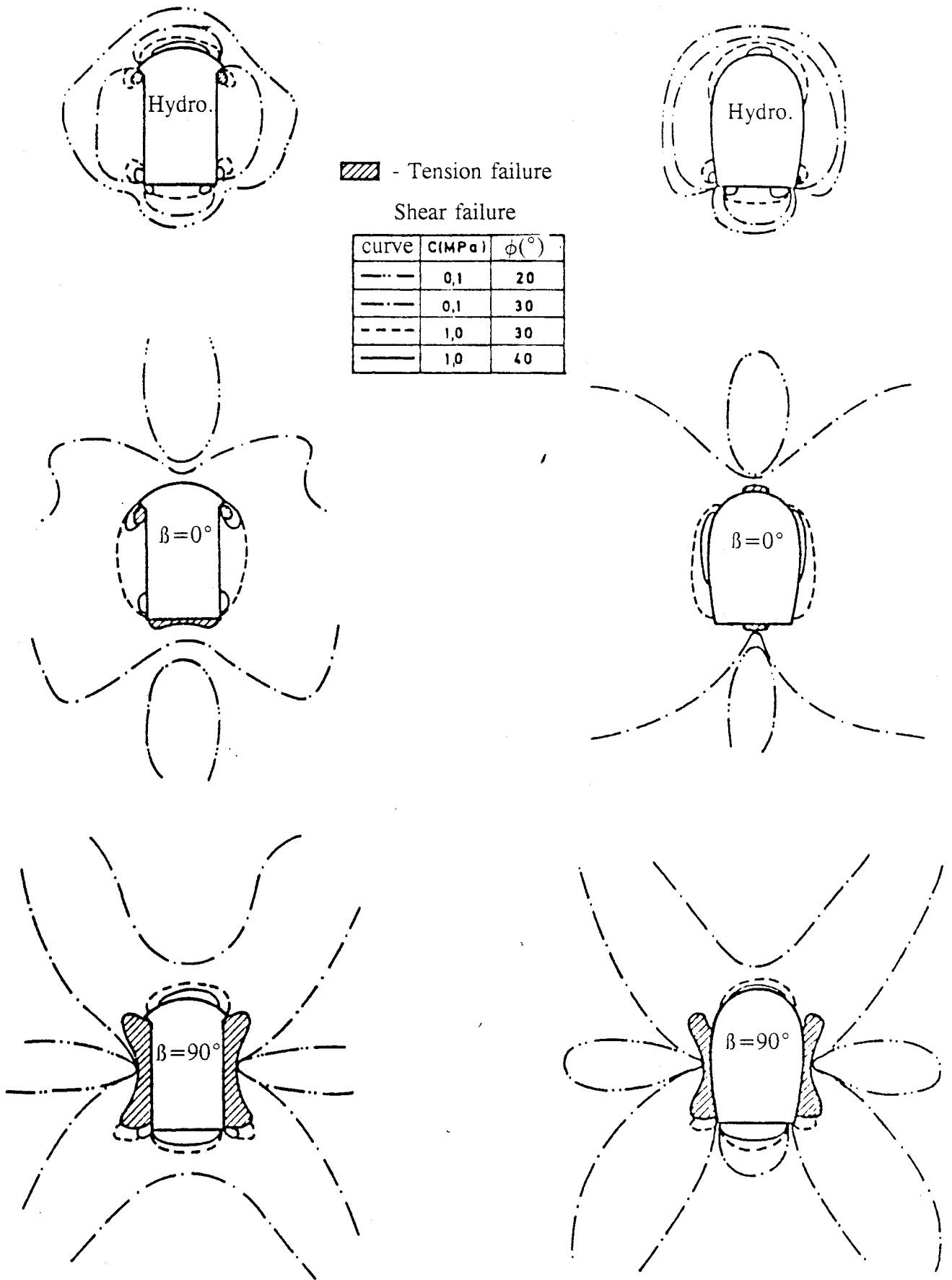


Fig. 4.6 - Failure zones for isolated caverns.

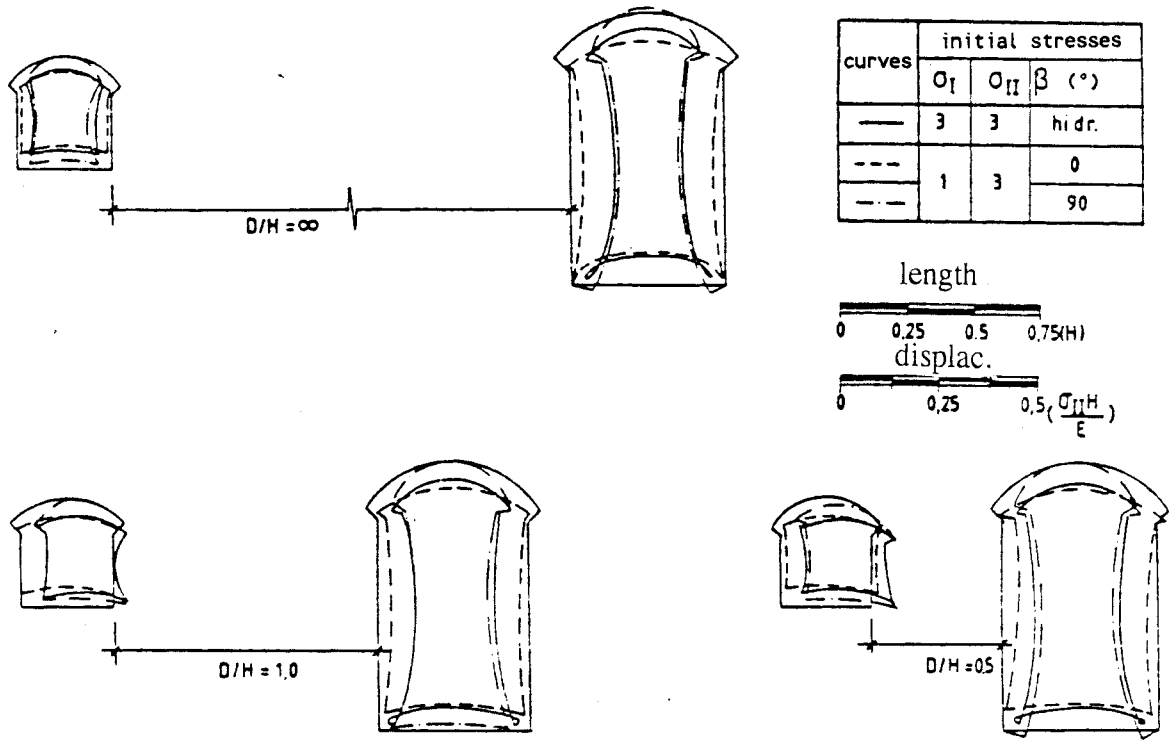


Fig. 4.7 - Boundary displacements for multiple caverns.

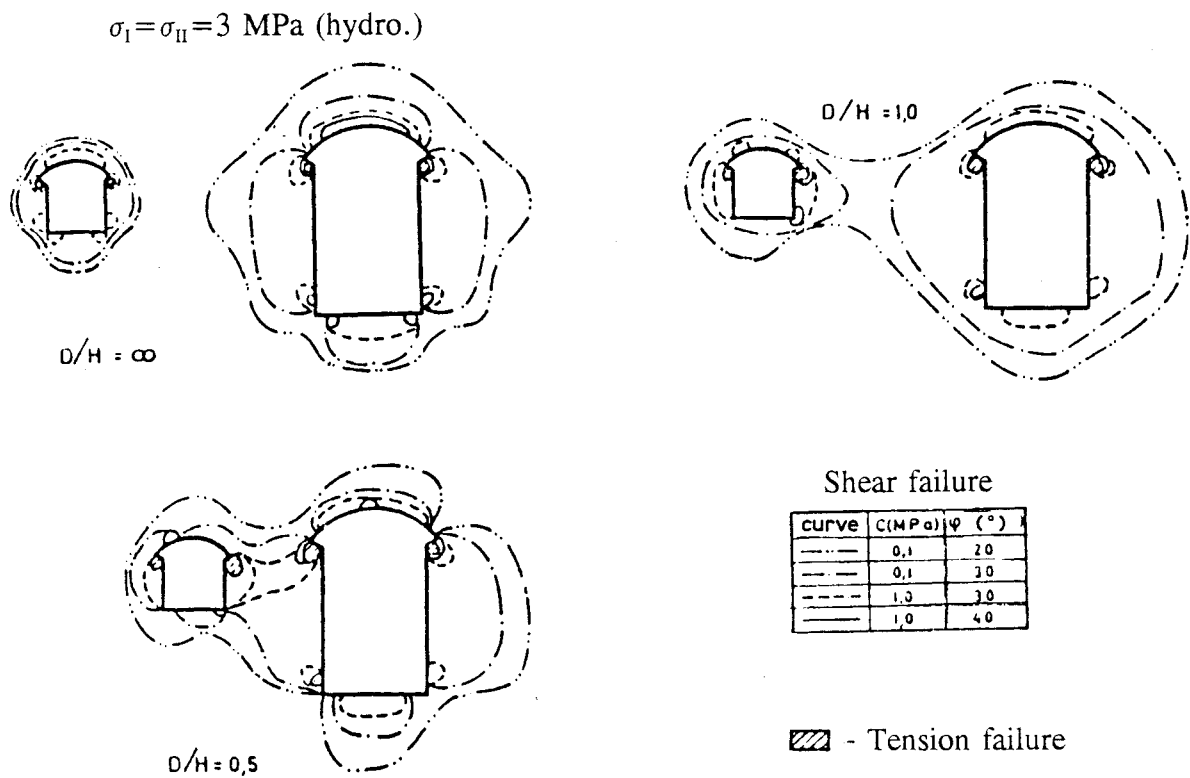


Fig. 4.8 - Failure zones for multiple caverns.

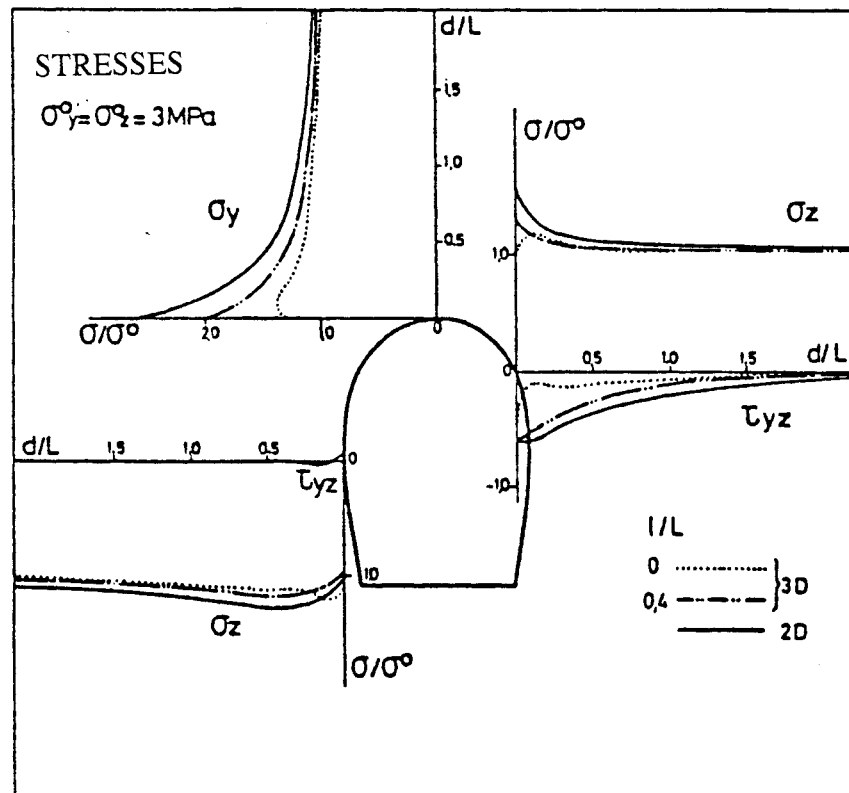
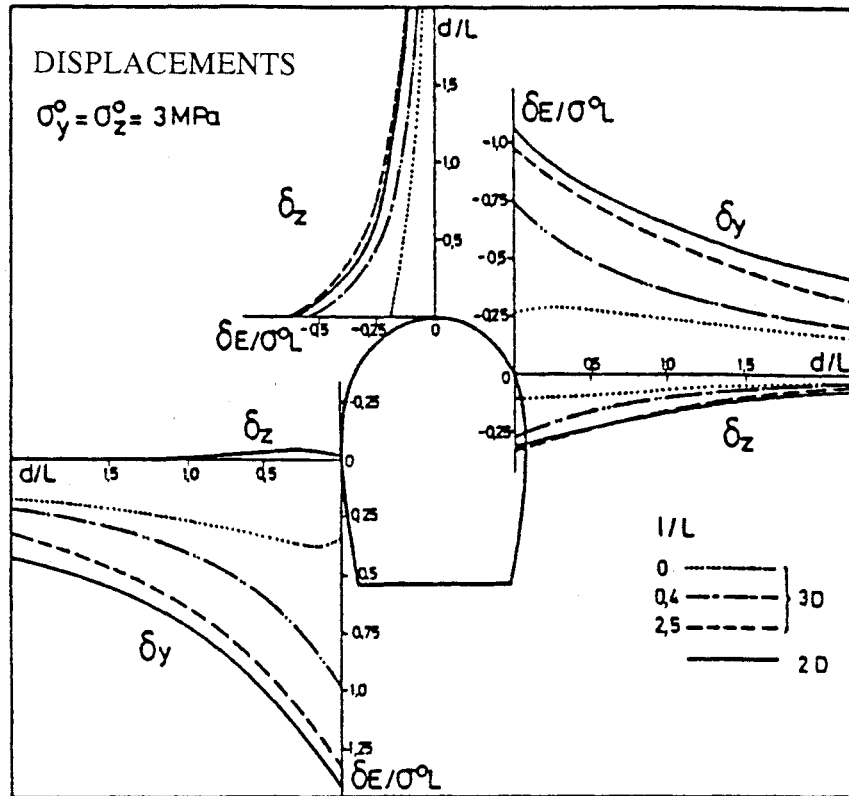
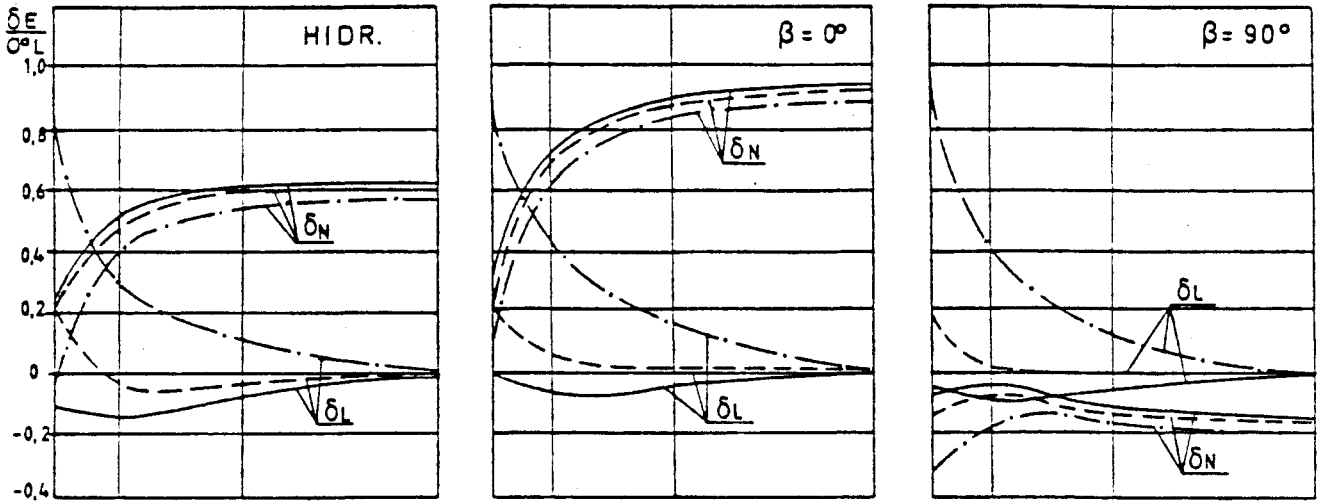
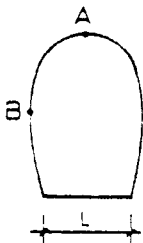
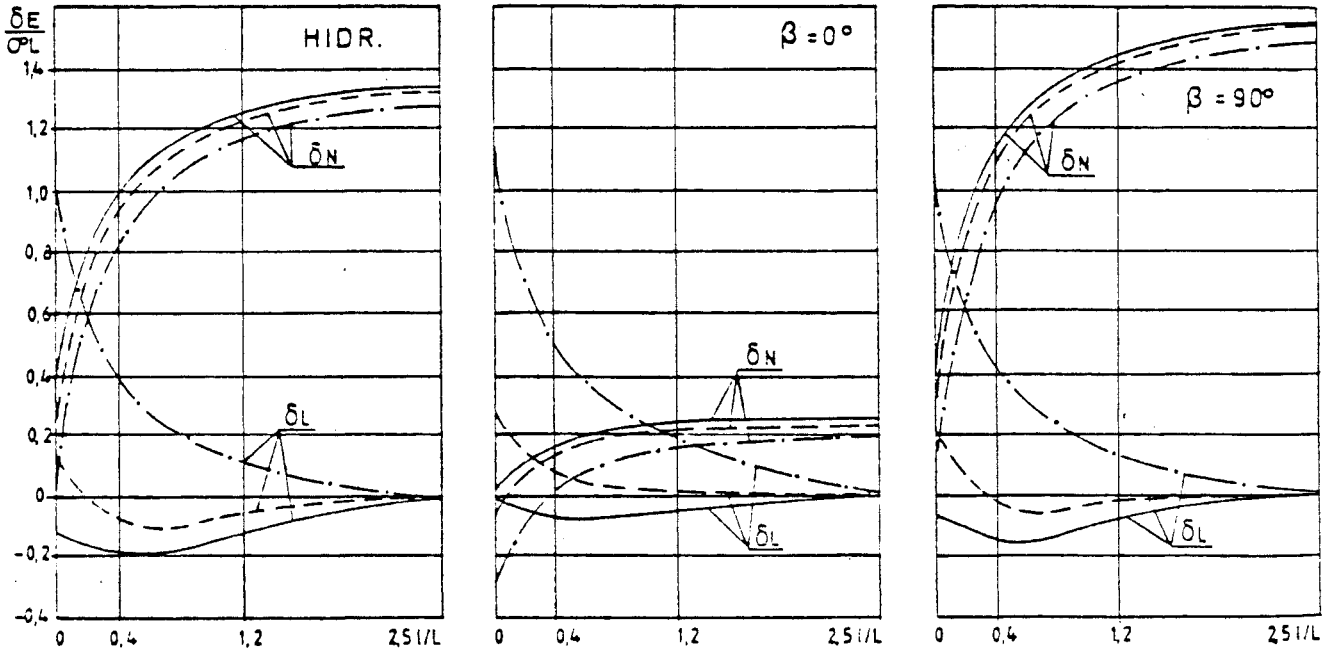


Fig. 4.9 - Results of 3D boundary element model for hydrostatic initial state of stress.
 LNEC - Proc.047/13/9246
 Proc.047/13/9249

POINT A



POINT B



curve	longitudinal stress σ_{III}
—	1.0
- - -	3.0
- · - ·	9.0

δ_N - normal displacement
 δ_L - longitudinal displacement
 $\sigma^0 = 3 \text{ MPa}$
 (+) - towards cavity

Fig. 4.10 - Displacements of 3D model for several longitudinal initial stresses.

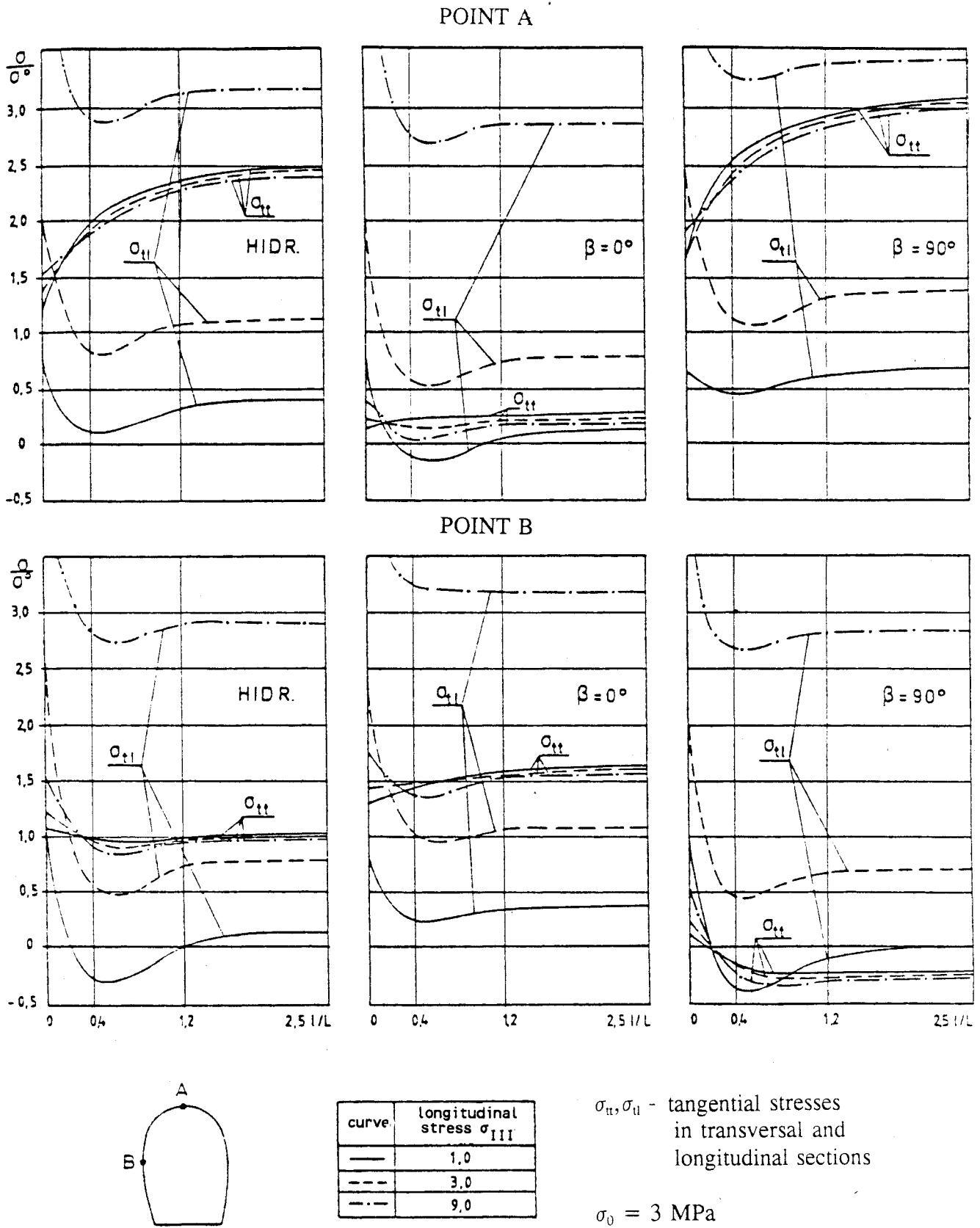
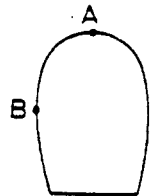
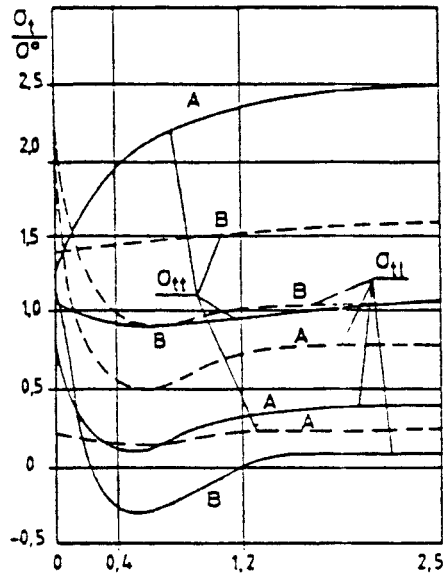
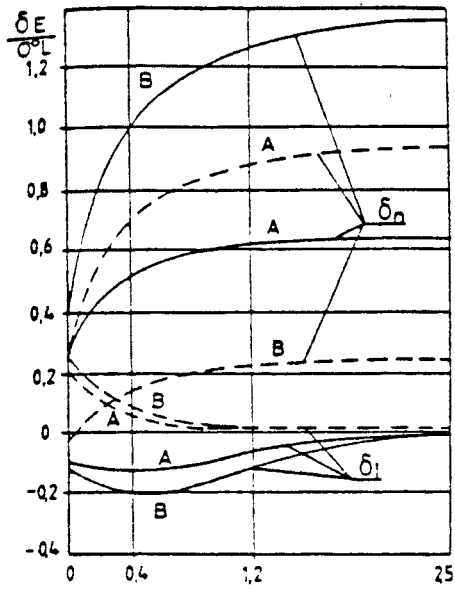


Fig. 4.11 - Tangential stresses of 3D model for several longitudinal initial stresses.

DISPLACEMENTS

TANGENTIAL STRESSES



curve	longitudinal stress (MPa)
—	1,0
- - -	3,0

δ_n, δ_t - normal and longitudinal displacements

σ_{tt}, σ_{ll} - tangential stresses in transversal and longitudinal sections

Fig. 4.12 - Influence of cavern orientation on displacements and stresses.

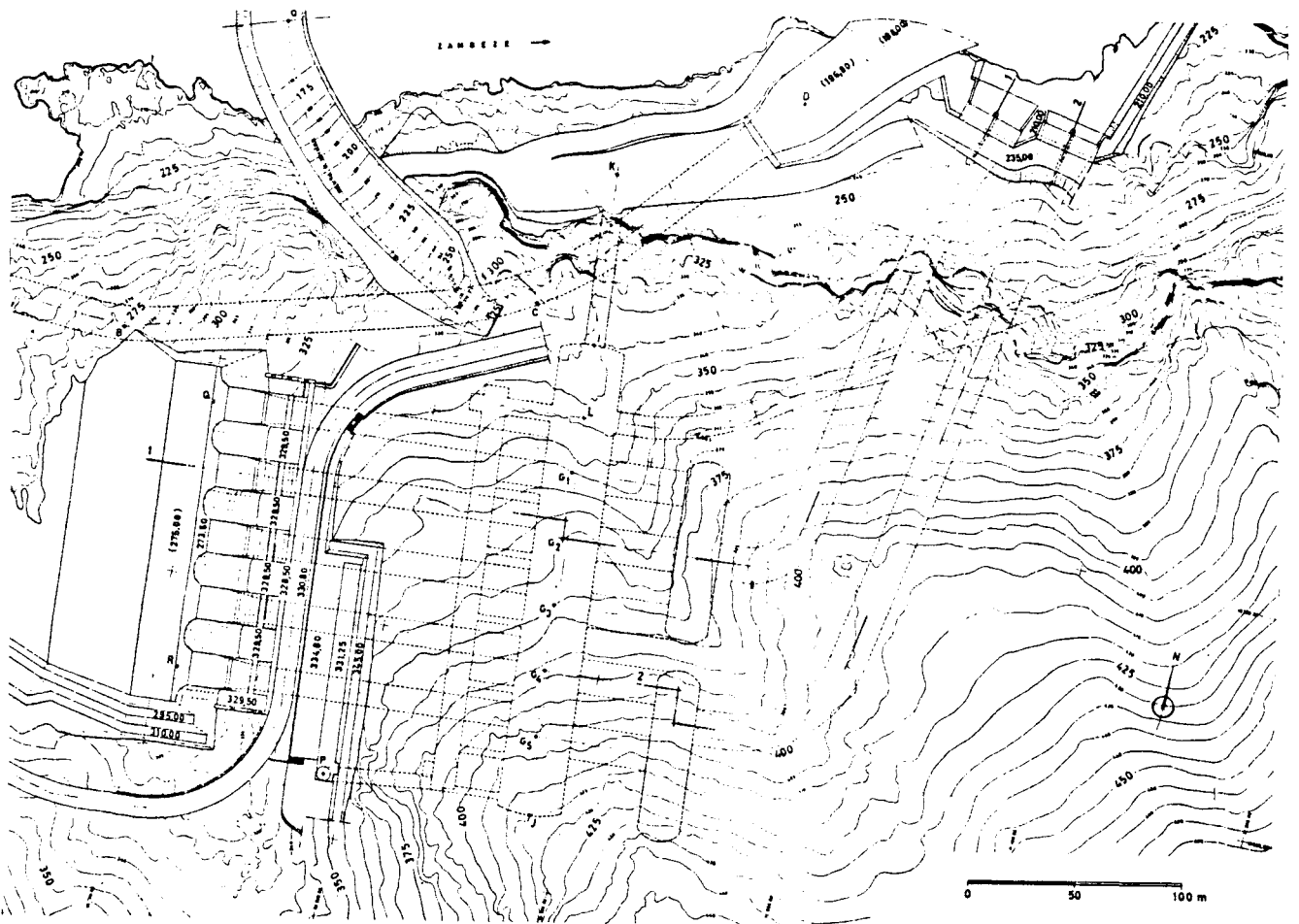


Fig. 5.1 - Cahora Bassa scheme. General plan of the powerhouse and hydraulic circuit (after Silveira et al., 1974)

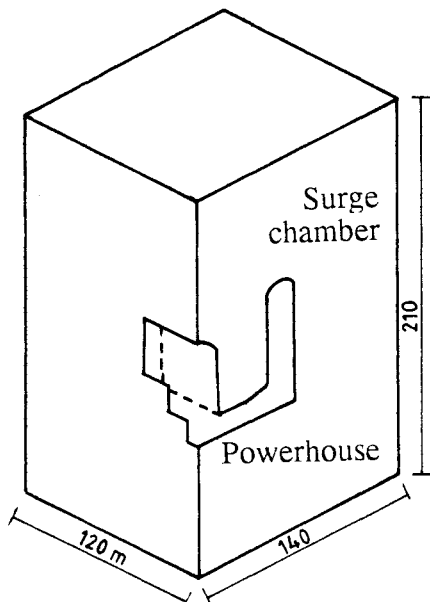


Fig. 5.2 - Block for the 3 D calculation model.

Table 5.1

Summary of in-situ test parameters

PARAMETER	VALUE
Rock mass modulus	
mean	65 GPa
maximum	116 GPa
minimum	23 GPa
Shear strength	
discont. in gneiss	C=0.3 MPa $\phi=33$ to 41°
lamprophyric dyke	C=0.2 MPa $\phi=20^\circ$
In situ stresses	
major princ. stress	13 to 18 MPa
minor princ. stress	9 to 12 MPa

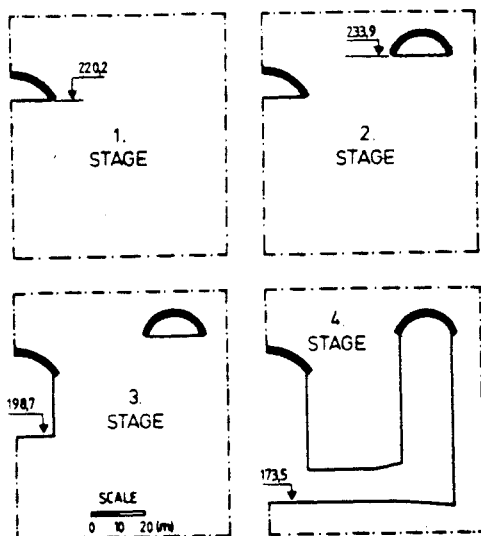


Fig. 5.3 - Construction sequence simulated by 3D model at section S_1

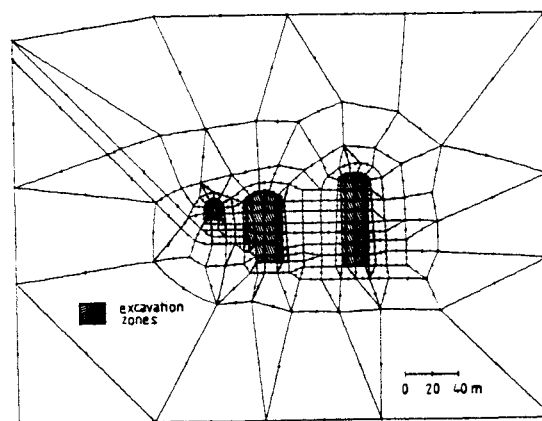


Fig. 5.4 - 2D finite element mesh

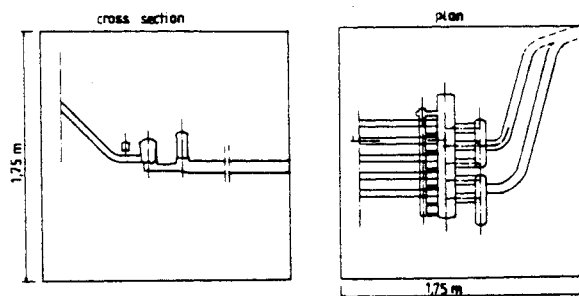


Fig. 5.5 - Schematic drawing of the laboratory model.

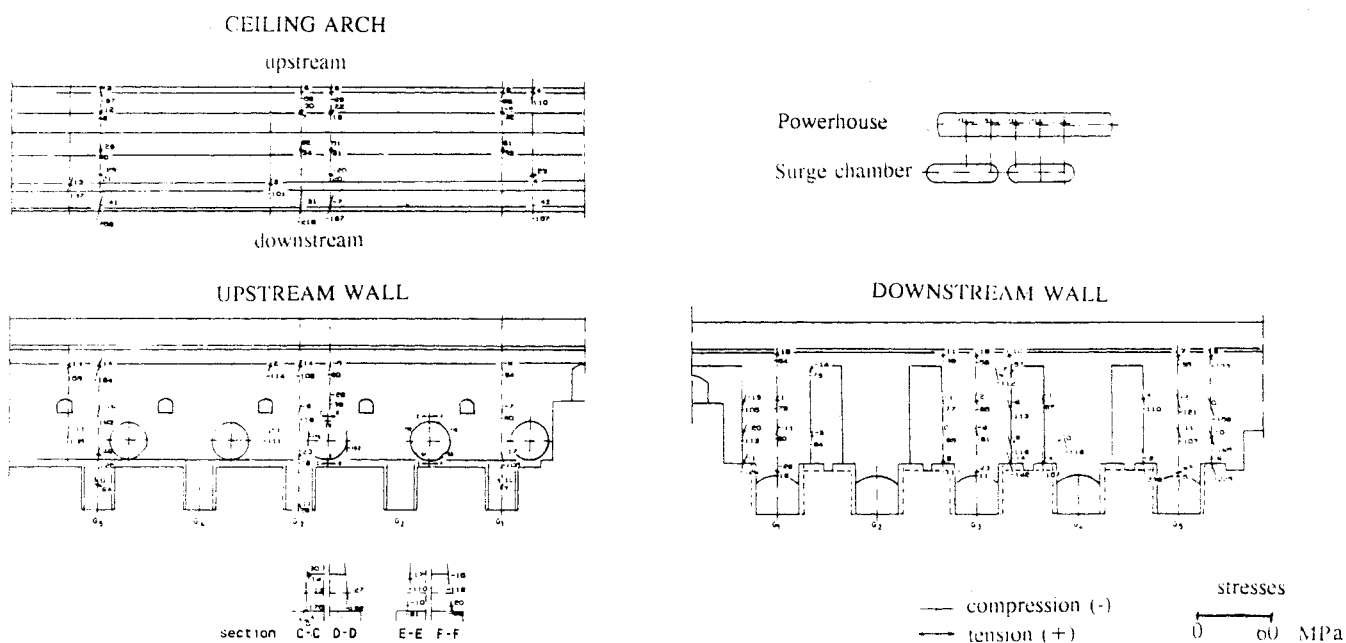


Fig. 5.6 - Principal stresses in the powerhouse cavern for a state of triaxial stress in the rock mass corresponding to $\sigma_v = 15$ MPa and $\sigma_H = 10$ MPa (after Silveira et al., 1974)

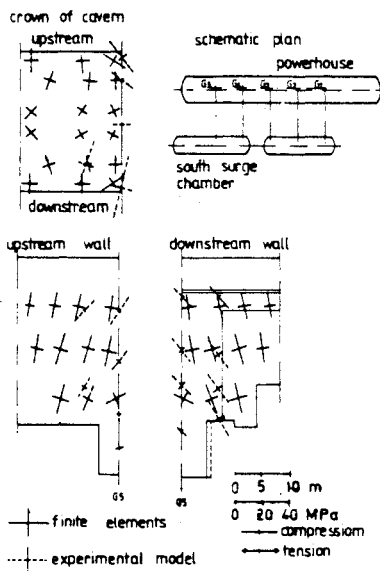


Fig. 5.7 - Principal stresses in the powerhouse cavern.

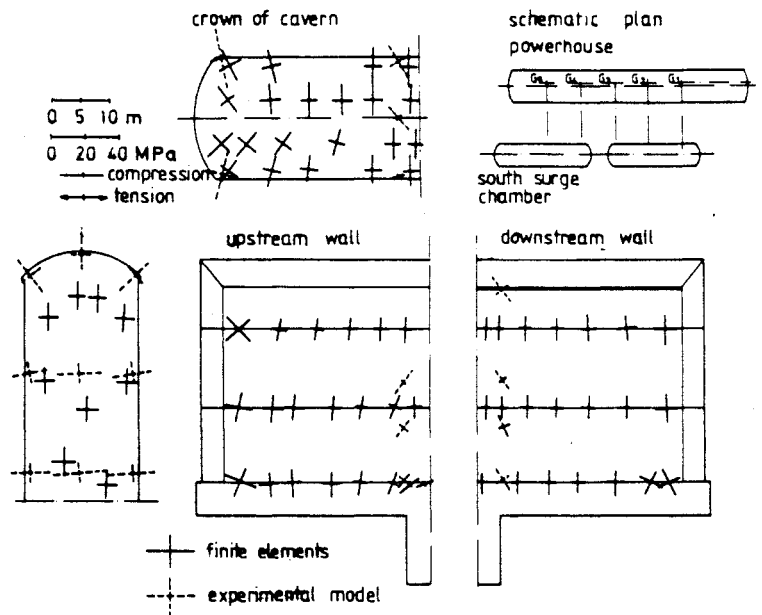


Fig. 5.8 - Principal stresses in the walls of the south surge chamber

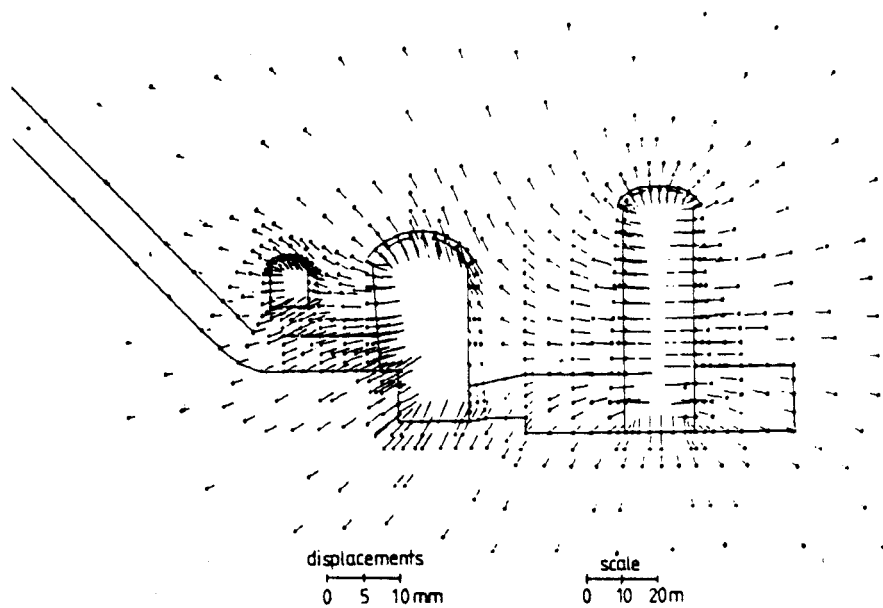


Fig. 5.9 - Displacements at section S_1 .

$C = 0,3 \text{ MPa}$ $\varphi = 41^\circ$

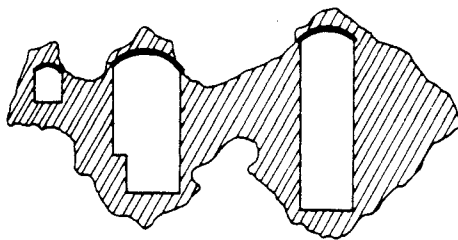


Fig. 5.10 - Plasticity zones

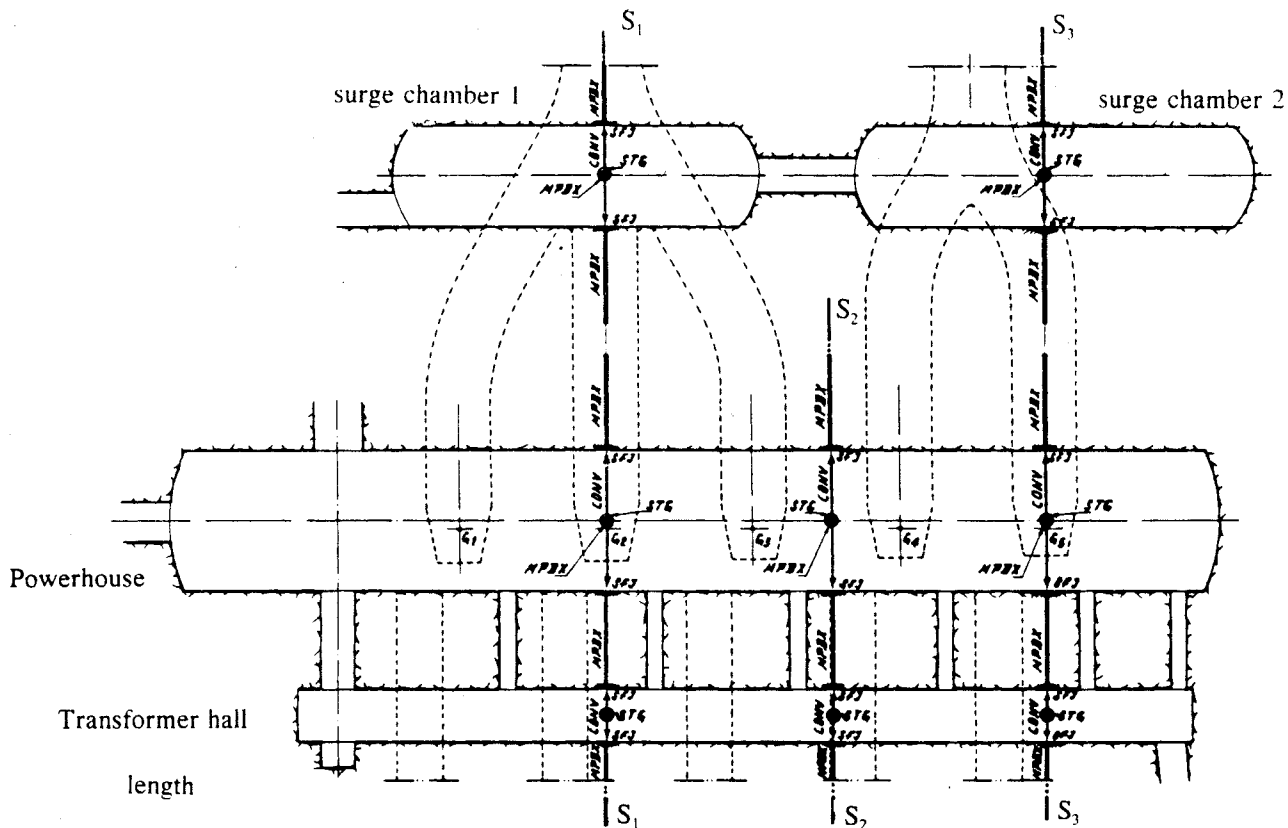


Fig. 5.11 - Observation plan of the powerhouse underground complex

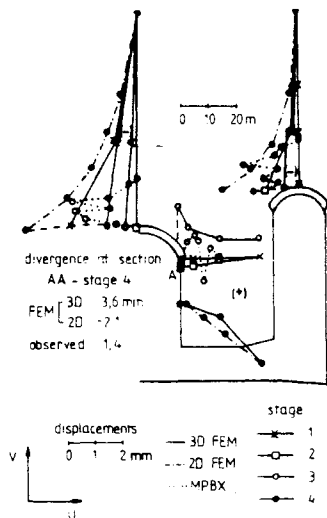


Fig. 5.12 - Comparison of observed and predicted behaviour

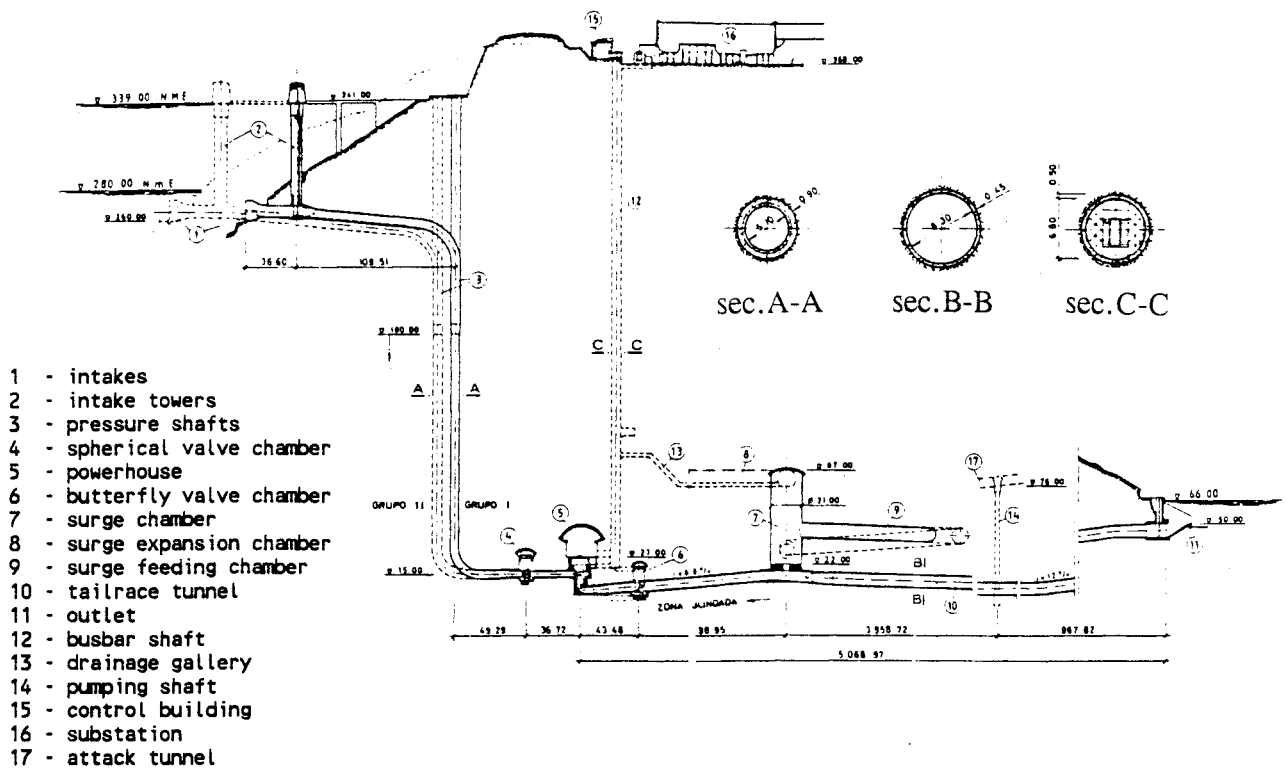


Fig. 6.1 - Hydraulic circuit of Alto Lindoso power scheme. Longitudinal profile (after EDP, 1991)

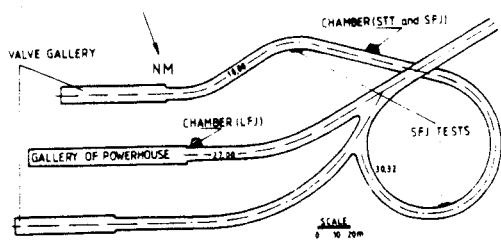
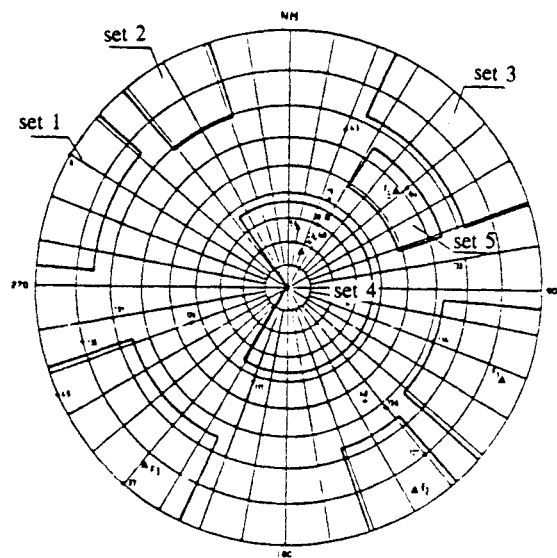


Fig. 6.2 - Sites of rock tests



F_i - Mean orientation for set i

Fig. 6.3 - Discontinuity sets

Table 6.1

Stability of blocks of an exploration gallery

Blocks	Ceiling ($\beta_f=90$)		Left wall ($\alpha_f/\beta_f=200/0$)		Right wall ($\alpha_f/\beta_f=20/0$)		Front side ($\alpha_f/\beta_f=290/0$)	
	Type	θ (°)	Type	θ (°)	Type	θ (°)	Type	θ (°)
1-2-3	D2	86	D12	83	D23	83	D1	84
1-2-4	D12	83	D12	83	N	--	D12	83
1-2-5	D12	83	D12	83	N	--	D12	83
1-3-4	V	--	D4	17	D13	79	D1	84
1-3-5	D1	84	D15	57	D13	79	D1	84
1-4-5	D15	57	D15	57	N	--	D5	58
2-3-4	V	--	D4	17	D23	83	D24	13
2-3-5	D2	86	D5	58	D23	83	D25	57
2-4-5	D5	58	D5	58	N	--	D25	57
3-4-5	V	--	D45	10	D35	12	D35	12

Table 6.2
Summary of joint shear tests result

<i>Parameter</i>	<i>minimum</i>	<i>mean</i>	<i>maximum</i>
<i>c</i> (MPa)	0.00	0.08	0.34
<i>tg φ</i>	0.604	0.740	0.910
<i>c'</i> (MPa)	0.00	0.06	0.25
<i>tg φ'</i>	0.410	0.581	0.681
<i>K_n</i> (GPa/m)	16	30	40
<i>K_s</i> (GPa/m)	2	4	8
<i>i</i> (°)	0	7	13

Table 6.3
Results of SFJ and STT tests

Results of SFJ tests

SFJ tests	Slot	Stresses (MPa)
SFJ ₁	horizontal	- 4.0
SFJ ₂	vertical	- 7.7
SFJ ₃	horizontal	- 0.4
SFJ ₄	horizontal	- 20.9

(-) compression

Results of STT tests

STT tests	Principal stresses (MPa)		
	σ_1	σ_2	σ_3
ST ₁₁	- 4.3	- 7.7	- 9.0
ST ₁₂	- 2.2	- 8.0	- 19.1
ST ₁₃	- 3.1	- 6.8	- 11.3
ST ₂₁	- 3.5	- 4.3	- 11.5
-ST ₂₂	- 2.6	- 8.8	- 14.4
ST ₃₁	- 5.6	- 11.6	- 14.3
ST ₃₂	- 5.4	- 11.2	- 13.5
ST ₄₁	- 2.6	- 9.6	- 14.4
ST ₄₂	- 3.3	- 5.1	- 14.9

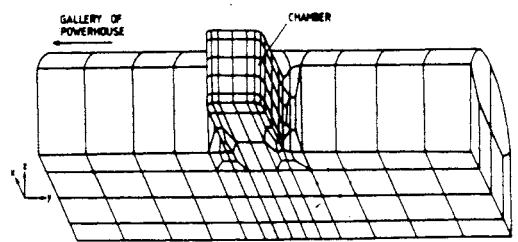


Fig. 6.4 - View of the boundary element mesh.

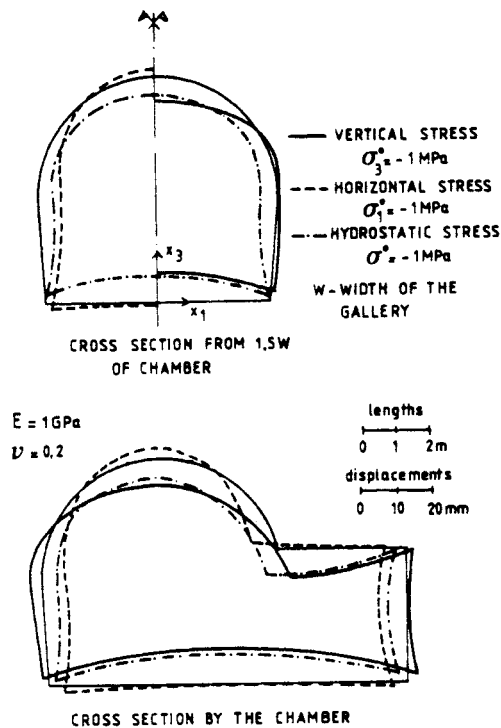


Fig. 6.5 - Displacements at the boundaries along the cross-sections.

Table 6.4
In-situ state of stress calculated

Stresses	Principal stresses
$\sigma_x = -12.6$	major stresses *
$\sigma_y = -10.7$	$\sigma_1 = -14.1$ at 007/61
$\sigma_z = -7.6$	intermediate stress
$\tau_{xy} = 1.3$	$\sigma_2 = -10.6$ at 135/18
$\tau_{yz} = 0.5$	minor stress
$\tau_{zx} = 2.9$	$\sigma_3 = -6.0$ at 232/21

* trend/plunge

phase 4 - concrete arch support

phase 5 - anchorage forces

phase 10 - concentrated forces
at powerhouse beam

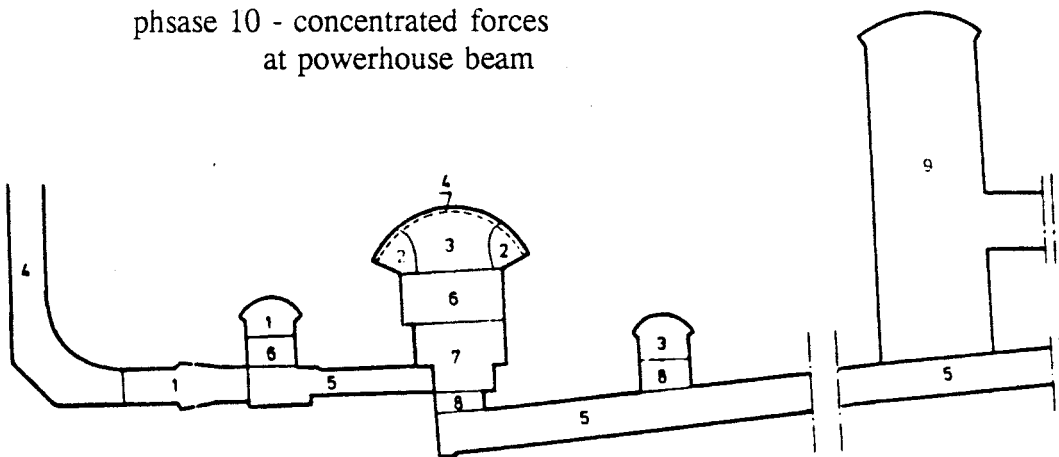


Fig. 6.6 - Construction sequence at section S₂

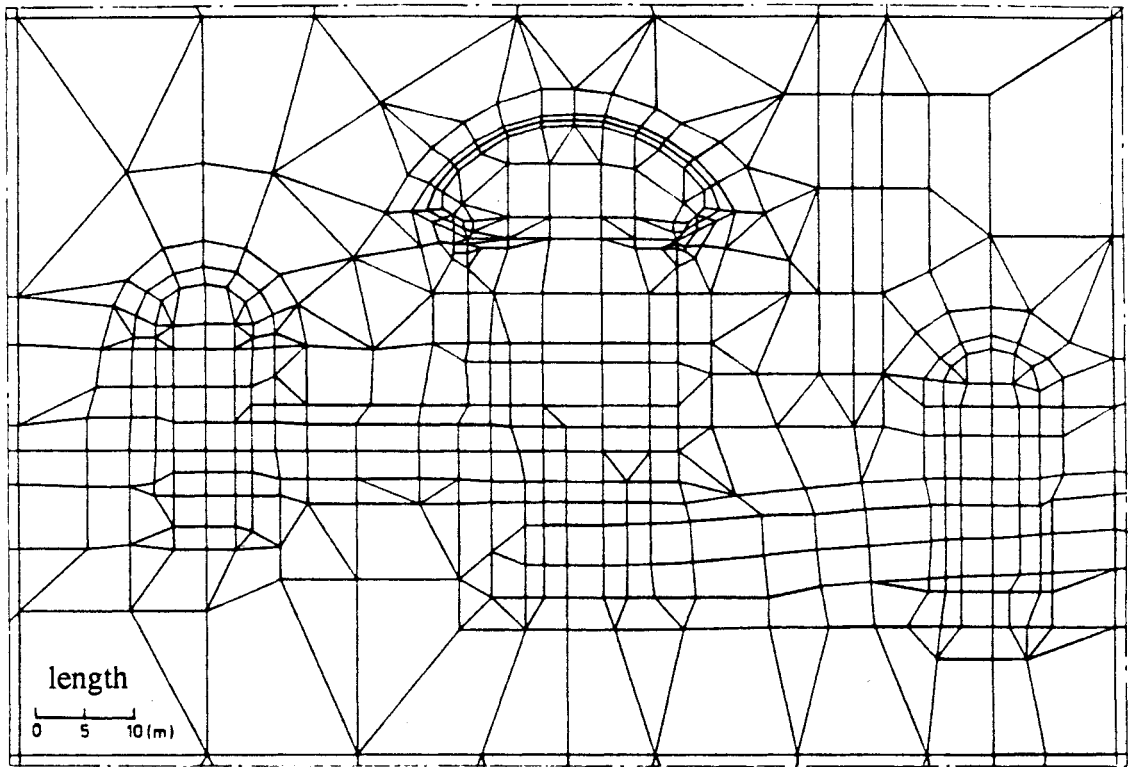


Fig. 6.7 - Detail of the finite element mesh.

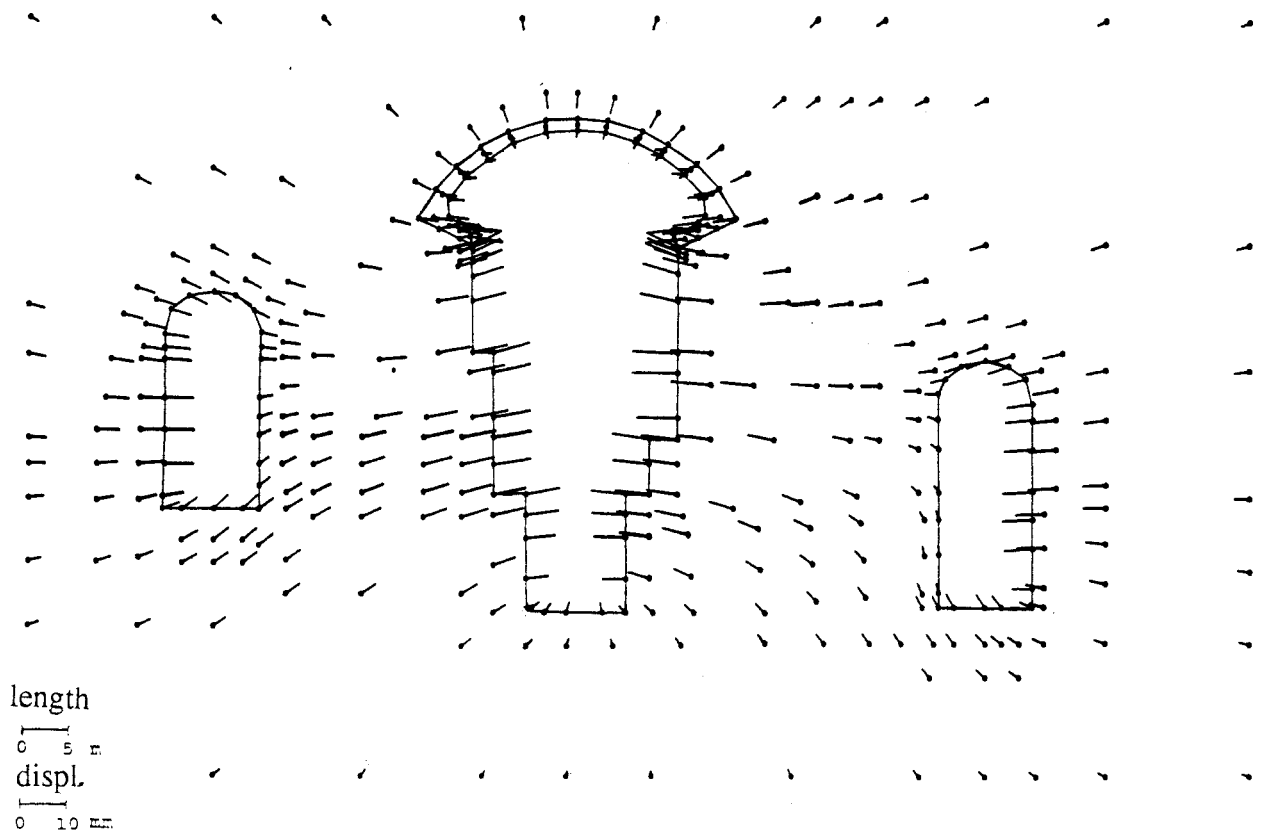


Fig. 6.8 - Displacements at phase 8.

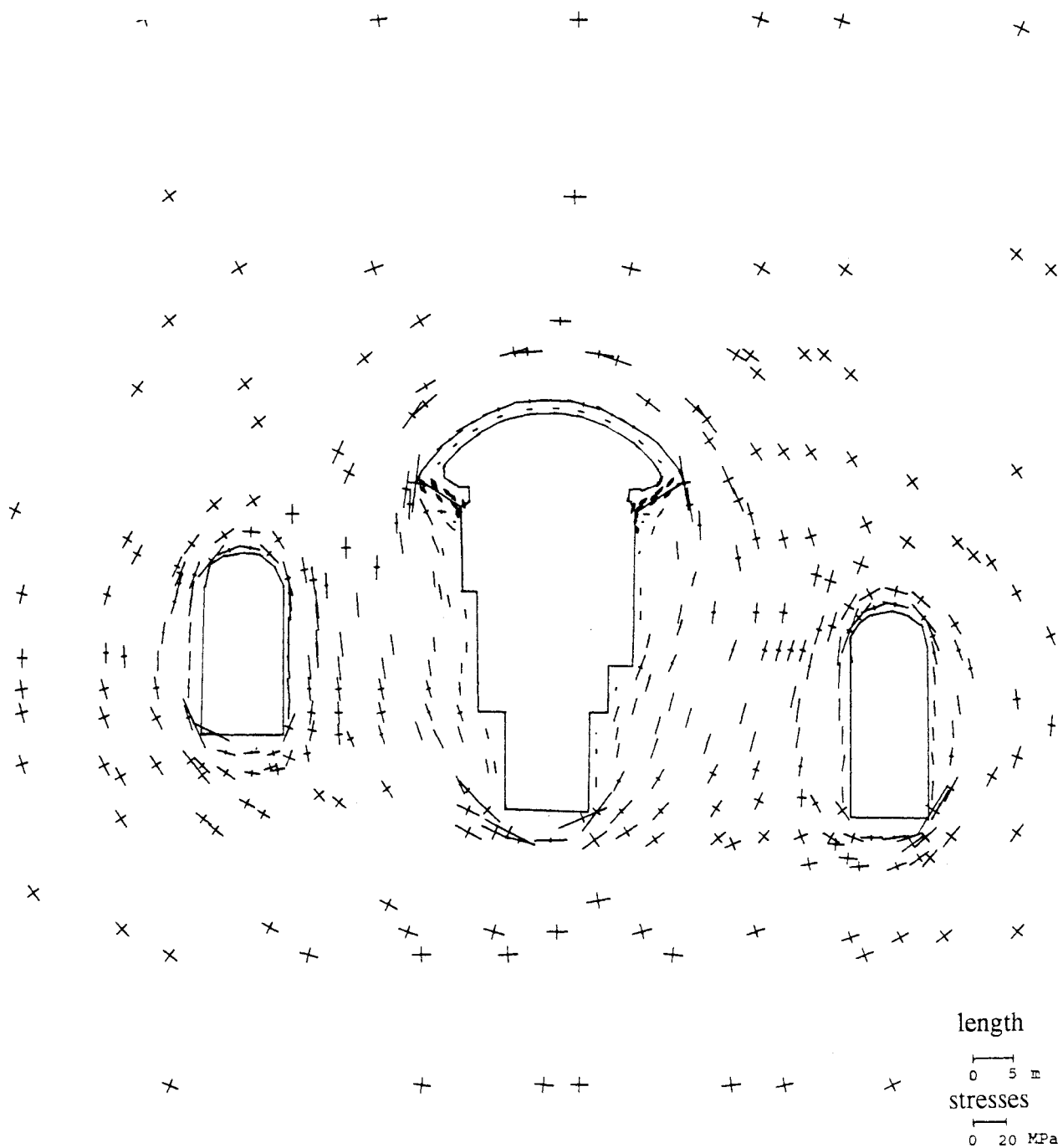


Fig. 6.9 - Principal stresses at phase 8.

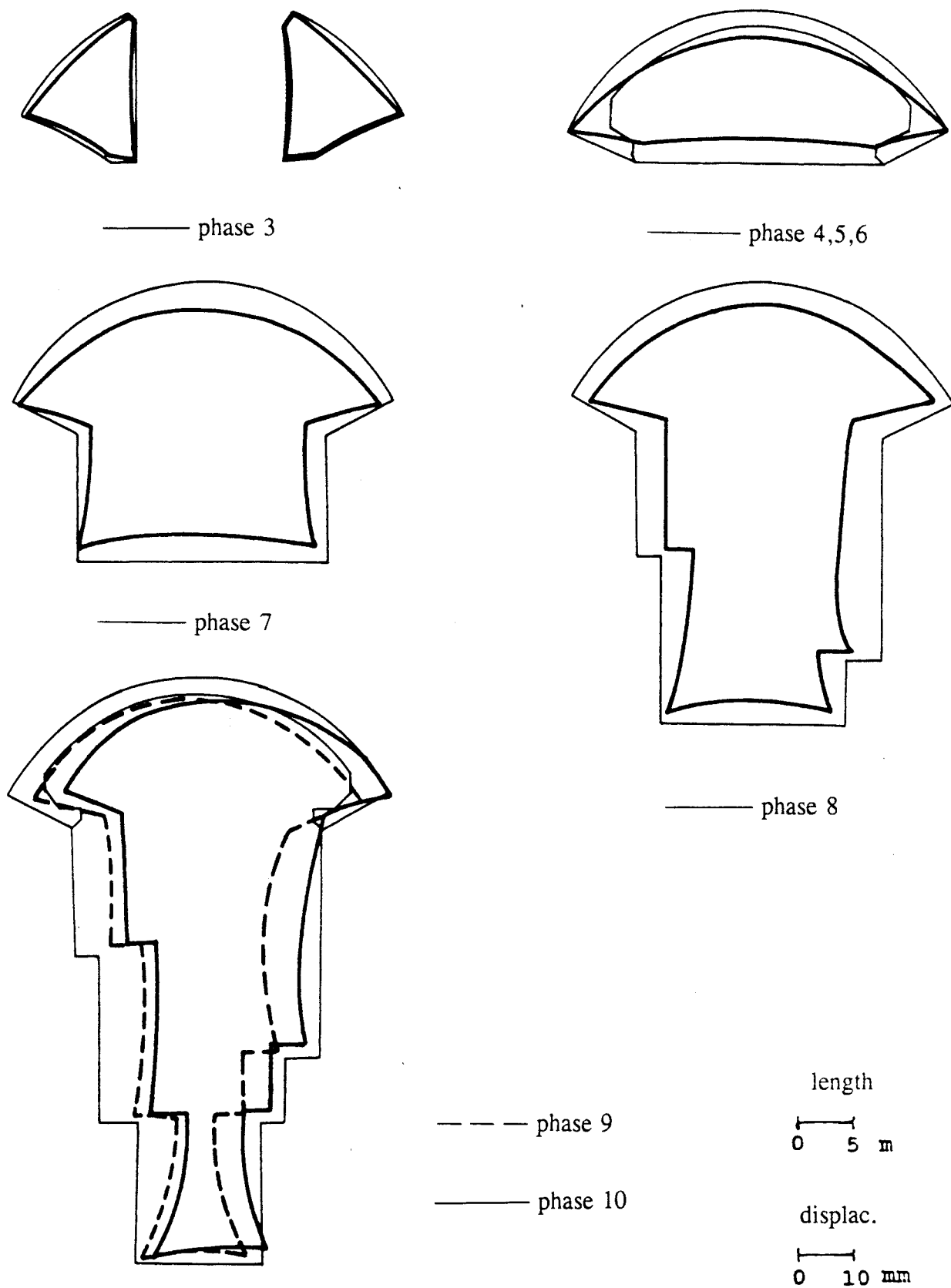


Fig. 6.10 - Displacements around powerhouse cavern for the different phases.

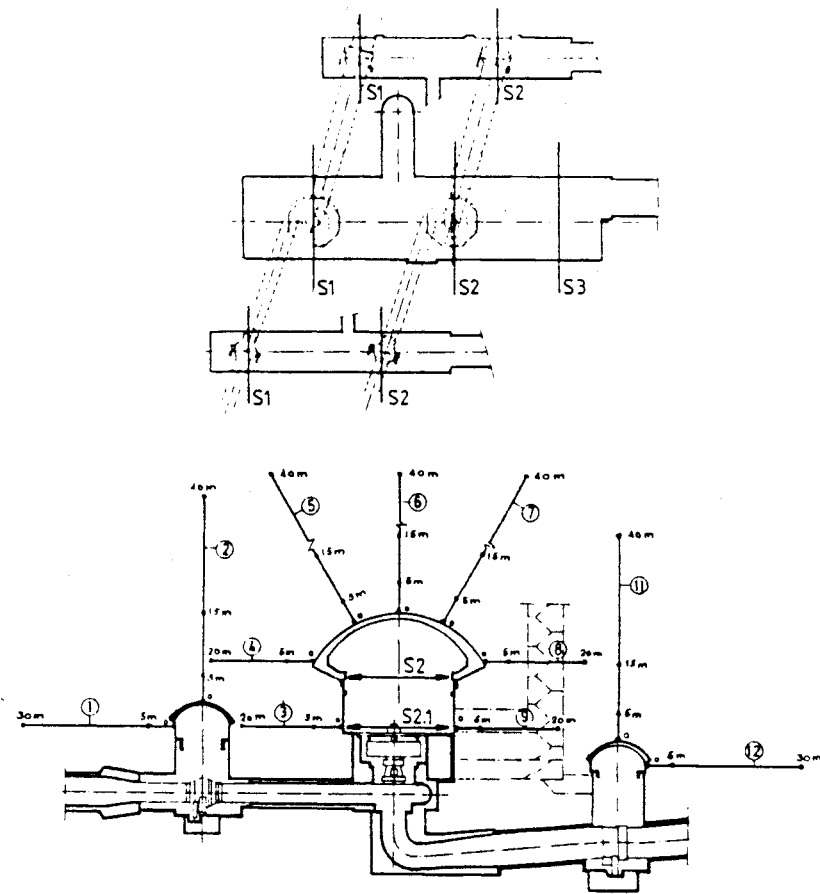


Fig. 6.12 - Observation plan of the powerhouse complex.

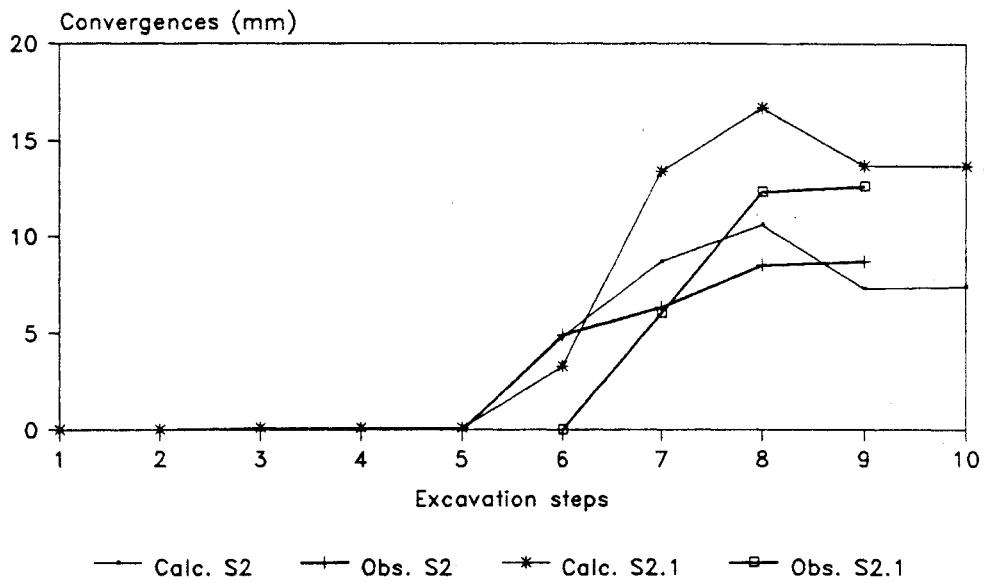
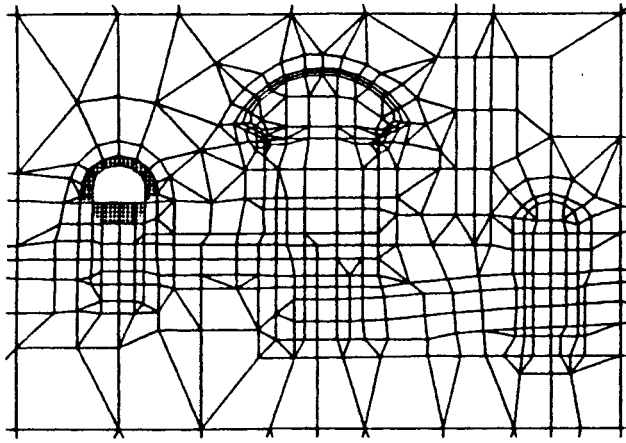
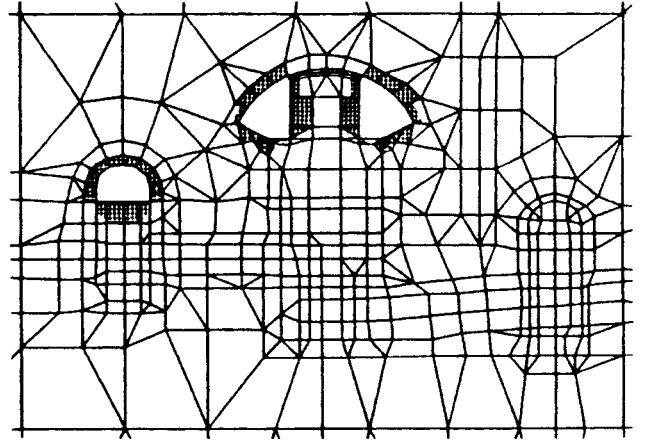


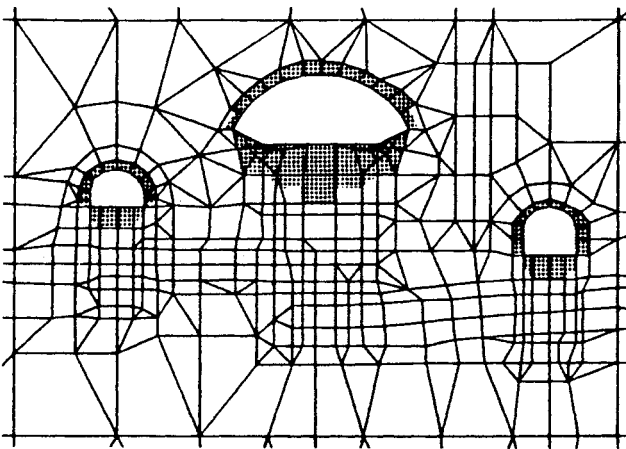
Fig. 6.13 - Comparison of observed and numerical convergences.



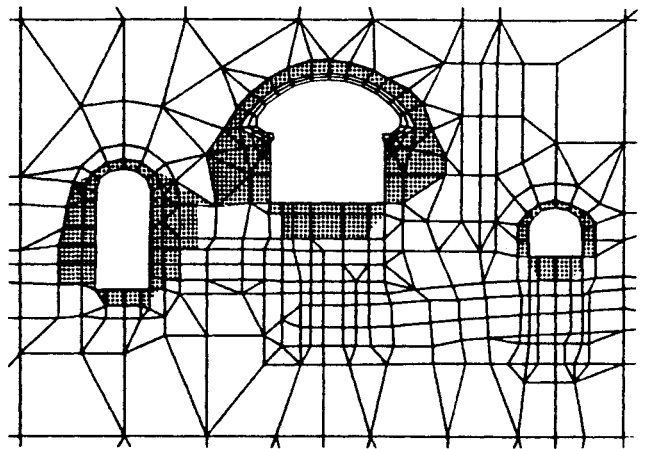
phase 1



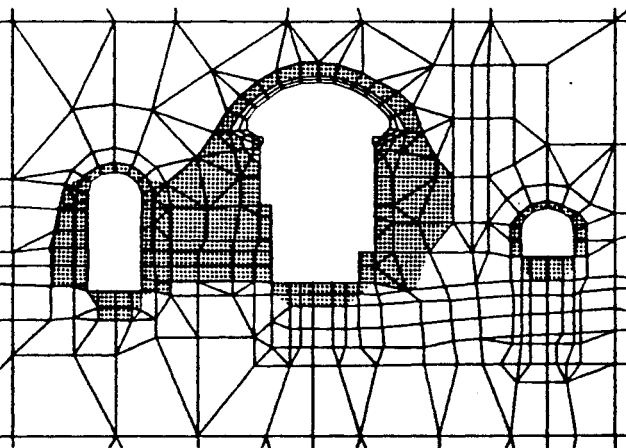
phase 2



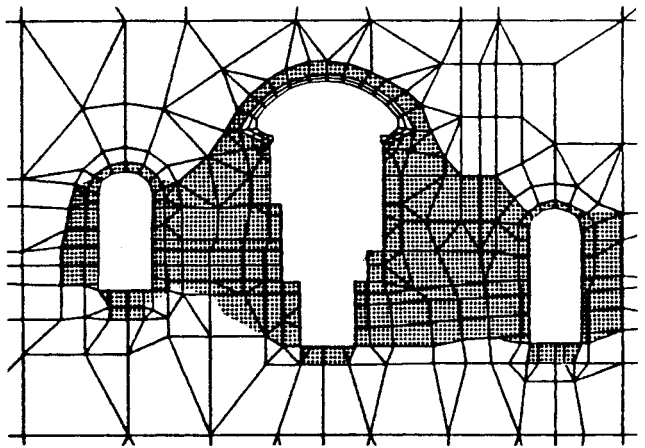
phase 3,4,5



phase 6



phase 7



phase 8,9,10

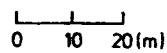


Fig. 6.11 - Failure zones around cavities with application of Coulomb criteria.

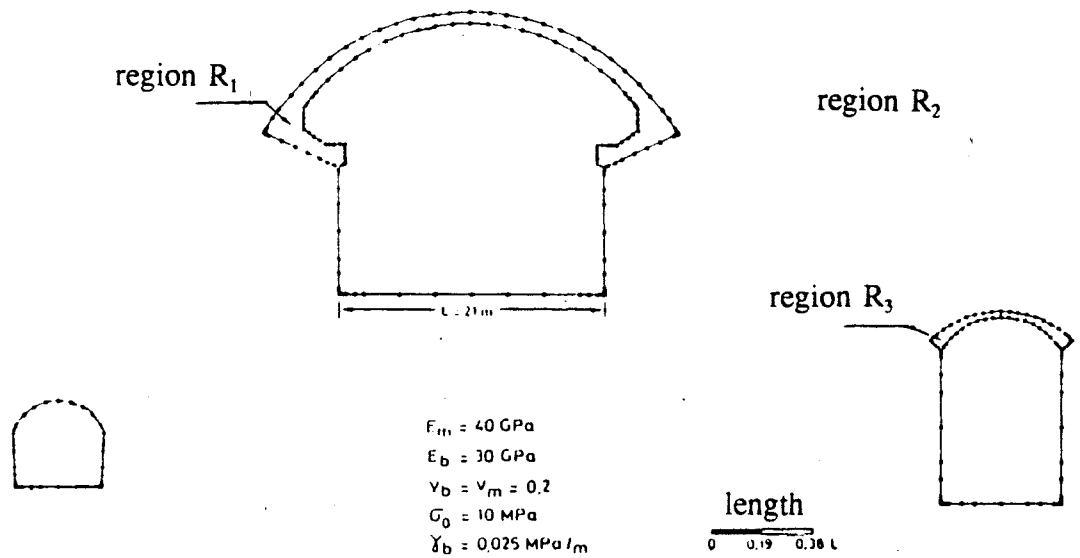


Fig. 6.14 - Boundary element model considering concrete arches (after Castro, 1989).

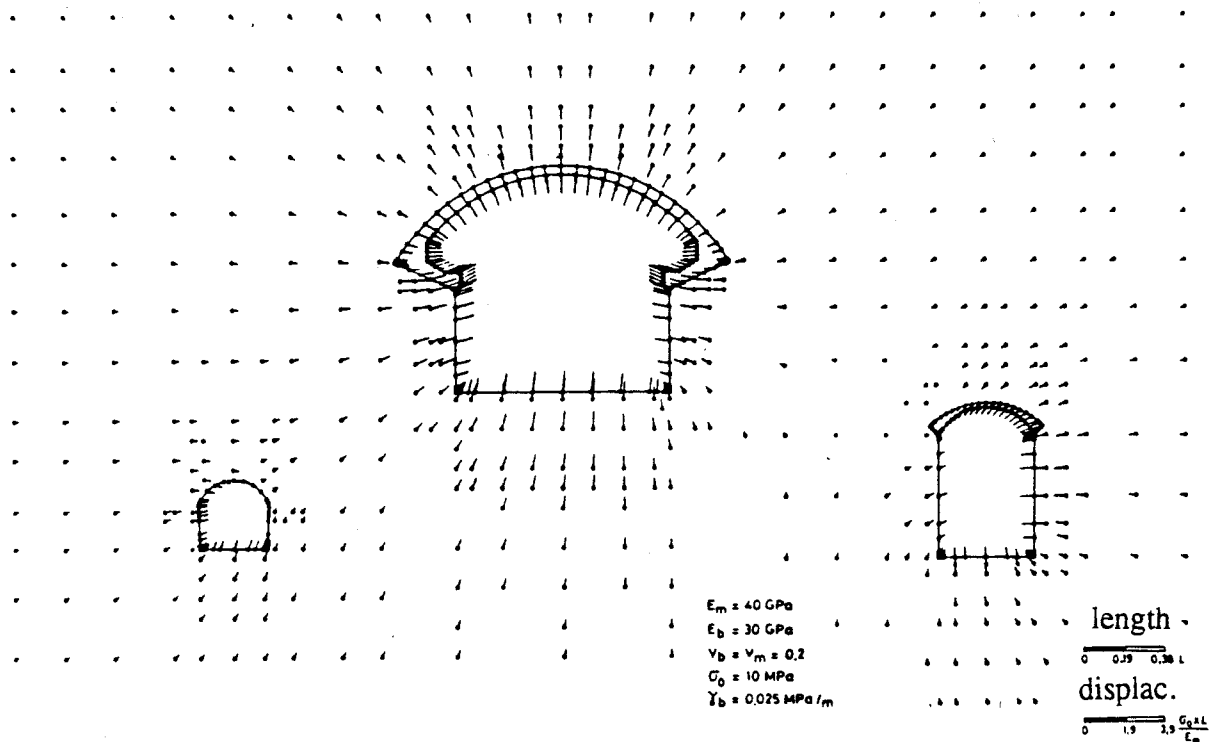


Fig. 6.15 - Displacements obtained with boundary element model (after Castro, 1989).

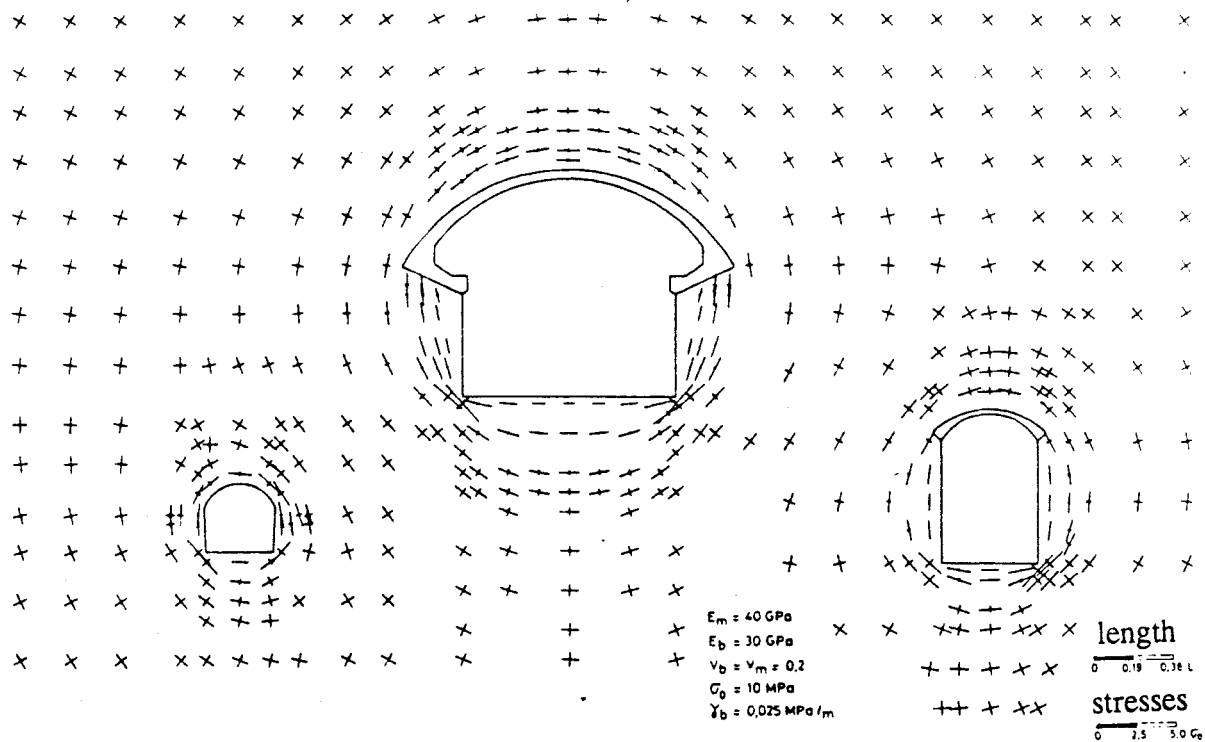


Fig. 6.16 - Principal stresses obtained with boundary element model (after Castro, 1989).

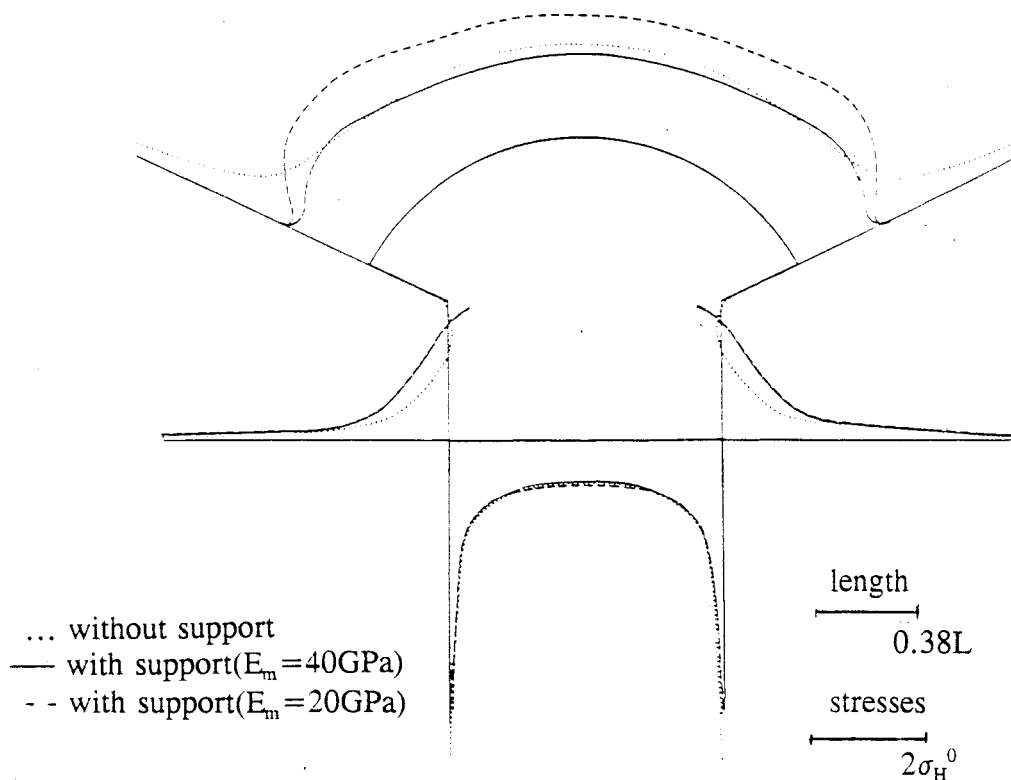


Fig. 6.17 - Tangential stresses along the boundaries of the powerhouse cavern (after Castro, 1989)

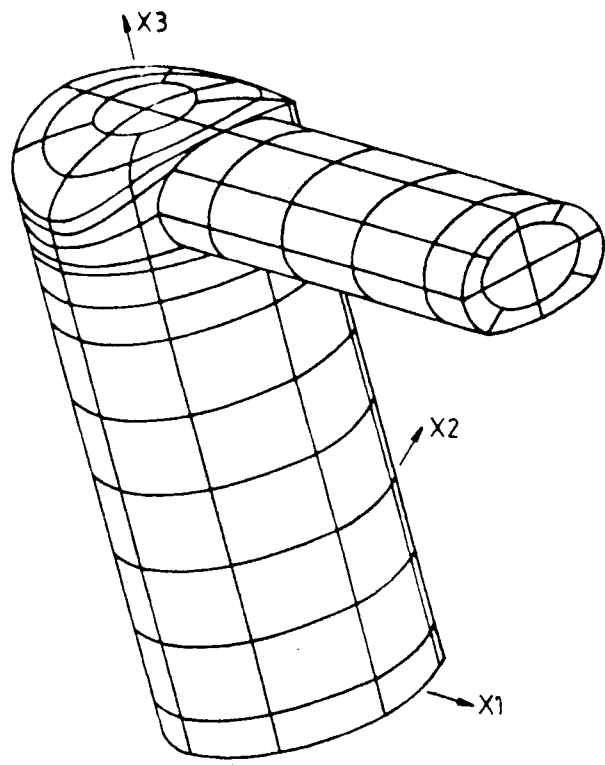


Fig. 6.18 - 3D boundary element mesh for the surge chamber

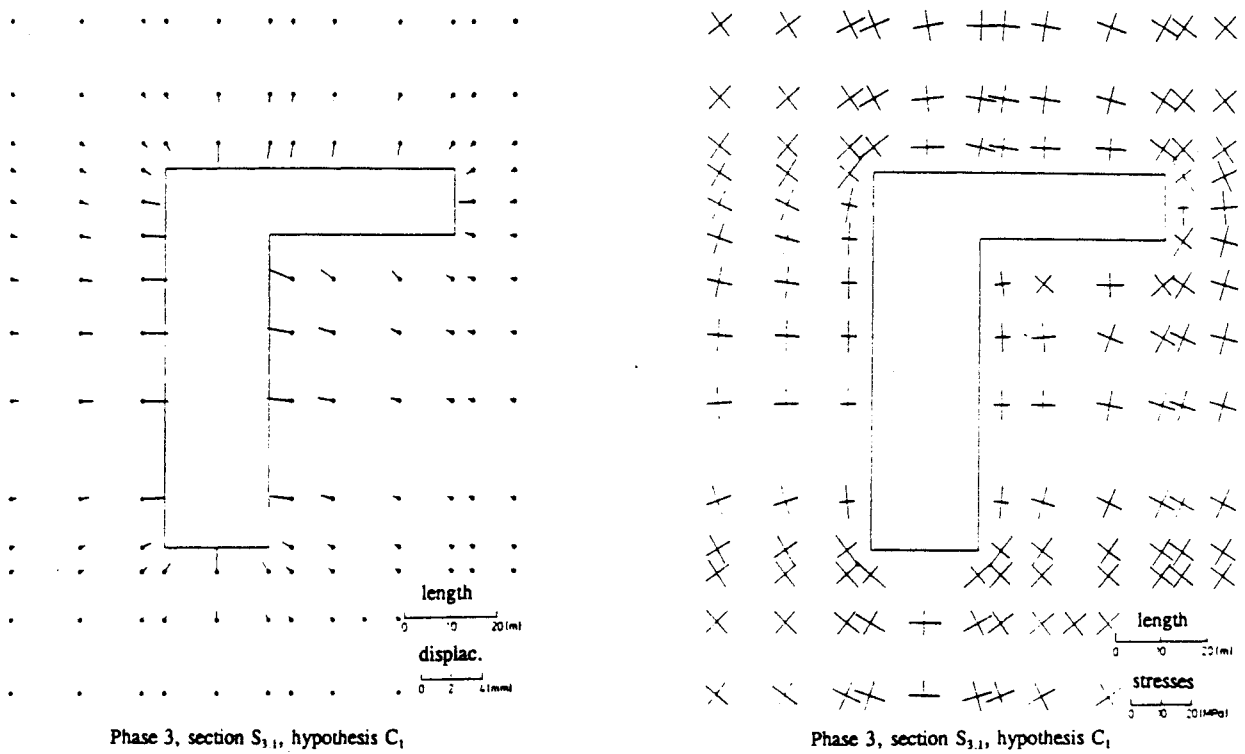
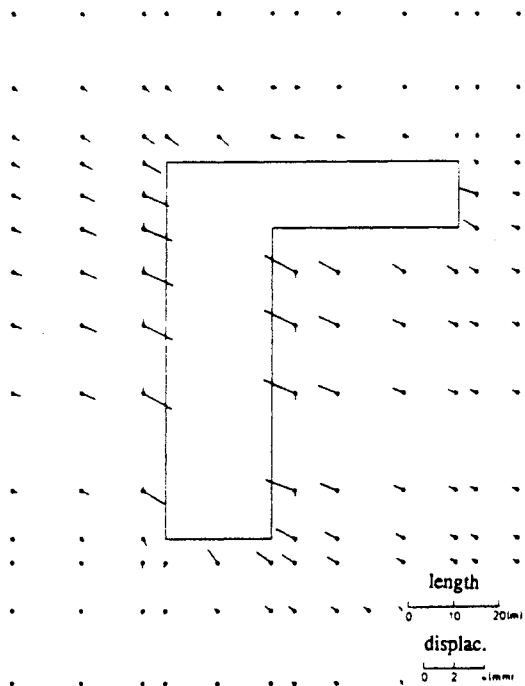
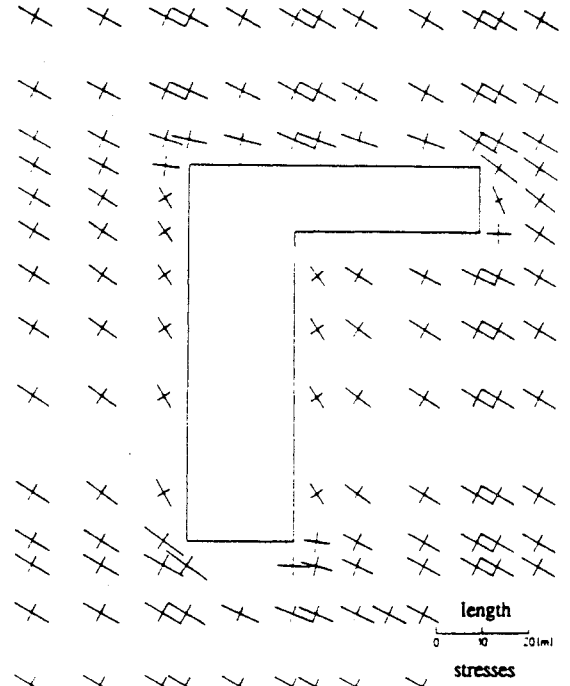


Fig. 6.19 - Displacements and principal stresses for phase 3, hypothesis C_1

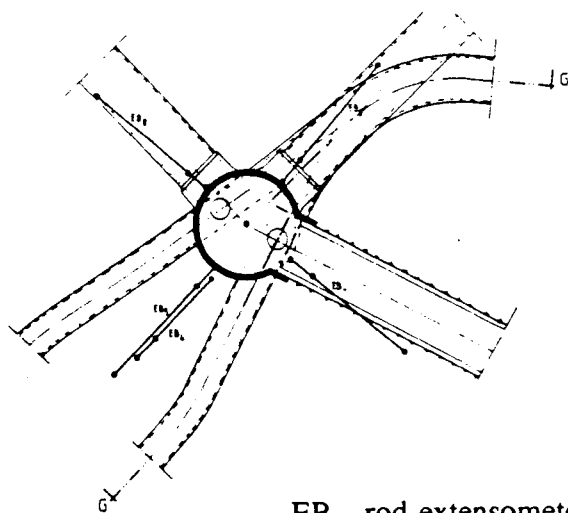


Phase 3, section $S_{3,1}$, hypothesis C_2



Phase 3, section $S_{3,1}$, hypothesis C_2

Fig. 6.20 - Displacements and principal stresses for phase 3, hypothesis C_2



EB - rod-extensometer

A - convergence section

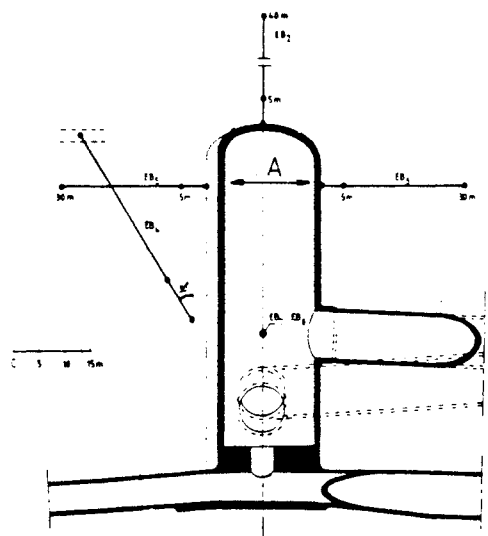


Fig. 6.21 - Observation plan of the surge chamber.

Convergence measurements

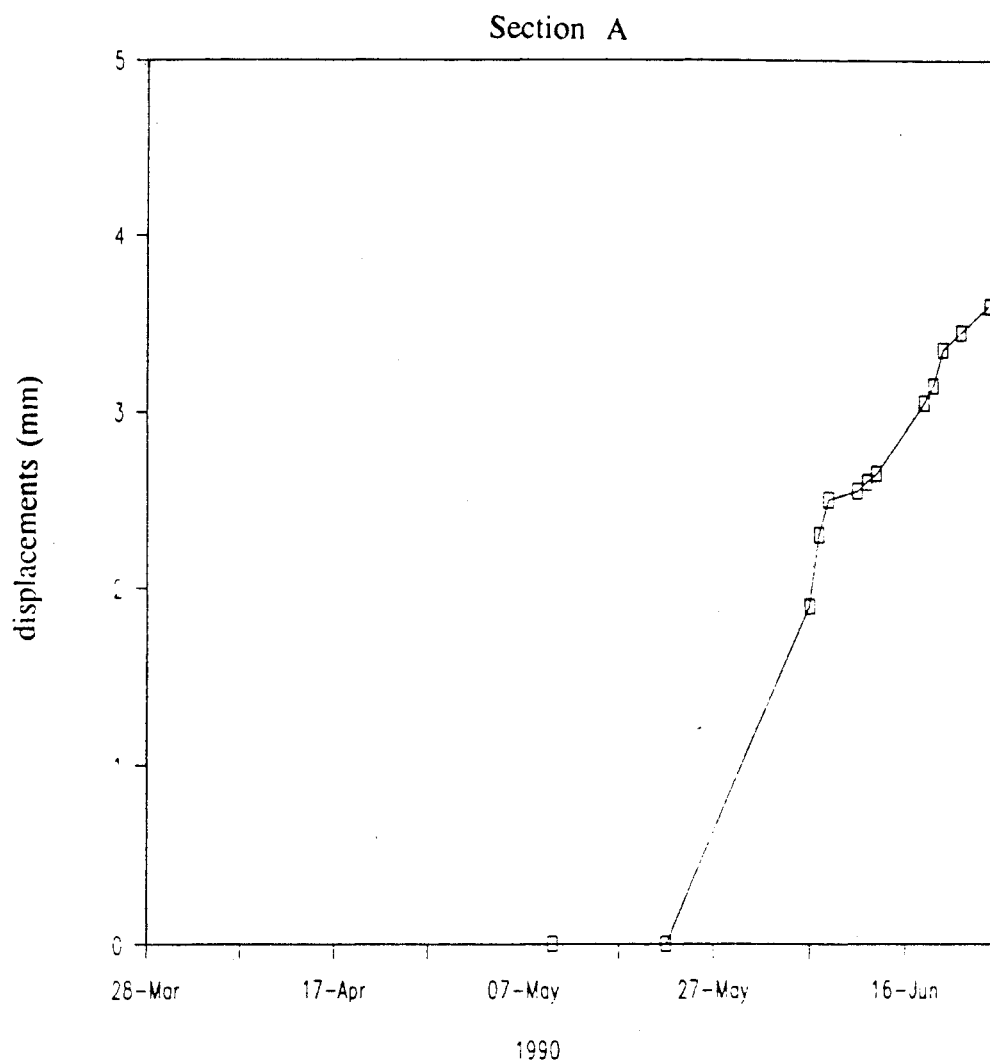


Fig. 6.22 - Convergence measurements at section A of the surge chamber.

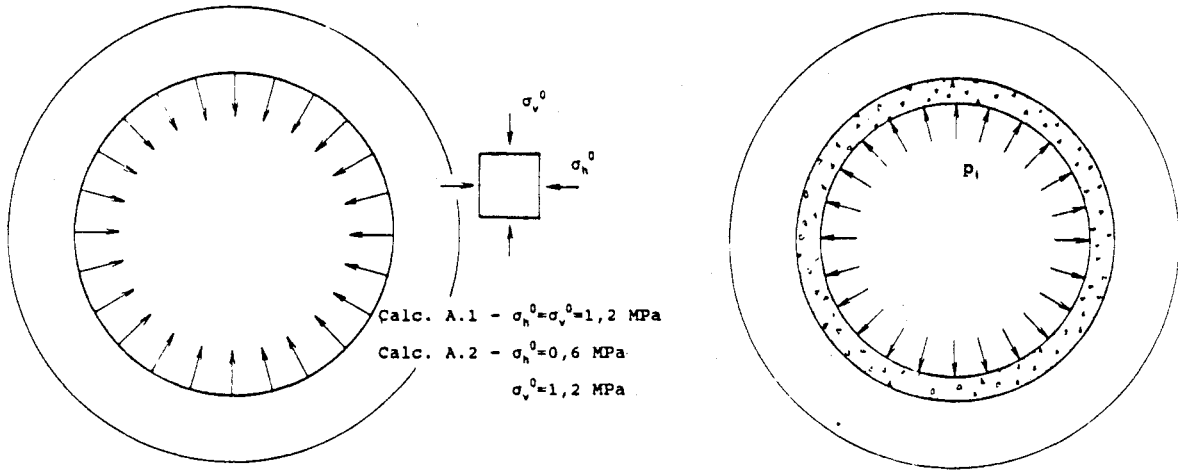


Fig. 7.3 - Conceptual model and construction sequence for the finite element model.

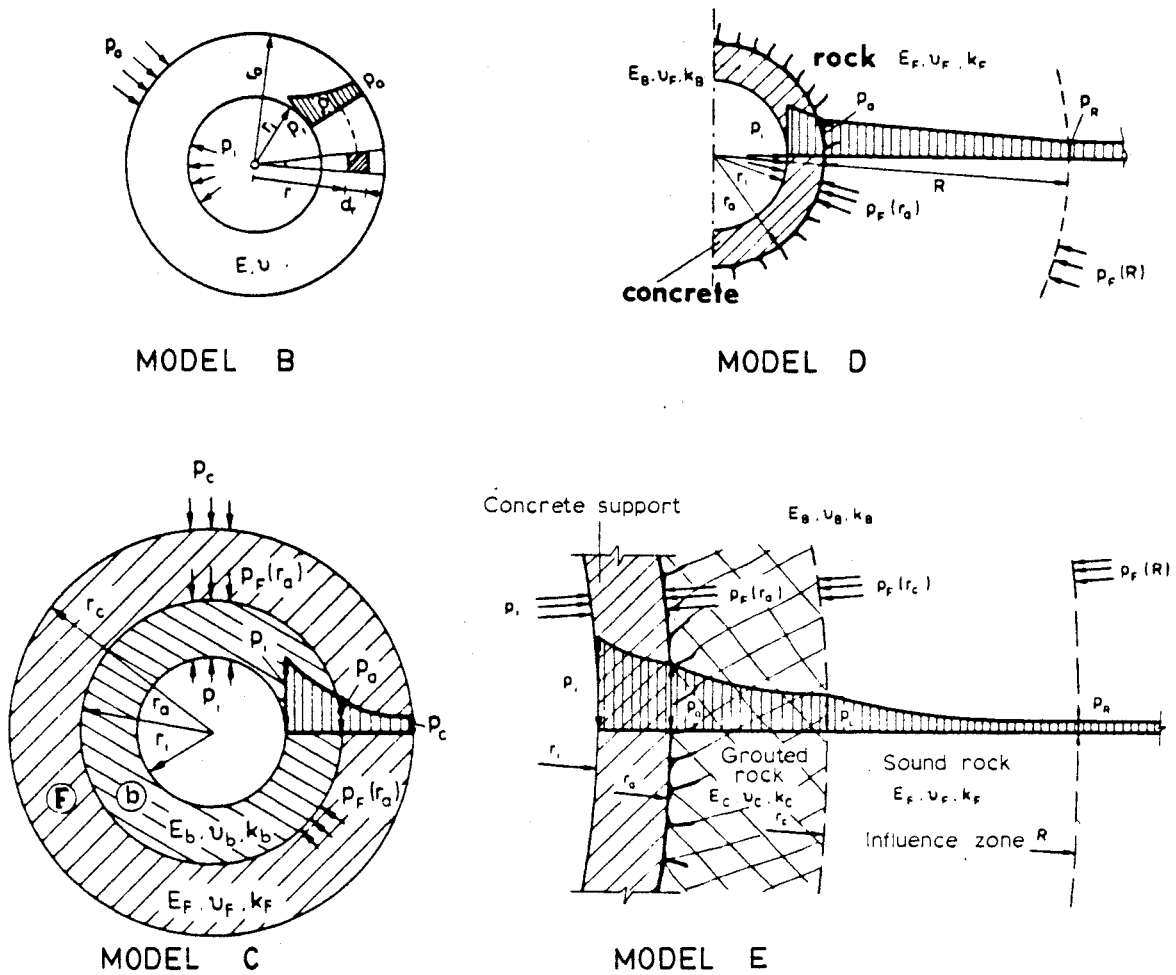


Fig. 7.4 - Conceptual models for the analytical solutions of the thick walled pervious rings (after Schleiss, 1986)

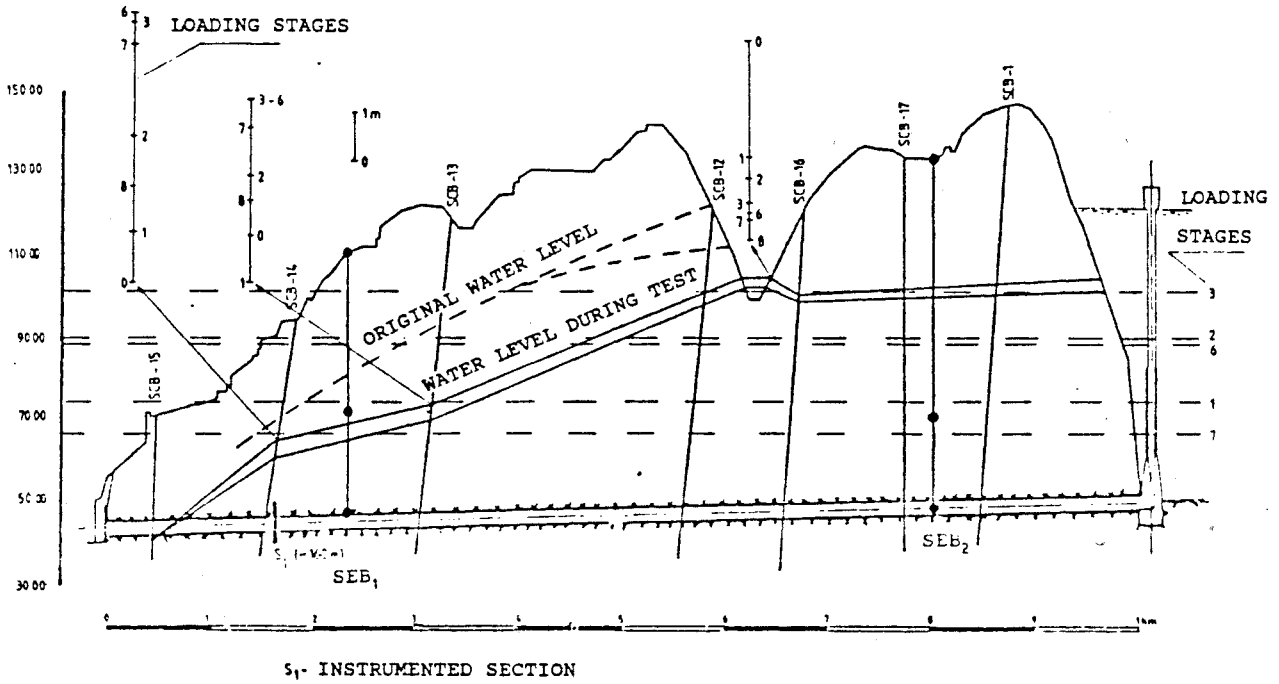


Fig. 7.1 - Castelo do Bode tunnel: vertical section.

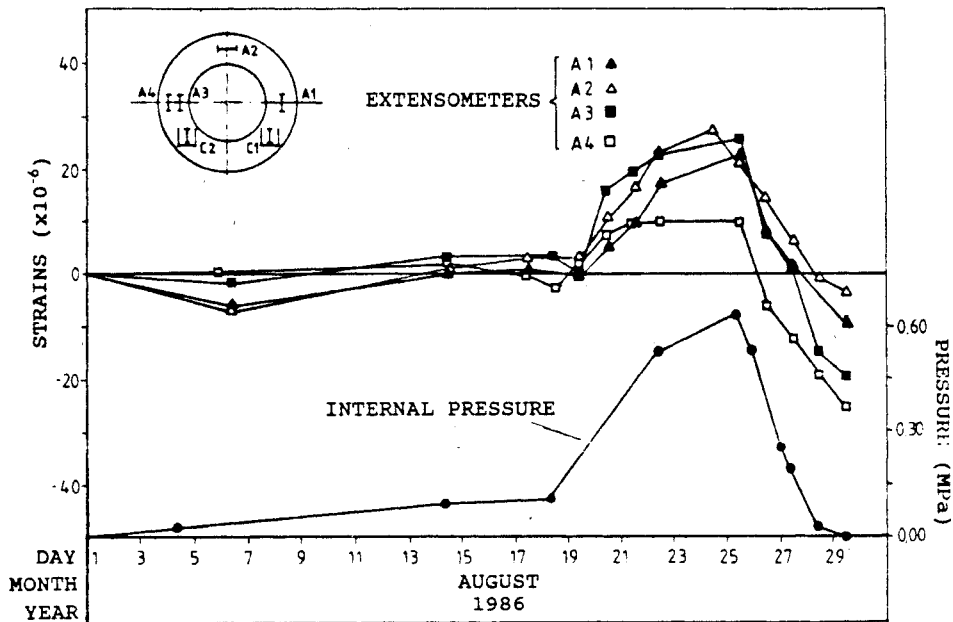


Fig. 7.2 - Loading test: internal water pressure and strains in the Carlson extensometers in the instrumented section

FIG. 7.5- TANGENTIAL STRESSES
IN THE CENTRE OF THE CONCRETE LINING

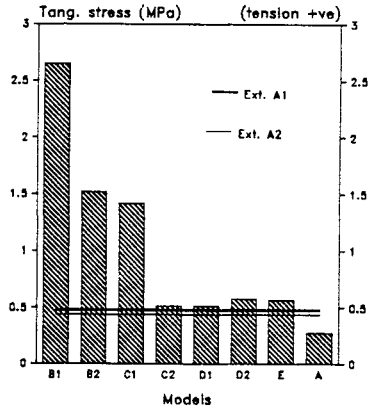


FIG. 7.6 - NORMAL STRESSES
IN THE LINING/ROCK CONTACT

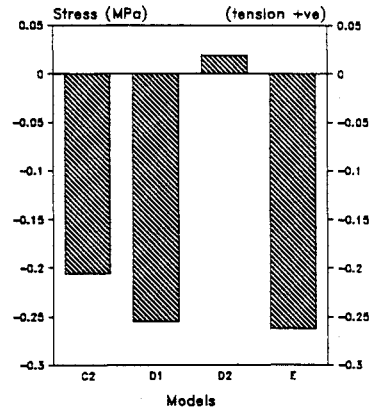


FIG. 7.7 - FLOW RATES
THROUGH THE CONCRETE LINING

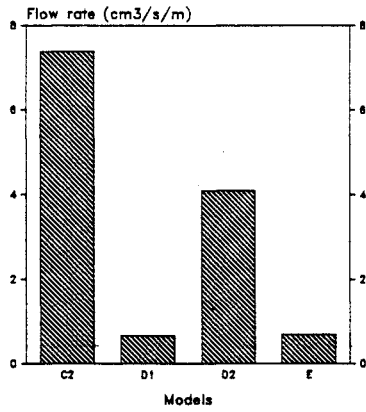


FIG. 7.8 - EXTENSOMETERS A1 AND A2
Tangential stresses

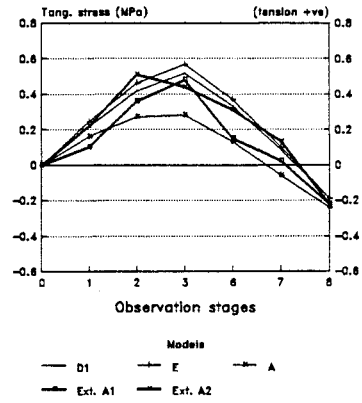


FIG. 7.9 - EXTENSOMETER A3
Tangential stresses

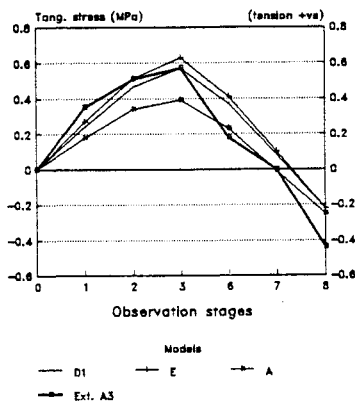
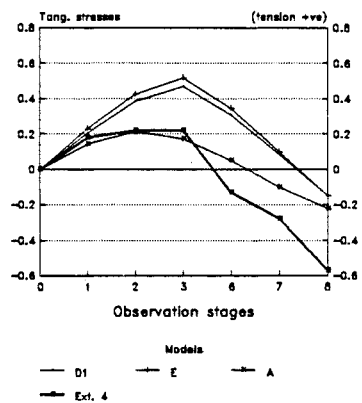


FIG. 7.10 - EXTENSOMETER A4
Tangential stresses





www.lnec.pt

AV DO BRASIL 101 • 1700-066 LISBOA • PORTUGAL
tel. (+351) 21 844 30 00
lnec@lnec.pt www.lnec.pt